

# Hadron Physics at J-PARC

H. Ohnishi,<sup>1</sup> F. Sakuma,<sup>2</sup> T. Takahashi,<sup>3</sup>

<sup>1</sup>Research Center for Electron Photon Science (ELPH),  
Tohoku University, Sendai 982-0826, Japan

<sup>2</sup>RIKEN Cluster for Pioneering Research (CPR),  
RIKEN, Wako 351-0198, Japan

<sup>3</sup>Institute of Particle and Nuclear Study (IPNS),  
High Energy Accelerator Research Organization (KEK),  
Tsukuba 305-0801, Japan

March 3, 2020

## Abstract

The aim of the hadron physics research programs conducted at J-PARC is to explore the structure of hadronic matter using the world's highest-intensity meson beams. Since the first beam was extracted at the hadron experimental facility (HEF) in February 2009, a wide variety of physics experiments have been proposed and performed to address open questions regarding quantum chromodynamics (QCD) at low energy. The high-intensity  $K^-$  and high-momentum beams available at J-PARC open a new era in hadron and nuclear physics, in which strange and charm quarks play an important role. We review the programs focused on addressing the hadron structure as strongly interacting composite particles, the origin of hadron mass, and interactions between hadrons under broken flavor SU(3) symmetry.

## Contents

<b>1</b>	<b>Introduction</b>	<b>2</b>
<b>2</b>	<b>J-PARC Hadron Experimental Facility</b>	<b>4</b>
2.1	Overview of J-PARC . . . . .	4
2.2	Overview of J-PARC . . . . .	4
2.3	Hadron Experimental Facility . . . . .	7
<b>3</b>	<b>Experiments at the J-PARC HEF</b>	<b>8</b>
3.1	QCD Vacuum and Hadron Structure . . . . .	10
3.1.1	Search for the $\Theta^+$ penta-quark baryon . . . . .	10
3.1.2	Search for the $H$ dibaryon . . . . .	12
3.1.3	Detailed investigations of nucleon resonances . . . . .	14
3.1.4	Hyperon resonance near the $\Lambda\eta$ threshold . . . . .	14
3.1.5	Charmed baryon spectroscopy . . . . .	15

3.1.6	Precise measurement of the spectral function of vector mesons via di-electrons . . . . .	17
3.1.7	Search for vector-meson nuclear bound states . . . . .	19
3.2	Antikaon-Nucleon Interaction . . . . .	20
3.2.1	Measurement of kaonic-deuterium $2p \rightarrow 1s$ X-rays . . . . .	22
3.2.2	Precise measurement of kaonic-helium $3d \rightarrow 2p$ X-rays . . . . .	25
3.2.3	Investigation of the $\Lambda(1405)$ line shape . . . . .	27
3.2.4	Search for kaonic nuclei . . . . .	31
3.3	Baryon-Baryon Interaction . . . . .	39
3.3.1	Neutron-rich $\Lambda$ hypernuclei . . . . .	40
3.3.2	$\gamma$ -ray spectroscopy of $\Lambda$ hypernuclei for detailed studies on $\Lambda$ interactions . . . . .	42
3.3.3	Investigation of in-medium $\Lambda$ properties by $\gamma$ -ray spectroscopy of $\Lambda$ hypernuclei . . . . .	46
3.3.4	Hyperon-Nucleon scattering . . . . .	47
3.3.5	Double- $\Lambda$ hypernuclei . . . . .	49
3.3.6	$\Xi$ hypernuclei . . . . .	53
3.3.7	X-ray spectroscopy of $\Xi^-$ -atoms . . . . .	57
<b>4</b>	<b>Future Prospects</b> . . . . .	<b>57</b>
4.1	Physics at HIHR . . . . .	58
4.2	Physics at K10 . . . . .	60
<b>5</b>	<b>Summary</b> . . . . .	<b>61</b>
<b>6</b>	<b>Acknowledgments</b> . . . . .	<b>62</b>

# 1 Introduction

Understanding the formation and interaction of a hadron is one of the fundamental goals of hadron physics. Nowadays, quantum chromodynamics (QCD) has succeeded in describing the interactions between quarks and gluons. However low energy phenomena, such as the formation of a hadron, are not clearly explained because perturbation theory does not work in the low energy regime.

The scientific programs at J-PARC aim to understand the formation and interaction of hadrons based on QCD. Especially, experimental programs underway and planned are intending to answer the following questions and issues:

- What are the effective degrees of freedom inside hadrons?
- How is the mass of the hadron acquired from the QCD vacuum?
- Can a meson exist in nuclear matter by holding the mesonic degrees of freedom?
- Reveal the hyperon-nucleon and hyperon-hyperon interaction to achieve a better understanding of nuclear forces.

QCD is supposed to generate constituent quarks dynamically as low-energy effective degrees of freedom. The constituent quark model assumes that the low-lying hadrons are composed of a few constituent quarks that carry color, spin, and flavor quantum numbers. The model successfully gives the number of states, their quantum numbers, and the flavor multiplet structure of their spectrum. The meson and baryon spectra suggest that the constituent quark has a dynamical mass of order 300 MeV/ $c^2$ , and that they are confined in a hadron. The model works very well for the ground state hadrons, while its prediction for the excited states is not satisfactory. Figure. 1 [1] shows a prediction of the negative-parity baryon spectrum in a constituent quark model. We notice that most of the low-lying

states are fairly well reproduced, but there is an exception – the  $\Lambda(1/2^-)$  state, where the prediction is off by 100 MeV from the observed state. It is also noted that many predicted states are not yet observed.

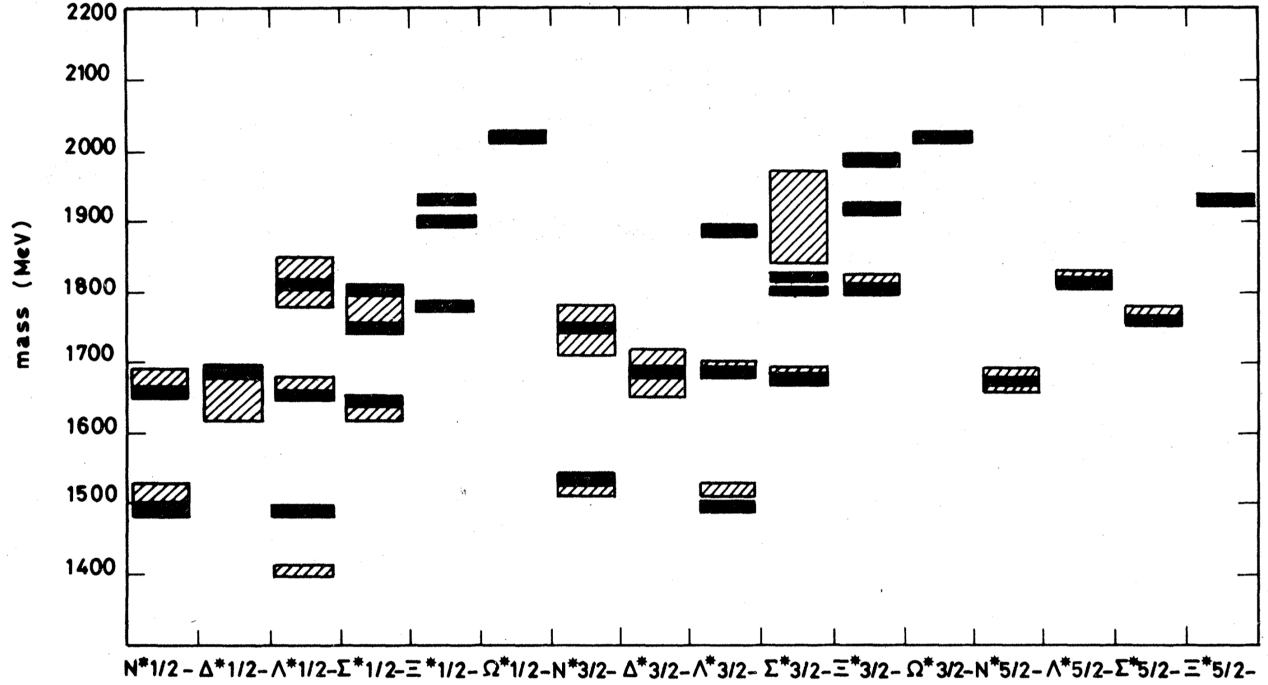


Figure 1: Mass spectra for negative-parity baryons. The hatched area shows experimental results and black bars represent the theoretical predictions. The figure is taken from Ref. [1].

Another deficiency of the constituent quark model is that the dynamics of confinement is not clear for multi-quark systems. QCD restricts hadrons to be color singlet but does not forbid multi-quark states, such as  $qq\bar{q}\bar{q}$ , or  $qqqq\bar{q}$ , referred to the tetra-quark and pentaquark baryons, respectively. The reason why the number of exotic hadrons is so small compared to ordinary hadrons with  $qqq$  or  $q\bar{q}$  configuration is not yet known.

The study of light hadrons in QCD sum rules revealed that their masses are generated by quark and gluon condensates in the QCD vacuum. The quark condensates are the direct consequence of spontaneous chiral symmetry breaking predicted by Y. Nambu and G. Jona-Lasinio [2, 3]. It is fascinating to confirm the relations between the hadron mass and the quark condensates from experiments. QCD also predicts that the chiral symmetry might be restored at high temperature or high baryon density. The embedded meson in a nucleus is a powerful tool to access the information on the QCD vacuum. One of the methods is to observe the change of the meson properties in nuclear matter, *i.e.*, modification of the spectral function. Vector mesons are used as a “probe” for this purpose. The other is trying to form a meson-nuclear bound state and draw out the information on binding energy and decay width of the state which will be connected with the QCD vacuum structure in the nucleus. Hereafter we are focusing on the research on anti-kaon ( $\bar{K}$ ) interactions with nucleons and nuclei, because the world’s highest-intensity kaon beam is available at J-PARC. The interaction between a  $\bar{K}$  and a nucleon is known to be strongly attractive, and there is a hyperon resonance below the sum of the  $\bar{K}$  and nucleon masses, *i.e.*,  $\Lambda(1405)$ . Thus  $\Lambda(1405)$  is expected to be a quasi-bound state of a  $\bar{K}$  and a nucleon. If so, it is reasonable to extend the idea that the  $\bar{K}$  embedded into a nucleus may form a kaonic nuclear

quasi-bound state. It should be noted that the density of the kaonic nuclear quasi-bound state could reach higher values than normal nuclear density, which will be connected to the physics inside neutron stars.

In the world of nuclei, a nucleon, *i.e.*, a proton or a neutron, is used as an effective degree of freedom to describe them, such as their structures and properties. One of the outstanding problems is the origin of short-range repulsion and spin-orbit force in nucleon-nucleon ( $NN$ ) interactions. Because in short-range parts, where nucleons and the exchanged mesons overlap each other, it is reasonable to consider quark and gluon degrees of freedom. The repulsive force in the short-range is essential to explain nuclear saturation properties due to the exquisite balance between the middle and long-range attractions. The spin-orbit force in nucleon-nucleus potentials and  $NN$  interactions are also essential to explain the periodical stability of nuclei – nuclear magic numbers. These important features which are originated in the short-range part must be understood based on QCD. One of the most effective methods to investigate and understand the short-range phenomena in nuclear forces is by introducing new degrees of freedom to the system, *i.e.*, strange ( $s$ ) quarks, which extends the  $NN$  interaction under the isospin symmetry of  $SU(2)$  to the interactions between octet baryons ( $B_8B_8$  interactions) under flavor  $SU(3)$  ( $SU(3)_f$ ) symmetry. Although the  $s$ -quark is heavier than  $u$  and  $d$  quarks, the mass difference is still sufficiently small to treat the system under  $SU(3)_f$  considering the QCD energy scale  $\Lambda_{QCD}$  of  $\sim 200$  MeV. These newly introduced hyperon-nucleon ( $YN$ ) and  $YY$  interactions should be determined by experiments in close cooperation with theoretical studies. Due to the difficulty of direct scattering experiments, spectroscopic studies on hypernuclei which contain one or more hyperons are essentially important to investigate  $YN$  and  $YY$  interactions.

The nature of QCD, *i.e.*, strong coupling phenomena in the low energy region, is thus a challenging problem to solve analytically. An approach to overcome this difficulty is lattice QCD simulation. From the effort of theorists together with the progress of supercomputers, some part of the hadron mass spectra and interaction between hadrons can be extracted from the QCD Lagrangian, and the results are consistent with the experimental data. However, difficulties to reproduce or predict the properties of hadrons still remain, especially for the properties and interactions of excited hadrons. Moreover, it has been extremely difficult to solve QCD at finite density by lattice QCD simulation. Therefore, experimental efforts could represent essential inputs to understanding the nature of QCD.

In this article, we provide a brief introduction to the facility in Sec. 2, including an overview of the J-PARC accelerator. In Sec. 3, we review the hadron physics experiments at J-PARC, focusing on “*QCD Vacuum and Hadron Structure*”, “*Antikaon-Nucleon Interaction*”, and “*Baryon-Baryon Interaction*”. The future prospects of the HEF extension are also presented in Sec. 4, which are expected to enhance the opportunities of hadron physics at J-PARC. Finally, a summary is given in Sec. 5.

## 2 J-PARC Hadron Experimental Facility

### 2.1 Overview of J-PARC

### 2.2 Overview of J-PARC

The Japan Proton Accelerator Research Complex (J-PARC) is a multi-purpose accelerator facility located in Tokai village, Japan [4, 5]. The aims of J-PARC are to promote a variety of scientific research programs ranging from the basic science of particle, nuclear, atomic and condensed matter physics and life science to applications for industry use and future nuclear transmutation, using various types of high-intensity secondary beams of neutrinos, muons, pions, kaons, protons, neutrons, and their antiparticles, as shown in Fig. 2. The J-PARC accelerator consists of three high-intensity proton accelerators, as shown in Fig. 3: a 400 MeV linac, a 3 GeV rapid cycling synchrotron (RCS), and a

main ring synchrotron (MR). Both the RCS and MR have a three-fold symmetry, and circumferences of 348.3 m and 1567.5 m, respectively.

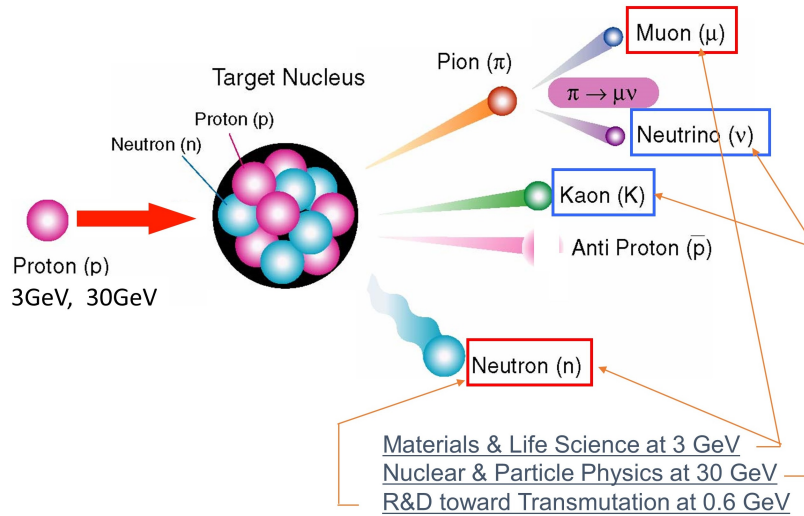


Figure 2: Multi purpose accelerator facility, J-PARC. A variety of particles produced by a high-intensity proton beam are provided as beams for a variety of experimental research on basic science to industrial applications. .

The linac is a beam injector to the RCS, which consists of a negative hydrogen ion source, a 3 MeV radio frequency quadrupole (RFQ), a 50 MeV drift tube linac (DTL), a 191 MeV separated-type DTL (SDTL), and a 400 MeV annular-ring coupled structure (ACS) [6]. At the linac, negative hydrogen ions instead of protons are accelerated up to 400 MeV because the charge-exchange injection scheme is adopted with a stripper foil at the RCS injection. The RCS, which is the world’s highest class of a high-power pulsed proton driver, accelerates the injected protons up to 3 GeV at a repetition rate of 25 Hz [7]. Most of the RCS beam pulses are delivered to the Material and Life Science Facility (MLF), while only a portion of the pulses are injected to the MR. Muon and neutron beams are available at the MLF, where beams are generated by colliding 3 GeV protons with carbon and mercury targets, respectively.

The protons injected from the RCS to the MR are accelerated up to 30 GeV, and delivered to the Neutrino Experimental Facility (NEF) and the Hadron Experimental Facility (HEF) with different extraction modes [8]. In the fast extraction mode (FX), all beam bunches are extracted within a one-turn time period to the NEF. Neutrino and anti-neutrino beams are used for the Tokai to Kamioka long-baseline neutrino oscillation experiment, T2K [9]. On the other hand, the beam is extracted to the HEF over several seconds in the slow extraction mode (SX). The uniform structure and low ripple noise of the slow extraction beam enables a wide variety of experiments to be performed, which generally requires the coincidence of several detectors to obtain the low-frequency occurrence events of interest among the large number of background interactions.

User operation was started in December 2008 at the MLF. In the MR, the beam was successfully accelerated to 30 GeV on December 23, 2008. The first beam was extracted to the HEF on February 23, 2009. Since then, the beam power has gradually increased by 536 kW at the RCS, ~ 500 kW at the MR-FX, and 51 kW at the MR-SX, as of the end of 2019. Now, further improvement of the beam power is proceeding and planned for each facility: a 1.2 MW equivalent test was successfully conducted with the RCS in 2018 for future ~ 1 MW operation at the MLF, and an upgrade of the MR main-magnet power supplies planned for 2021 will realize ~ 1 MW operation of the MR-FX and over

# J-PARC

## Japan Proton Accelerator Research Complex

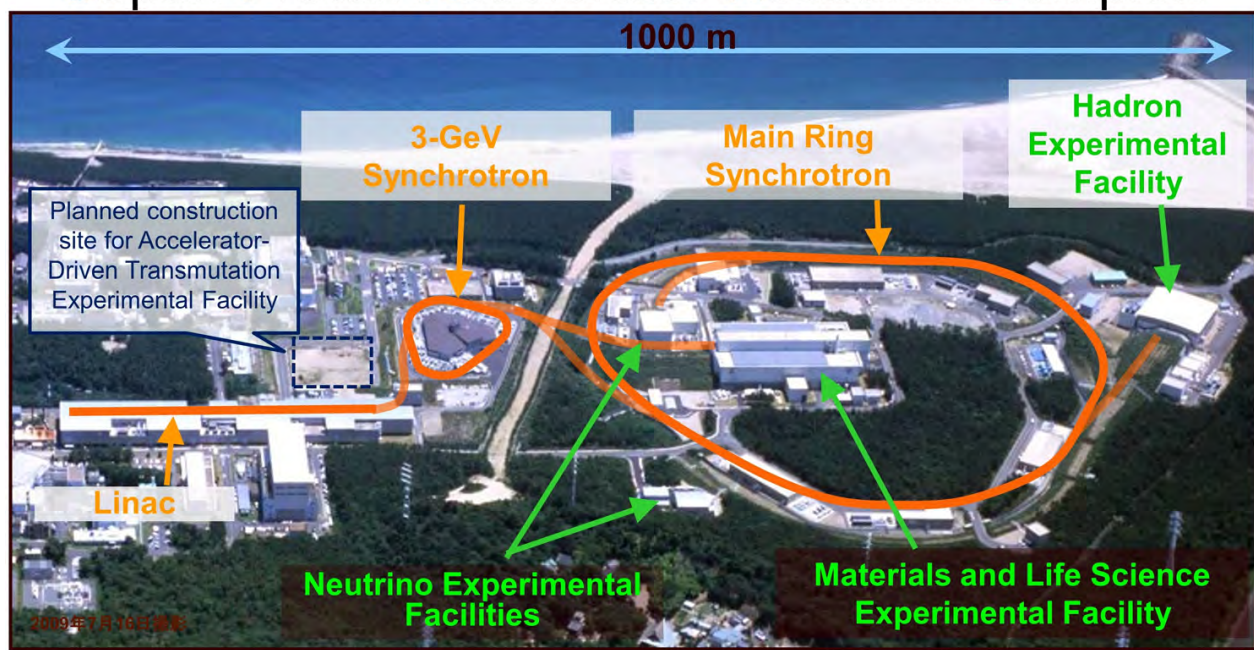


Figure 3: Aerial photograph of J-PARC. J-PARC consists of three high-intensity proton accelerators: linac, 3 GeV synchrotron and main ring synchrotron, and three experimental facilities, the Material and Life Science Facility, the Hadron Experimental Facility, and the Neutrino Experimental Facility. The construction of an accelerator-driven transmutation facility is planned.

100 kW operation of the MR-SX by operation with a higher repetition rate than that at the present.

## 2.3 Hadron Experimental Facility

The HEF focuses on particle and nuclear physics using the primary 30 GeV proton beam and secondary beams of pions, kaons, antiprotons, and muons. The 30 GeV proton beam slowly extracted from the MR is transported through a beam-switching yard (SY) to a secondary-particle production target (T1) located in the hadron experimental hall (HD-hall) with a width of 60 m and 56 m in length [10].

In the SY, which is  $\sim 200$  m long along the primary beamline, the primary beam is shifted up by 2.9 m to avoid beam halo originated from beam loss at the extraction devices. In the middle of the beam transport line, a beam branching device (a Lambertson magnet at present) is installed, so that a small fraction of the beam is transported to the new beamline under construction. The new beamline is branched to the high momentum (high-p) and COMET beamlines in the HD-hall.

Secondary beams produced at the T1 target are extracted from the primary beamline to three charged secondary beamlines (K1.8, K1.8BR, and K1.1) [11] and one neutral secondary beamline (KL). Figure. 4 shows a layout of the HD-hall and the south hall.

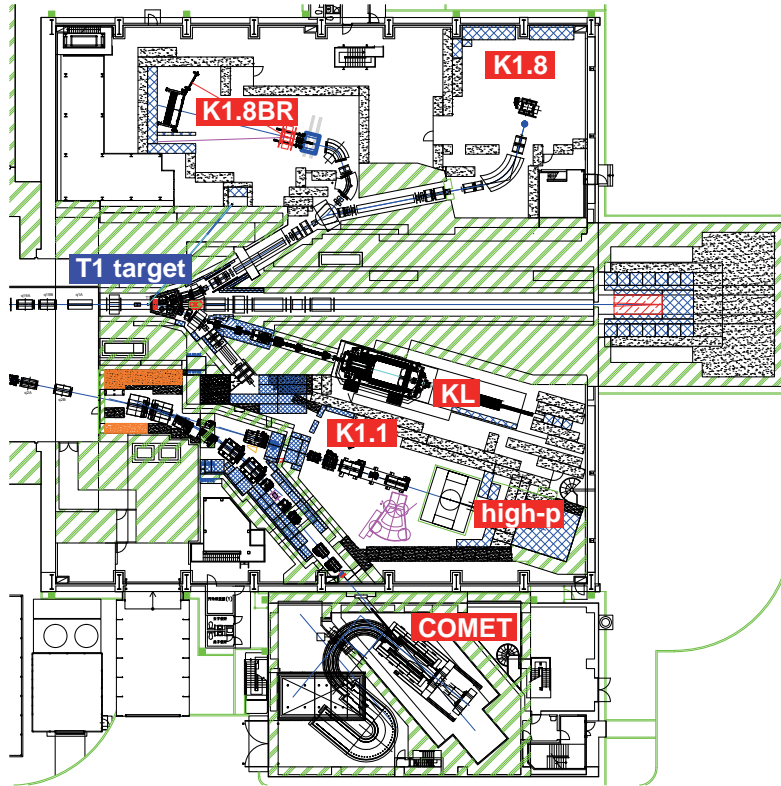


Figure 4: Layout of the hadron experimental (HD) hall and the south experimental hall. Three secondary beamlines, K1.8, K1.8BR, and KL, are in operation. The high-p beamline will be ready for operation in February 2020.

The K1.8 beamline is mainly designed for systematic studies of the double strangeness systems via the  $(K^-, K^+)$  reactions, such as a spectroscopic study of  $\Xi$  hypernuclei [12]. A maximum central momentum of  $\sim 2$  GeV/c is available at K1.8 because the cross section of the  $p(K^-, K^+)\Xi$  reaction is known to be a maximum at 1.8 GeV/c. The K1.8 beamline is composed of 4 sections: the front-end section, the first mass separation section, the second mass separation section, and the beam analyzer section. The total length of the beamline is 45.8 m. In the front-end section, secondary particles from the primary beam are extracted with  $6^\circ$ , where the kaon production cross section is expected to be a

maximum according to the Sanford-Wang parametrization [13]. Two 6 m long electrostatic separators (ES) are employed to separate kaons from pions in the first and second mass separation sections. The beam trajectory and momentum are determined in the beam analyzer section, called the K1.8 beam spectrometer, where point-to-point optics are realized between the entrance and exit of the section with a QDQQ magnet configuration. A set of tracking detectors and beam timing counters installed at the entrance and exit of the QDQQ provide precise beam information.

The K1.8BR beamline is a branch line of the K1.8 beamline designed as a short beamline to deliver a low-momentum mass-separated kaon beam of 0.7–1.1 GeV/ $c$ , of which the total length is 31.3 m. The cross sections of the quasi-elastic reactions of  $K^- N \rightarrow \bar{K} N$  are maximal around 1 GeV/ $c$ ; therefore, the K1.8BR beamline is suitable for experimental studies of the  $\bar{K} N$  interactions via the  $(K^-, N)$  reactions with light nuclear targets [14]. The beamline shares the upstream components of K1.8, *i.e.* the front-end section and the first mass separation section of K1.8. The beam is bent to the opposite side of K1.8 at the D magnet after the first mass separation section, and transported to the experimental target through a momentum analyzer section composed of QDQD magnets.

The KL beamline is a neutral secondary beamline used to search for the rare CP-violating kaon decay,  $K_L^0 \rightarrow \pi^0 \nu \bar{\nu}$  (the KOTO experiment) [15]. The beamline consists of a 1<sup>st</sup> collimator, a sweeping magnet, and a 2<sup>nd</sup> collimator. The  $K_L^0$  beam is extracted with 16° and transported to a detector system mainly composed of a CsI electromagnetic calorimeter and a charged-particle veto counter.

The K1.1 beamline is constructed on the opposite side of the K1.8 beamline. A maximum momentum of 1.1 GeV/ $c$  is available, where mainly precise measurements of  $\Lambda$  hypernuclei are conducted. The beamline consists of a front-end section, a mass-separation section with two stages of cross field type ES with 2 m of length, and a beam analyzer section with a DQQ magnet configuration. The total length of the beamline is 27.1 m. Experiments at K1.1 will be performed after the completion of the first stage experiments at the high-p beamline, by rebuilding the layout of the magnets and the experimental area at the south side of the HD-hall. This is due to interference of space between the high-p and the K1.1 beamlines.

The construction of the high-p beamline was completed in 2020 January. It will provide a primary 30 GeV proton beam with an intensity of up to  $\sim 10^{10}$  per pulse. The beam commissioning will start from March 2020. The beamline was originally designed to investigate the in-medium spectral change of vector mesons produced via the  $p + A$  reactions. The use of secondary high-momentum but mass-unseparated beams of pions, kaons, and antiprotons up to 20 GeV/ $c$  is also planned in the future by placing a thin production target at the branching point. Charmed baryon spectroscopy will be performed via the  $(\pi^-, D^{*-})$  reactions at  $\sim 20$  GeV/ $c$  to explore the effective degrees of freedom to describe hadrons. The COMET beamline at the south experimental hall under construction is dedicated to deliver 8 GeV protons in the bunched slow extraction mode for the experiment to search for  $\mu^-$  to  $e^-$  conversion, COMET [16].

As of April 2019, a beam power of 51 kW was achieved with a 2.0 s beam spill length in a 5.2 repetition cycle, which corresponds to  $5.4 \times 10^{13}$  protons per pulse. Up to the spring of 2019, the beam power was limited by the production target system composed of a gold target and an indirect water-cooling system [17]. To increase the beam power for the HEF, a new production target system, allowable to 95 kW, was installed in November 2019. A new target system up to >150 kW is also under development, which employs a directly-cooled rotating-target system.

### 3 Experiments at the J-PARC HEF

In this section, we describe details of individual experiments conducted at the HEF. Table 1 summarizes the current status of the experiments classified as “completed”, “ongoing”, “forthcoming”, and “planned”.

Table 1: Summary of the status of the experiments at the HEF described in this article.

	Experiment	Beamline	Beam particle	Status
E03	Measurement of X-rays from $\Xi$ -atom	K1.8	$K^-$	forthcoming
E05	Spectroscopic study of $\Xi$ -hypernucleus, $^{12}_{\Xi}\text{Be}$ , via the $^{12}\text{C}(K^-, K^+)$ reaction	K1.8	$K^-$	completed
E07	Systematic study of double strangeness system with an emulsion-counter hybrid method	K1.8	$K^-$	completed
E10	Production of neutron-rich $\Lambda$ -hypernuclei with the double charge-exchange reactions	K1.8	$\pi^-$	completed
E13	Gamma-ray spectroscopy of light hypernuclei	K1.8	$K^-$	completed
E15	A search for deeply-bound kaonic nuclear states by in-flight $^3\text{He}(K^-, n)$ reaction	K1.8BR	$K^-$	completed
E16	Electron pair spectrometer at the J-PARC 50-GeV PS to explore the chiral symmetry in QCD	high-p	$p$	ongoing
E19	High-resolution search for $\Theta^+$ pentaquark in $\pi^- p \rightarrow K^- X$ reactions	K1.8	$\pi^-$	completed
E26	Direct measurements of $\omega$ mass modification in $\Lambda(\pi^-, n)\omega$ reaction and $\omega \rightarrow \pi^0\gamma$ decays	K1.8	$\pi^-$	planned
E27	Search for a nuclear $\bar{K}$ bound state $K^- pp$ in the $d(\pi^+, K^+)$ reaction	K1.8	$\pi^+$	completed
E29	Study of in medium mass modification for the $\phi$ meson using $\phi$ meson bound state in nucleus	K1.8BR	$\bar{p}$	planned
E31	Spectroscopic study of hyperon resonances below $\bar{K}N$ threshold via the $(K^-, n)$ reaction on deuteron	K1.8BR	$K^-$	completed
E40	Measurement of the cross sections of $\Sigma p$ scatterings	K1.8	$\pi^\pm$	ongoing
E42	Search for $H$ -dibaryon with a large acceptance hyperon spectrometer	K1.8	$K^-$	forthcoming
E45	3-body hadronic reactions for new aspects of baryon spectroscopy	K1.8	$K^-$	forthcoming
E50	Charmed baryon spectroscopy via the $(\pi^-, D^{*-})$ reaction	high-p	$\pi^-$	planned
E57	Measurement of the strong interaction induced shift and width of the 1st state of kaonic deuterium at J-PARC	K1.8BR	$K^-$	forthcoming
E62	Precision spectroscopy of kaonic helium $3\ ^3d \rightarrow 2p$ X-rays	K1.8BR	$K^-$	completed
E63	Proposal of the 2nd stage of E13 experiment	K1.1	$K^-$	planned
E70	Proposal for the next E05 run with the $S$ -2 $S$ spectrometer	K1.8	$K^-$	forthcoming
E72	Search for a narrow $\Lambda^*$ resonance using the $p(K^-, \Lambda)\eta$ reaction with the hypTPC detector	K1.8BR	$K^-$	forthcoming

## 3.1 QCD Vacuum and Hadron Structure

Hadrons are the excitations of the QCD vacuum itself, which hold basic information regarding non-perturbative QCD. Precise spectroscopy of a nucleon resonance, *i.e.*, the spectroscopy of  $N^*$ , is known to be a way to access that information. However, most of the nucleon resonances have a large width, so that there is no easy way to extract the pole position of the nucleon resonance. Therefore, partial wave analysis (PWA) to obtain the pole position of the resonance is mandatory. The study of nuclear resonances has a long history, and precise data for  $\pi N$  interactions have already been accumulated. However, a high-quality data set, such as  $\pi N \rightarrow \pi\pi N$ , for the non-strangeness sector and  $\pi N \rightarrow KY$ , where  $Y$  represents a baryon with a strange quark, are still missing. These measurements will be a key to accessing non-perturbative QCD vacuum structure via the spectroscopy of nucleon resonances. An experimental program to accumulate these missing data is now in preparation at the J-PARC K1.8 beamline, referred to as the J-PARC E45 experiment.

QCD allows for the existence of a hadron with non-meson and non-baryon configurations, the so-called exotic hadron, such as the tetra-quark ( $qq\bar{q}\bar{q}$ ), pentaquark-baryon ( $qqqq\bar{q}$ ), dibaryon ( $qqqqqq$ ), and so forth. One of the critical missions for hadron physics is to clarify the existence of exotic hadrons and to identify their properties. The search for the pentaquark-baryon with strangeness = +1, *i.e.*,  $\Theta^+$ , which consists of  $uudd\bar{s}$ , was performed as the J-PARC E19 experiment. On the other hand, research to find one of the dibaryon states, the  $H$ -dibaryon, which consists of  $uuddss$ , is planned as the J-PARC E42 experiment.

Another question needs to be answered with respect to understanding the effective degrees of freedom (DoF) to describe a hadron itself. For ordinary mesons and baryons, especially for the ground state hadrons, constituent quarks are known to be reasonable degrees of freedom to describe their properties, such as mass and spin-parity. However, especially for excited baryons or mesons, the correlation between a quark pair, *i.e.*,  $qq$  inside the hadron, will be enhanced and those correlated quark pairs, which are referred to as a di-quark correlation, will be acting as DoF. One of the best ways to reveal the importance of a di-quark correlation is the spectroscopy of a baryon with a heavy quark, such as charmed baryons. An experiment to show the di-quark correlation in charmed baryons is planned at the J-PARC high momentum beamline as the J-PARC E50 experiment.

Another significant issue for hadron physics is the origin of hadron mass, *i.e.*, to reveal the mechanism whereby mass is acquired from the QCD vacuum [18]. In the sector of light quarks, the underlying mechanism is accompanied by the spontaneous breaking of chiral symmetry. Efforts to access the information experimentally are in progress internationally. Partial restoration of the chiral symmetry in a nucleus is expected theoretically, and such partial restoration will lead to a reduction of the magnitude of the condensate,  $|\langle\bar{q}q\rangle|$ . QCD sum rules connect hadron spectral functions to such condensates. Therefore, spectral functions of mesons in the nucleus could be modified [19, 20, 21, 22]. Precise measurement of the vector meson spectral functions, such as  $\rho$ ,  $\omega$  and  $\phi$  mesons, is under preparation as the J-PARC E16 experiment.

The other way to access information regarding the partial restoration of the chiral symmetry is to search for the meson-nuclear bound state, and determine its binding energy and decay width [23]. The existence of the meson-nuclear bound state indicates a reduction of the meson mass in nuclear media. Experiments to search for the meson nuclear bound state, especially for  $\omega$  and  $\phi$  mesons, have been proposed as the J-PARC E26 and E29 experiments.

Details of obtained and expected results for each experiment are reviewed in the following sections.

### 3.1.1 Search for the $\Theta^+$ penta-quark baryon

In 2003, the  $S = +1$  baryon was observed via the  $\gamma n \rightarrow K^- K^+ n$  reaction at the SPring-8/LEPS experiment [24]. The results showed a peak structure in the  $K^+n$  invariant mass spectrum at 1535 MeV/ $c^2$ . The obtained width is surprisingly narrow; it is less than 25 MeV/ $c^2$ , which is consistent with

the experimental resolution. The quantum number of the observed baryon can be identified as  $S=+1$ , and the width is much less than an ordinary nucleon resonance, which is of the order of  $100 \text{ MeV}/c^2$ . Thus the observed baryon is expected to be a candidate for an exotic hadron, *i.e.*, a pentaquark baryon with one anti-strange quark ( $uudd\bar{s}$ ). The baryon was named  $\Theta^+$ , and it is expected to be one of the lightest anti-decuplet members of the set of baryons with four quarks and one anti-quark, which was predicted by D. Diakono, V. Petrov, and M. Polyakov in 1997 [25]. In 2009, the SPring-8/LEPS collaboration presented a new result for  $\Theta^+$  via the  $\gamma d \rightarrow K^+ K^- pn$  reaction with high statistics [26]. They confirmed the previous result, namely, the existence of the peak structure in the  $K^+ n$  invariant mass spectrum at the same position,  $M_{K^+ n} = 1535 \text{ MeV}/c^2$ . Intensive studies to confirm the existence of  $\Theta^+$  have been performed in photoproduction at Jefferson Lab [27], with proton–proton collisions at COSY [28], and in high energy collider experiments [29, 30]. However, no clear evidence has been reported. Results from KEK 12 GeV proton synchrotron (KEK-PS) E522 show a bump structure at  $1530.6^{+2.2}_{-1.9}(\text{stat.})^{+1.9}_{-1.3}(\text{syst.}) \text{ MeV}$  via the  $\pi^- p \rightarrow K^- X$  reaction, for an incident pion momentum of  $1.92 \text{ GeV}/c$ , even though the statistical significance for the measurement was only  $2.5 - 2.7\sigma$  [31]. Thus it is clear that a new experiment with a hadron beam is required to conclude whether the  $\Theta^+$  baryon exists.

Figure 5 shows diagrams for  $\Theta^+$  production via the  $(\pi^-, K^-)$  reaction. To identify  $\Theta^+$  production in the J-PARC E19 experiment, missing mass spectroscopy was performed by high precision analysis of the incident  $\pi^-$  and out-going  $K^-$  momenta using the high-resolution beamline spectrometer and the superconducting kaon spectrometer (SKS) placed on the K1.8 beamline, respectively. The experiment collected data for two different incident  $\pi$  momenta settings,  $1.92 \text{ GeV}/c$  and  $2.01 \text{ GeV}/c$ , to investigate the excitation function of  $\Theta^+$  production for this production channel. The achieved missing mass resolution for  $\Theta^+$  production was found to be  $1.72 \text{ MeV}$  and  $2.13 \text{ (FWHM)}$ , for incident pion momenta of  $1.92 \text{ GeV}/c$  and  $2.01 \text{ GeV}/c$ , respectively.

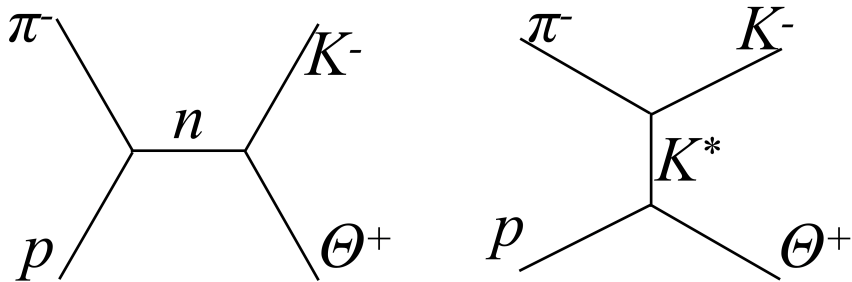


Figure 5: Feynman diagram for  $\Theta^+$  production via  $(\pi^-, K^-)$  reaction.

Figure 6 shows the obtained results from the E19 experiment [32, 33]. The right and left figures show the missing mass spectra reconstructed via the  $p(\pi^-, K^-)$  reaction with incident pion momenta of  $1.92 \text{ GeV}/c$  and  $2.01 \text{ GeV}/c$ , respectively. No clear peak structure was observed around the expected  $\Theta^+$  mass region for either momentum setting.

The E19 experiment also determined the upper limit of the production cross section of  $\Theta^+$  for this reaction, as summarized in Figure 7. The obtained upper limit is  $0.28 \mu\text{b}/\text{sr}$  at 90% confidence level (CL) in the mass region  $1.510$  to  $1.550 \text{ GeV}$  for both  $1.92$  and  $2.01 \text{ GeV}/c$ , which is an order of

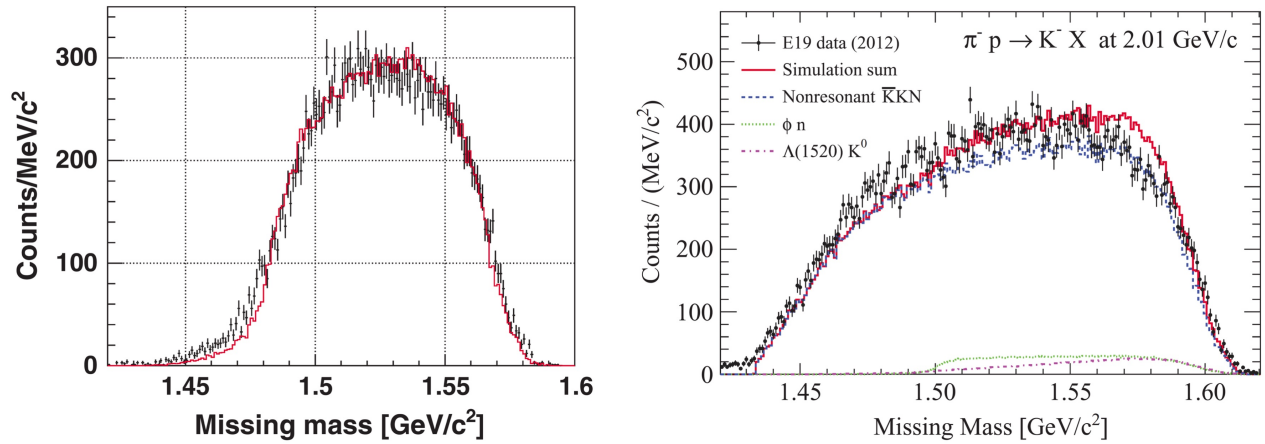


Figure 6: Missing mass spectra of  $\pi^- p \rightarrow K^- X$  reaction at 1.92 GeV/c (left) and 2.01 GeV/c (right). The red lines show simulation results for both figures. No clear peak structure is seen around the mass of  $\Theta^+$ ,  $M \sim 1530$  MeV/ $c^2$ . The figures are taken from Ref. [32] (left) and Ref. [33] (right).

magnitude lower than the previous E522 result of  $2.9 \mu\text{b}/\text{sr}$ . The decay width at the 90% CL upper limit was also evaluated and derived to be less than 0.36 and 1.9 MeV for the assumed spin-parities of the  $\Theta^+$  of  $1/2^+$  and  $1/2^-$ , respectively, by combining the theoretical calculations using the effective Lagrangian.

### 3.1.2 Search for the $H$ dibaryon

In 1977, R.L. Jaffe predicted the existence of a hadron with six quarks including two strange quarks, as a compact object [34]. The object was named  $H$ -dibaryon.

Recently, lattice QCD calculations have shown strong evidence for the existence of  $H$ -dibaryon near and above the double  $\Lambda$  threshold region [35, 36]. Thus, a new experimental program with high statistics and high precision is necessary. Many experimental efforts to find the  $H$ -dibaryon have been performed, including  $K^-$  induced fixed-target experiments and collider experiments. However, no positive results have been reported to date apart from the KEK-PS E224 [37] and E522 [38] experiments. The E224/E522 experiments measured the invariant mass spectrum of two  $\Lambda$ s in the  $(K^-, K^+)$  reaction on a carbon target and found a peak structure near the double  $\Lambda$  threshold. However, the significance of the signal is very poor due to low statistics. Therefore, the experiment could not conclude the existence of  $H$ -dibaryon from the data.

A new experiment to search for the  $H$ -dibaryon is under preparation as the J-PARC E42 experiment [39]. A schematic view of the E42 spectrometer (Hyperon Spectrometer) is shown in Fig. 8. The experiment will be performed at the K1.8 beamline with a newly installed superconducting Helmholtz magnet with a large time projection chamber (HypTPC). A high intensity  $K^-$  beam transported by the K1.8 beamline spectrometer is focused on a diamond target where two  $\Lambda$ s will be produced via the  $(K^-, K^+)$  reaction at 1.8 GeV/c. The outgoing  $K^+$  will be detected and identified by the scattered particle KURAMA spectrometer. The KURAMA spectrometer consists of a large dipole magnet together with tracking chambers and a time-of-flight (ToF) wall to determine the particle species. Some fraction of the interaction may produce  $H$ -dibaryons, which immediately decay into two  $\Lambda$ s. The Hyperon Spectrometer will reconstruct those two  $\Lambda$ s by detecting its decaying particles, *i.e.*, two  $\pi^-$ s and two protons.

The expected double  $\Lambda$  invariant mass resolution is  $1.5$  MeV/ $c^2$  at the  $\Xi N$  mass threshold. 10,000  $\Lambda\Lambda$  events will be accumulated over a data gathering period of 33 days, together with 1440  $H$ -dibaryon signals. These statistics are about 120 times higher than in the previous E522 experiment.

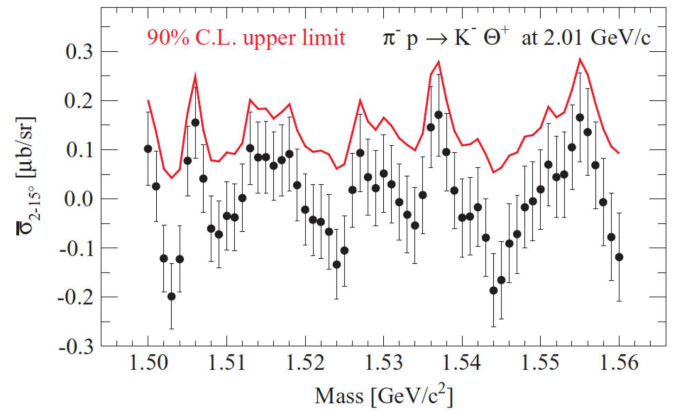
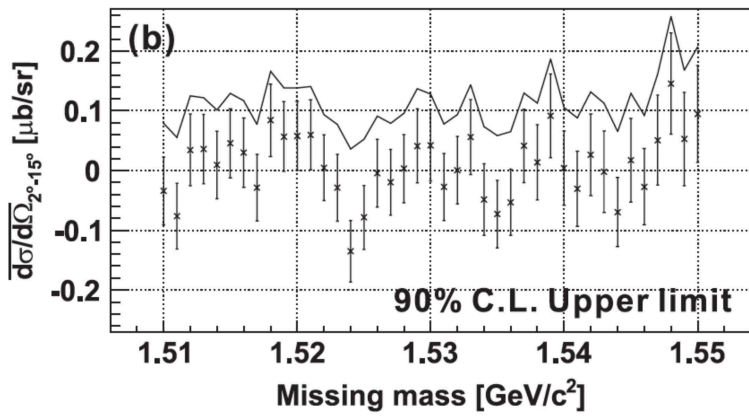


Figure 7: Production cross section of  $\Theta^+$  as a function of its mass for incident pion beam momenta of 1.92 GeV/c (Left) and 2.01 GeV/c (right). The line indicates the upper limit of the production cross section at the 90% confidence level. The figures are taken from Ref. [32] (left) and Ref. [33] (right).

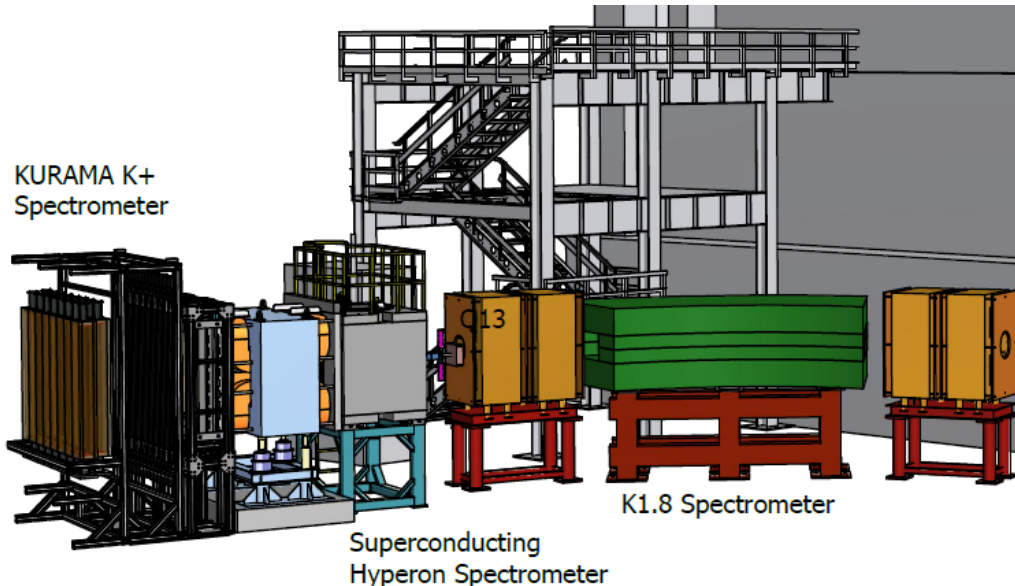


Figure 8: Schematic view of the E42 detector setup. The Hyperon Spectrometer consists of a superconducting Helmholtz-type magnet and a time projection chamber (HypTPC) with a KURAMA spectrometer [40, 41].

### 3.1.3 Detailed investigations of nucleon resonances

Due to the non-perturbative nature of the QCD in the low energy regime, the QCD vacuum structure shows a complex aspect. It is known that a baryon is an excitation of the QCD vacuum. Thus, one way to reveal the QCD vacuum structure is to investigate the baryon spectrum, especially for excited state baryons.

Spectroscopic studies of baryons, especially for nucleon resonances, have gathered considerable data on  $\gamma N \rightarrow \pi N$  and  $\pi N \rightarrow \pi N$ , and intensive analyses of the data have been performed. A clear description of the nucleon resonances has been developed, though as yet no precise details on nucleon resonances with masses more than  $1.6 \text{ GeV}/c^2$ , which is above the  $N\pi\pi$  threshold, have been obtained because of the lack of data available. Therefore, high statistics and high-quality data are required to improve our knowledge of nucleon resonances for  $M > 1.6 \text{ GeV}/c^2$ .

The J-PARC E45 experiment [42] will accumulate high statistics and high-quality data on  $\pi N \rightarrow \pi\pi N$  and  $\pi N \rightarrow KY$  reactions. The experiment will be performed at the K1.8 beamline using the E42 spectrometer (Hyperon Spectrometer) with a large acceptance. This will allow a partial wave analysis to extract detailed resonance parameters.

### 3.1.4 Hyperon resonance near the $\Lambda\eta$ threshold

A new hyperon resonance has been observed in the invariant mass of the  $pK^-$  spectrum [43] in the Dalitz plot analysis of  $\Lambda_c \rightarrow pK^-\pi^+$  [44]. The mass of the resonance was found to be 1663 MeV, and the width of the resonance was extremely narrow, about 10 MeV. Because no such narrow resonance has been observed to date [45], the newly found resonance might be a candidate for an exotic  $\Lambda^*$  resonance.

On the other hand, based on old data presented by the Crystal Ball collaboration for the differential cross section for the  $K^-p \rightarrow \Lambda\eta$  reaction [46], two theoretical groups have indicated the existence of a new  $\Lambda^*$  resonance around this mass region. The ANL-Osaka-KEK group claimed, based on a partial wave analysis, the existence of a narrow  $\Lambda^*$  resonance at  $1671_{-8}^{+2}$  MeV with  $J^P = 3/2^+$  [47, 48]. Unfortunately, a lack of information regarding the polarization observables in the data of the Crystal Ball collaboration means that the new  $\Lambda^*$  cannot be confirmed unambiguously. On the other hand,

B.C. Liu and J.J. Xie concluded, based on their reaction model approach, the presence of a narrow  $\Lambda^*$  resonance at 1669 MeV with  $J^P = 3/2^-$  [49, 50]. Therefore, the properties of the resonance are still undetermined.

The existence of the  $\Lambda^*$ , which strongly coupled with  $\eta\Lambda$ , needs to be identified together with its spin and parity to answer the question of whether new narrow  $\Lambda^*$  resonance exists or not. The E72 experiment aims to search for the  $\Lambda^*$  resonance with  $J = 3/2$  near the  $\Lambda\eta$  threshold via the  $p(K^-, \Lambda)\eta$  reaction at around 735 MeV/c [51]. A detailed shape study of the differential cross section measurements in a narrow center-of-mass region around 1669 MeV will allow us to determine the spin of the resonance. Polarization measurements can also be used for the parity determination. The experiment will be performed at the K1.8BR or K1.1 beamline with a large solid angle detector, HypTPC. The experiment is under preparation.

### 3.1.5 Charmed baryon spectroscopy

Understanding the effective degree of freedom to describe a hadron is a fundamental question in hadron physics. Previously, a model based on the “constituent quark” was used to describe the properties of a ground state hadron, such as the mass and magnetic moment. However, the model fails to reproduce excited state hadrons. A possible approach to address this discrepancy is to introduce a new degree of freedom, correlated di-quarks, inside the excited hadron. Interactions between quarks, especially the color-magnetic interaction inside a hadron, can be written as follows:

$$V_{CMI} \sim \frac{\alpha_s}{m_i m_j} (\lambda_i \cdot \lambda_j) (\vec{\sigma}_i \cdot \vec{\sigma}_j), \quad (1)$$

where  $\lambda$  and  $\sigma$  are the color and spin of the quarks, respectively.

The equation shows that the strength of the interaction between two quarks is proportional to the inverse of the quarks’ masses. For a baryon, we use the Jacobi coordinate system to solve the three-body equation. One coordinate is  $\lambda$  and the other is  $\rho$ . Figure 9 illustrates this coordinate systems. For an excited nucleon,  $N^*$ , where the three constituent quarks (written as qqq) have almost the same masses, we cannot distinguish the  $\rho$  and  $\lambda$  directions. However, let us introduce a heavy-quark Q in a baryon, such as a charm quark or even a strange quark, to form a “qqQ” system. In such a system, the color-magnetic interaction for “qq” is naturally stronger than the interaction for “qQ.” Therefore, a strong “qq” correlation appears inside a baryon. The next question is how the effect of the di-quark correlation appears in the observables. The answer is illustrated in Figure 9. As we mentioned, for a  $N^*(qqq)$ , it is not possible to separate the  $\lambda$  and  $\rho$  coordinates. Thus, the excitation of the  $\rho$  and  $\lambda$  directions cannot be distinguished and thus the energy level of the excitation in the  $\rho$  and  $\lambda$  directions is degenerate. On the other hand, for a baryon with one heavy quark, the  $\rho$  and  $\lambda$  coordinates can be defined. Let us assume the coordinate between “qq” is  $\rho$  and “Q–qq” is  $\lambda$ . In this case, an excitation of the  $\lambda$  direction, which corresponds to a rotation of two light quarks around one heavy quark, is easier than a  $\rho$  mode excitation, where two light quarks are rotated. This leads to a separation of the  $\rho$  mode and the  $\lambda$  mode in baryon mass spectrum. Moreover, as shown in Figure 10, an excited baryon in a  $\rho$  or  $\lambda$  mode is expected to have favored decay channels. For example, light-meson ( $\pi$ ) – heavy-baryon ( $Y_c$ ) decay will be dominant for a  $\rho$  mode excited charmed baryon. On the other hand, a heavy-meson (D) and light-baryon (N) decay mode will be favored for  $\lambda$  mode excited baryons. In addition, a systematic comparison between charmed baryon (baryon with one charm quark) and hyperon (baryon with one strange quark) mass spectra, including the decay modes, will confirm whether the di-quark correlation in hadrons exists.

The main goal of the J-PARC E50 experiment is to obtain evidence for di-quark correlation in baryons via charmed baryon spectroscopy [53]. The E50 experiment focuses on charmed baryon production with t-channel  $D^*$  exchange in the  $p(\pi^-, D^{*-})Y_c^*$  reaction up to 20 GeV/c, where  $Y_c^*$  denotes an excited charmed baryon. A typical production diagram is shown in Fig. 11.

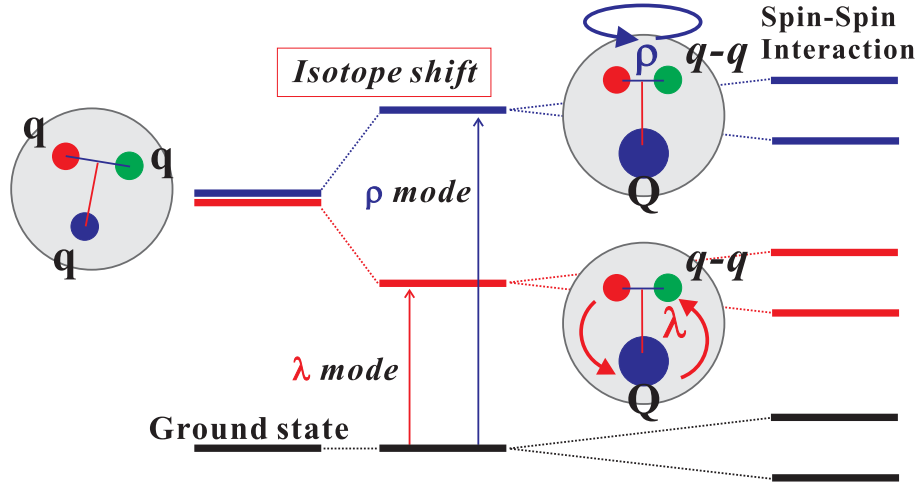


Figure 9: Schematic view of the  $\rho$  and  $\lambda$  excitations in  $N^*$  and  $Y_c^*$ . Degeneracy of the energy level for the  $\rho$  and  $\lambda$  mode excitations is expected in nucleon resonances ( $N^*$ ), while those levels are expected to be separate in excited charmed baryons. The figure is taken from Ref. [52].

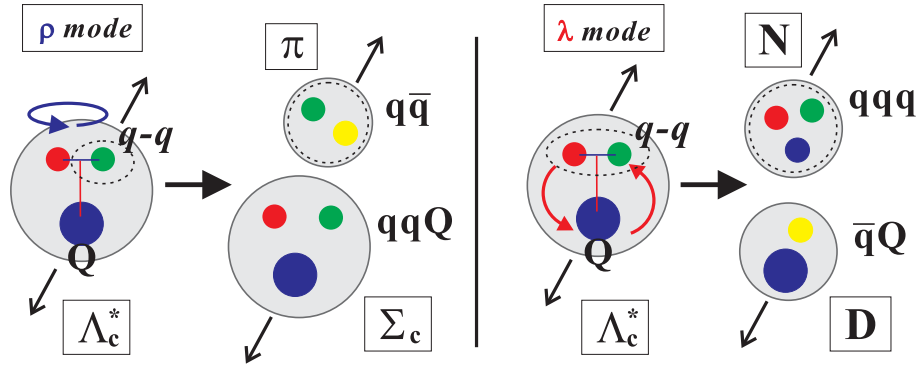


Figure 10: Expected decay channel for  $Y_c^*$ . A charmed baryon with a  $\rho$  mode excitation will favorably decay to a charmed baryon and a light meson, while a decay with a nucleon and charmed meson will be enhanced in the  $\lambda$  mode excited charmed baryon. The figure is taken from Ref. [52].

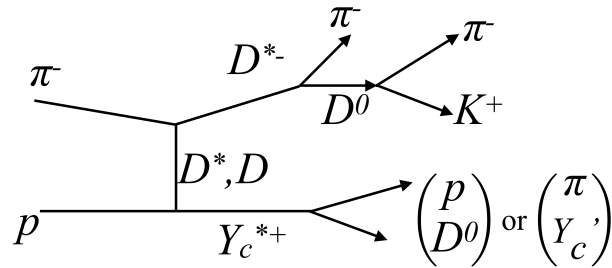


Figure 11: Feynman diagram for charmed baryon production via the  $(\pi^-, D^{*-})$  reaction. The production of a charmed baryon can be identified via missing mass analysis by detecting forward going  $D^*$  mesons.

The key to the experiment is a high momentum resolution beamline spectrometer, and a large acceptance and high precision decay particle spectrometer. A schematic view of the decay particle spectrometer is shown in Fig. 12. The spectrometer consists of a large-gap dipole magnet, wire chambers, and high-resolution ToF detectors to identify outgoing  $D^*$  mesons and decay products of charmed baryons.

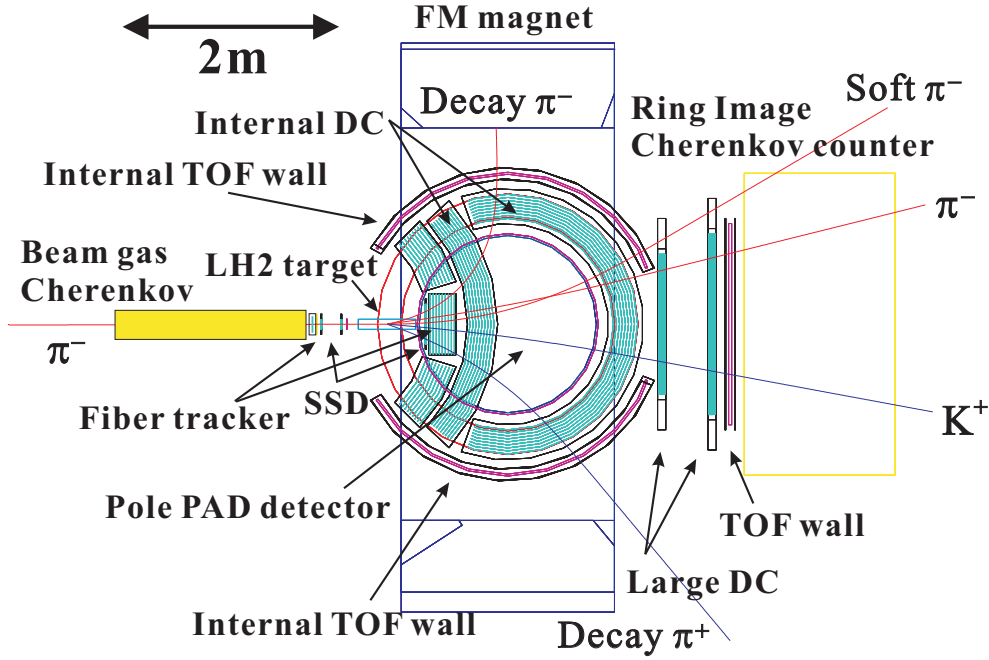


Figure 12: Schematic view of the E50 spectrometer. The figure is taken from Ref. [52].

and high-resolution ToF detectors to identify outgoing  $D^*$  mesons and decay products of charmed baryons.

Figure 13 shows the expected charmed baryon spectrum for one hundred days of beam time. If the strong di-quark correlation exists as expected, a two-peak structure which corresponds to the spin doublets (the  $\rho$  and  $\lambda$  mode excited charmed baryons) will appear in the spectrum [54].

On the other hand, we can access the structure of an excited hyperon and explore the existence of the di-quark correlation in it by using  $K^-$  as beam particles instead of  $\pi^-$ . Due to the relatively high production cross section of excited hyperons compared with charmed baryons, hyperon spectroscopy will be an essential upgrade to the E50 experiment. We may find evidence for the existence of di-quark correlation by hyperon spectroscopy, which can be confirmed by charmed baryon spectroscopy.

The beamline construction was completed during 2019, and a secondary target will be installed at the branch point of the high-momentum beamline to realize high-momentum  $\pi^-$  and  $K^-$  beams in the HEF. The detector construction for charmed baryon spectroscopy is underway.

### 3.1.6 Precise measurement of the spectral function of vector mesons via di-electrons

QCD sum rules establish a link between hadron masses and spontaneous chiral symmetry breaking in the QCD vacuum. One way to confirm this is to investigate meson properties in nuclear matter, where the symmetry is expected to be partially restored. The vector mesons,  $\rho$ ,  $\omega$  and  $\phi$ , have attracted attention as powerful probes to investigate the spectral function in nuclear matter for two reasons. The first is that vector mesons have di-lepton decay channels,  $e^+e^-$  and  $\mu^+\mu^-$ , which do not cause spectral shape distortion via the strong interaction. The second is the narrow natural width of the order of 10 MeV, which makes it relatively easy to identify.

To date, the KEK-PS E325 experiment has discovered a significant modification of the spectral function of  $\rho$ ,  $\omega$  and  $\phi$  mesons in a nucleus via di-electron spectrum [56, 57]. On the other hand, the

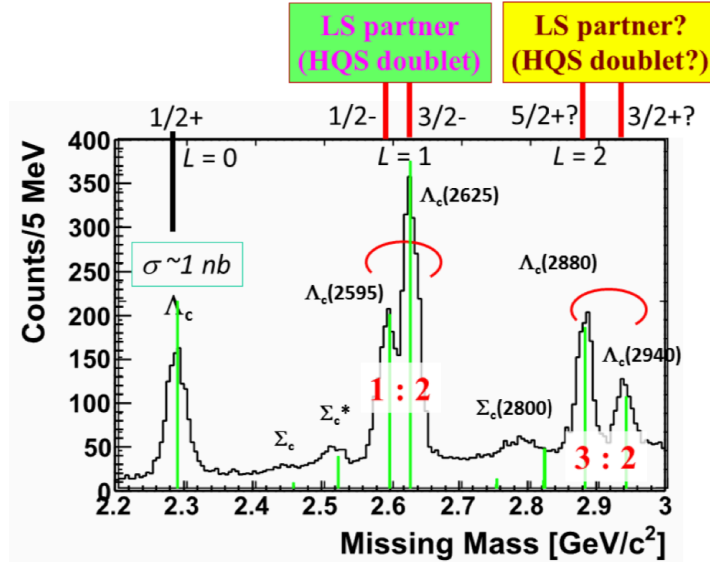


Figure 13: Expected missing mass spectrum simulated with the known charmed baryon states. The detector resolutions are included for this simulation. The production cross section for a charmed baryon is assumed to be  $\sigma(\Lambda_c^+) = 1$  nb, which can be evaluated with a theoretical calculation [55]. Clear spin double states,  $\Lambda_c(2595)$  and  $\Lambda_c(2625)$ , and  $\Lambda_c(2880)$  and  $\Lambda_c(2940)$ , are seen. For this simulation, the spin-parity of  $\Lambda_c(2940)$  is assumed to be  $3/2^+$ . The figure is taken from Ref. [54].

CLAS experiment at Jefferson Lab observed width broadening of the vector meson spectral function in heavier target nuclei (Fe, Ti) without shifting of the pole position [58]. The difference between the E325 experiment and the CLAS experiment may be due to the production mechanism of the vector mesons, namely hadron-production and photoproduction. Unfortunately, both experiments have only a limited amount of data. Therefore, new high statistics data are required to make detailed investigations on the spectral functions of vector mesons in nuclear matter.

The J-PARC E16 experiment is the successor to the previous E325 experiment, with a significant detector upgrade incorporating acceptance for a high-intensity beam but maintaining a high mass resolution [59]. The main goal of the E16 experiment is to accumulate a hundred times more statistics than the previous E325 experiment. The new data will allow access to the spectral functions of vector mesons as a function of their momenta [60, 61]. This will subsequently allow measurements of the dispersion relation of vector mesons in nuclear matter. Figure 14 shows a schematic view of the E16 spectrometer. The spectrometer consists of four major subsystems. The first is a high precision and high rate tracking detector with a gas electron multiplier (GEM) [63], with a low material budget to reduce the external radiative effect and multiple scattering of electrons and positrons, which distort the reconstructed mass spectrum. The GEM tracker is used to compensate for the expected background hit rate of up to  $5 \text{ kHz/mm}^2$  [64]. The second system is a hadron blind detector (HBD), which detects the electrons using Cherenkov light in  $\text{CF}_4$  gas, and does not respond to pions [65, 66]. The third is a lead-glass calorimeter (LG) for identifying electrons together with HBD signals. The pion misidentification probabilities of the HBD and LG are estimated to be 0.6% and 5%, respectively [67]. Finally, a layer of silicon strip detector (SSD) is introduced to reduce the possible effects of accidental hits due to the 10-MHz interaction rate at the target.

The phase one experiment, with part of the detector, will be performed in 2020, followed by experiments with the full detector setup in the near future.

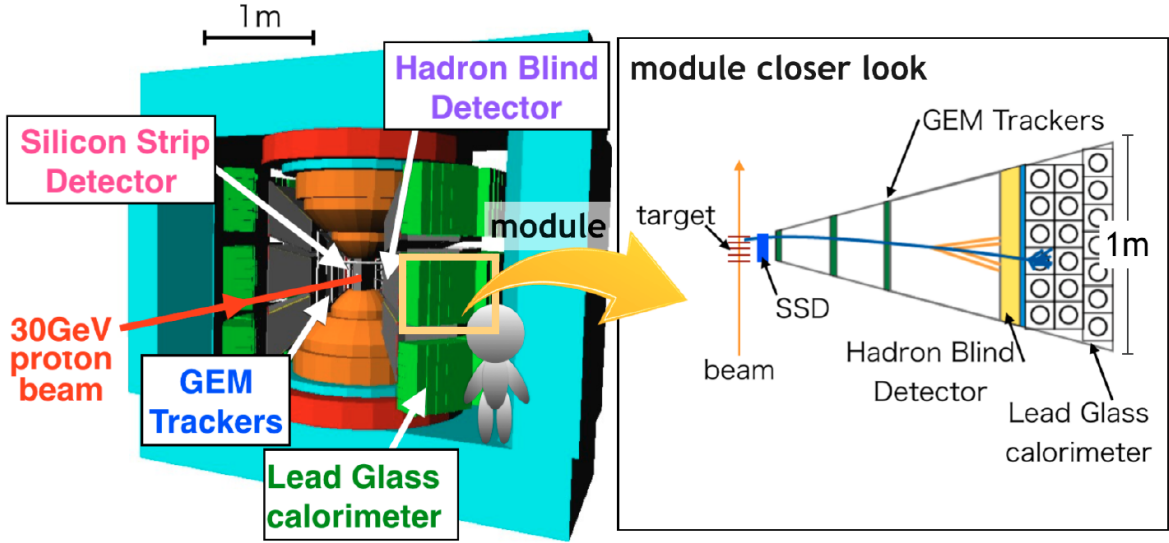


Figure 14: Schematic view of the E16 spectrometer. The figure is taken from Ref. [62]

### 3.1.7 Search for vector-meson nuclear bound states

As we discussed in the previous section, the mass of the hadron is strongly correlated with the expectation value of the chiral condensation,  $\langle \bar{q}q \rangle$ , in the environment where the hadron exists. The value of  $\langle \bar{q}q \rangle$  is expected to be reduced as a function of the nuclear matter density. Thus, the mass of a hadron, such as a vector meson, is expected to be reduced inside the nucleus. The mass reduction can be considered to indicate the existence of an attractive force between the vector meson and nuclear matter, raising the issue as to whether vector meson nuclear-bound states exist.

The J-PARC E26 experiment is planned to be performed at the J-PARC K1.8 beamline, in an effort to search for the  $\omega$  meson bound state [68]. Figure 15 shows a schematic view of the measurement. The  $\omega$  meson will be produced at a proton in the nucleus via the  $p(\pi^-, n)\omega$  reaction. Neutron emission in the beam direction (*i.e.*,  $0^\circ$ ) will be required for this experiment. In this situation, the direction of the produced  $\omega$  meson will be the backward direction in the center-of-mass frame, *i.e.*, a low momentum  $\omega$  meson in the laboratory frame will be produced. The typical momentum produced in this kinematics is  $\sim 100$  MeV/ $c$ . If the  $\omega$ -nucleus interaction is strong enough, a  $\omega$  meson nuclear-bound state will be formed. Soon after the  $\omega$ -meson bound state is formed, some fraction of  $\omega$ , which remains inside the nuclear matter, will decay via the  $\omega \rightarrow \pi^0\gamma$  mode. The invariant mass of  $\pi^0\gamma$  from the  $\omega$  meson will contain information on the  $\omega$  mass in the nucleus, which is related to chiral condensation in the nucleus. The E26 experiment can identify the meson nucleus bound state via missing mass analysis and measurements of the spectral function of the  $\omega$  meson via the invariant mass reconstruction by its decay products, simultaneously.

The J-PARC E29 experiment will search for  $\phi$  meson bound nuclei [69]. The E29 experiment will focus on the  $\bar{p}p \rightarrow \phi\phi$  reaction as a source for producing  $\phi$  mesons in nuclei. An advantage of using this reaction as an elementary process is that double  $\phi$  meson production is the dominant channel for the double  $\bar{s}s$  pair production around the production threshold, where the corresponding  $\bar{p}$  beam momentum will be  $\sim 1.0$  GeV/ $c$  [70]. Thus, detecting  $\phi$  mesons in the reaction automatically assures that another  $\phi$  meson has been produced. Moreover, if we require the production direction of one  $\phi$  meson to be in the incoming beam direction, the momentum of the other  $\phi$  in the laboratory frame will be  $\sim 200$  MeV/ $c$ . This momentum is comparable with the Fermi momentum in the nucleus. Therefore, the probability of a  $\phi$  meson sticking in the nucleus will be enhanced if the interaction between  $\phi$  meson and nucleus is sufficiently strong.

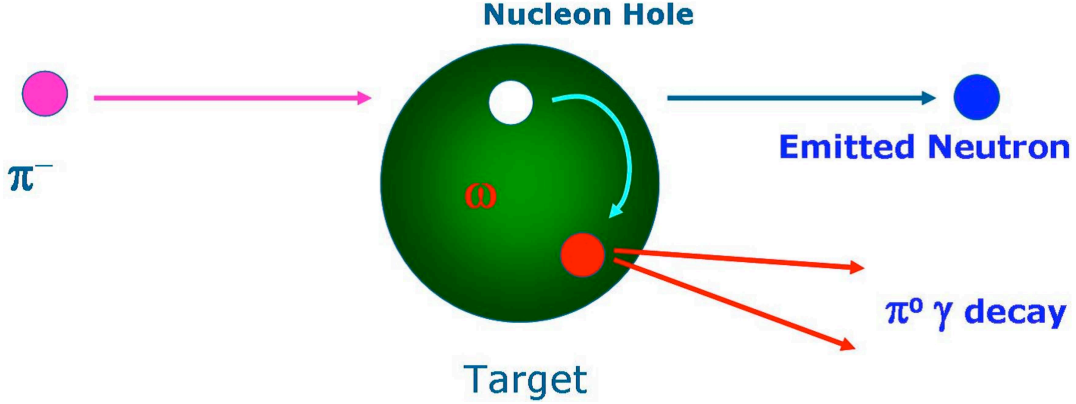


Figure 15: Schematic view of the production mechanism for the  $\omega$  meson nucleus bound state.

Figure 16 shows a schematic view of the process of searching for the  $\phi$  meson bound nucleus. The experiment is planned to be performed at the K1.8BR beamline. A high intensity  $\bar{p}$  beam will impact a carbon target and the  $\bar{p}p \rightarrow \phi\phi$  reaction will occur in the nucleus. A  $\phi$  meson will be ejected in the forward direction and a residual nucleus will capture the other  $\phi$  meson by a strong interaction, forming a  $\phi$  meson nuclear-bound state. Soon after the  $\phi$  meson nuclear-bound state formation, the nucleus will absorb the bound  $\phi$  meson via the  $\phi p \rightarrow K^+\Lambda$  reaction in the nucleus.

Formation of a  $\phi$ -meson bound nucleus can be identified by missing mass analysis via the forward emitted  $\phi$  meson. In addition, the existence of a  $\bar{s}s$  pair in the residual nucleus is assured by the detection of  $\Lambda$  from the target. As discussed above, the double  $\phi$  meson production is dominant in double strange quark pair production. Thus the required  $\Lambda$  is already good evidence for the existence of a  $\phi$  meson in the nucleus.

### 3.2 Antikaon-Nucleon Interaction

The meson-baryon interactions close to the mass thresholds provide crucial information on the interplay between spontaneous and explicit chiral symmetry breaking. Among meson-baryon interactions, the antikaon-nucleon ( $\bar{K}N$ ) interaction is an important probe to understand this important aspect of low-energy QCD. The  $\bar{K}N$  interaction in the  $I = 0$  channel is known to be strongly attractive, which has been revealed from extensive measurements of anti-kaonic hydrogen atoms [71, 72, 73] and low-energy  $\bar{K}N$  scattering [74].

From the point of view of this strong interaction between the antikaon and nucleus at the low-energy limit, kaonic atoms in which an electron is replaced by a  $K^-$  meson have been well studied in precise experiments of characteristic X-ray spectroscopy. The effects of strong interaction can be measured as a level shift from the binding energy calculated by only the electromagnetic interaction, and the broadening width due to absorption of the kaon by the nucleus. Information on the  $\bar{K}$ -nucleus potential can be extracted using the comprehensive data set of the shifts and widths obtained by the kaonic atom

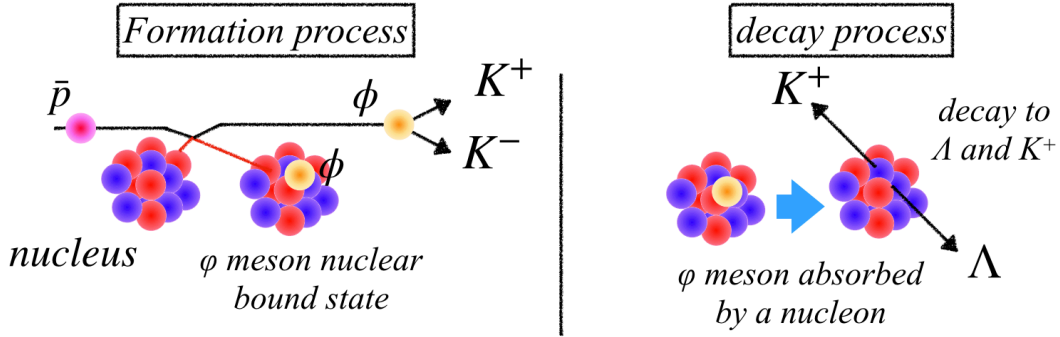


Figure 16: Schematic view of the production mechanism for the  $\phi$  meson nucleus bound state.

measurements from lithium (Li) to uranium (U) with density dependent optical potentials. However, the obtained  $\bar{K}$ -nucleus potential still remains controversial; the two major theoretical approaches with phenomenological models and chiral unitary models have provided conflicting results. With a view to clarify this controversial situation, in the J-PARC E62 experiment, high-precision spectroscopy of the isotope shift between the kaonic- $^3\text{He}$  and kaonic- $^4\text{He}$   $2p$  states was performed using a superconducting transition-edge-sensor (TES) microcalorimeter with resolution one order of magnitude better than conventional semi-conductor detectors.

The discrepancy of the calculated  $\bar{K}$ -nucleus potential is closely related to the different approach to calculations of the most essential  $\bar{K}N$  interaction. Extensive efforts have revealed the  $\bar{K}N$  interaction to be strongly attractive in the  $I = 0$  channel, and now the  $K^-p$  scattering amplitude in the low energy region has been precisely obtained from the results of SIDDHARTA at DAΦNE [73] and from theoretical calculations based on this measurement [75, 76, 77]. To determine the isospin dependent  $\bar{K}N$  scattering length, which is the most important but missing information in the  $\bar{K}N$  interaction field, kaonic deuterium X-ray measurements have now been launched as the J-PARC E57 experiment.

However, due to the presence of the  $\Lambda(1405)$  state located just below the  $\bar{K} + N$  mass threshold as shown in Fig. 17, theoretical investigations of the  $\bar{K}N$  interaction are very complicated and thus difficult. The  $\Lambda(1405)$  state is still an unclear state because it cannot be described by simple constituent quark models as an ordinary three-quark state [1]; therefore, there is a long-standing discussion on the interpretation of the  $\Lambda(1405)$  state, such as a meson-baryon ( $\bar{K}N$ ) quasi-bound state [78] or other exotic states such as a pentaquark baryon [79, 80]. Among the interpretations of the  $\Lambda(1405)$  state, the meson-baryon scenario is widely supported because the  $\Lambda(1405)$  state can be naturally described as a quasi-bound  $\bar{K}N$  state in the  $\bar{K}N$ - $\pi\Sigma$  coupled-channel system. In such models, energy independent phenomenological models are constructed to reproduce the  $\Lambda(1405)$  mass pole with a single pole structure, which show the mass pole of around 1405 MeV with deep  $\bar{K}N$  potential [81, 82]. On the other hand, the chiral unitary approaches, which are based on a chiral effective Lagrangian and are thus energy dependent, have given shallow potential and predicted a double pole structure of  $\Lambda(1405)$ ;

$\pi\Sigma$  and  $\bar{K}N$  coupled channels appear in lower and higher poles, respectively, and consequently, the spectrum shape has a peak around 1420 MeV [83, 84, 85, 86]. The “ $\Lambda(1405)$  problem” is one of the most important issues to be solved in the field of hadron physics, because the meson-baryon molecule picture of the  $\Lambda(1405)$  state can also be applied to other candidates of hadronic molecular states, such as the recently observed  $XYZ$  [87, 88, 89] and  $P_c$  states [90, 91]. At J-PARC, the E31 experiment was performed to reveal the  $\Lambda(1405)$  line shape by using and focusing on the most promising channel of  $\bar{K}N \rightarrow \pi\Sigma$ .

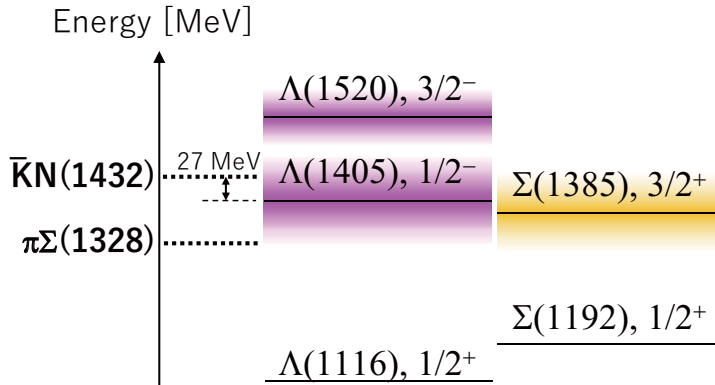


Figure 17: Level scheme of  $Y^*$  resonances around the  $\pi\Sigma$  and the  $\bar{K}N$  mass thresholds.

The possible existence of kaon-nuclear quasi-bound states has been widely discussed, based on the concept of the  $\Lambda(1405)$  state as the  $\bar{K}N$  quasi-bound state. The kaon-nuclear quasi-bound states have been well studied theoretically with various frameworks and the existence of these states is claimed today. Among the kaonic nuclear states, the  $\bar{K}NN$  system (symbolically denoted as “ $K^-pp$ ”) has attracted strong interest in both theoretical and experimental studies because it is the lightest predicted  $S = -1$   $\bar{K}$  nucleus. Many theoretical calculations have been conducted based on few-body calculations using the  $\bar{K}NN-\pi\Sigma N-\pi\Lambda N$  coupled formalism; however, predictions of the binding energy and width are still widely divergent, so that there are as yet many uncertainties of the  $\bar{K}N$  interaction below the mass threshold of  $\bar{K} + N$ . Experimental investigations of the kaon-nuclear quasi-bound states have also been performed over the last few decades. Despite these extensive efforts, only a small amount of experimental information has become available; however, it is still insufficient to discriminate between a variety of conflicting interpretations. To pin down the strength of the  $\bar{K}N$  interaction below the threshold and to clarify the controversial situation of the kaon-nuclear quasi-bound states, the J-PARC E27 and E15 experiments were conducted to search for the “ $K^-pp$ ” state via different reactions using the world’s highest-intensity  $\pi^-$  and  $K^-$  beams, respectively.

### 3.2.1 Measurement of kaonic-deuterium $2p \rightarrow 1s$ X-rays

The  $K^-p$  interaction at around the threshold energy has been studied by precise kaonic hydrogen X-ray spectroscopy measurements of the  $2p \rightarrow 1s$  transition ( $K_\alpha$ ). The strong-interaction effects can be derived via the shift ( $\epsilon$ ) and the width ( $\Gamma$ ) of the atomic levels relative to the electromagnetic values, which are caused by the strong interaction between kaons and protons. The strong interaction shift  $\epsilon_{1s}$  is defined as

$$\epsilon_{1s} = E_{2p \rightarrow 1s}^{\text{measured}} - E_{2p \rightarrow 1s}^{\text{EM}}, \quad (2)$$

where  $E_{2p \rightarrow 1s}^{\text{measured}}$  and  $E_{2p \rightarrow 1s}^{\text{EM}}$  are the measured  $2p \rightarrow 1s$  transition energy and that calculated with only the electromagnetic interaction, respectively. The obtained  $\epsilon_{1s}$  and  $\Gamma_{1s}$  are used to derive the complex  $S$ -wave  $K^-p$  scattering length  $a_{K^-p}$  with the Deser-type formula by taking into account the

isospin-breaking corrections at the next-to-leading order [92, 93, 94]:

$$\epsilon_{1s} + i\frac{\Gamma_{1s}}{2} = 2\alpha^3\mu_r^2 a_{K^-p} \times \{1 - 2\alpha\mu_r(\ln\alpha - 1)a_{K^-p}\}, \quad (3)$$

where  $\alpha$  and  $\mu_r$  denote the fine-structure constant and the reduced mass of the  $K^-p$  system,  $m_K M_p / (m_K + M_p)$ , respectively. The most precise values of the strong-interaction shift and width of the kaonic hydrogen 1s state were obtained by the SIDDHARTA experiment [73].

The obtained scattering length from the SIDDHARTA results is

$$a_{K^-p} = (-0.65 \pm 0.10) + i(0.81 \pm 0.15) \text{ fm}. \quad (4)$$

Together with the total cross sections of the  $K^-p$  scattering amplitude and the threshold branching ratios, the complex  $S$ -wave  $K^-p \rightarrow K^-p$  scattering amplitude can be evaluated with strong constraint at the mass threshold, and then extrapolated to the sub-threshold region [75, 76, 77].

The  $K^-p$  scattering amplitude has thus been determined, especially at around and above the threshold. However, the information on the isospin dependent  $\bar{K}N$  scattering length is still missing. Due to isospin conservation, only the averaged scattering length in the isospin  $I = 0$  and  $I = 1$  ( $a_0$  and  $a_1$ ) channels is obtained from the kaonic hydrogen measurement:

$$a_{K^-p} = \frac{1}{2}(a_0 + a_1). \quad (5)$$

Measurement of the kaonic deuterium 1s state is required to determine the individual isoscalar  $a_0$  and isovector  $a_1$  scattering lengths. The complex  $S$ -wave  $K^-d$  scattering length  $a_{K^-d}$ , can be obtained from the shift and the width of the  $2p \rightarrow 1s$  transition using a similar formula to the  $K^-p$  case [95]:

$$\epsilon_{1s} + i\frac{\Gamma_{1s}}{2} = 2\alpha^3\mu_r^2 a_{K^-d} \times \{1 - 2\alpha\mu_r(\ln\alpha - 1)a_{K^-d}\}, \quad (6)$$

where  $\mu_r$  denotes the reduced mass of the kaon-deuteron system. Information on  $a_0$  and  $a_1$  can then be obtained from the combination of  $a_{K^-p}$  and  $a_{K^-d}$ :

$$a_{K^-n} = a_1, \quad (7)$$

$$a_{K^-d} = \frac{4(m_N + m_K)}{2m_N + m_K}Q + C, \quad (8)$$

where

$$Q = \frac{1}{2}(a_{K^-p} + a_{K^-n}) = \frac{1}{4}(a_0 + 3a_1). \quad (9)$$

The first and second terms of  $a_{K^-d}$  in Eq. 8 represent the lowest-order impulse approximation of the  $K^-N$  scattering in the  $K^-d$  system, *i.e.*,  $K^-$  scattering with each nucleon in deuterium, and higher-order corrections such as the  $K^-d$  three-body interaction, respectively.

There are many theoretical calculations on the  $K^-d$  scattering length that give consistent values of the shift and width, as summarized in Table 2. However, no experimental results have yet been obtained due to the difficulty of the measurement, which is caused by large absorption in the  $2p$  state [96, 97, 98, 99]. To date, only the SIDDHARTA group has shown an exploratory measurement on the X-rays from kaonic deuterium, and the upper limits for the yield of the  $K$ -series transitions were reported at a liquid deuterium density of 1.5% (13.9 times the STP density): total and  $K_\alpha$  yields of  $Y(K_{tot}) < 0.0143$  and  $Y(K_\alpha) < 0.0039$  (90% CL), respectively [100]. The yield is one order of magnitude smaller than the kaonic-hydrogen yield, which is known to be  $\sim 0.01$  for  $K_\alpha$  [71, 101].

The J-PARC E57 experiment at the K1.8BR beamline has been proposed to measure the shift and width of the kaonic-deuterium 1s state with an accuracy of 60 eV and 140 eV, respectively [108]. The

Table 2: Calculated  $K^-d$  scattering length  $a_{K^-d}$ , and corresponding experimental observables,  $\epsilon_{1s}$  and  $\Gamma_{1s}$ . The values are taken from Ref. [102].

$a_{K^-d}$ (fm)	$\epsilon_{1s}$ (eV)	$\Gamma_{1s}/2$ (eV)	Reference
$-1.66 + i1.28$	-884	665	[95]
$-1.42 + i1.09$	-769	674	[103]
$-1.46 + i1.08$	-779	650	[104]
$-1.48 + i1.22$	-787	505	[105]
$-1.58 + i1.37$	-887	757	[106]
$-1.42 + i1.60$	-670	508	[107]

experiment uses a gaseous deuterium target at a density of 4% of the liquid deuterium density (30 K with 0.35 MPa,  $\sim 30$  times the STP density), where a  $K_\alpha$  yield of  $\sim 0.1\%$  is expected [96, 97]. To efficiently measure low-yield X-rays with a large width, a large solid angle is covered with many arrays of silicon drift detectors (SDDs) [109, 110, 111]. In addition, a cylindrical detector system (CDS) is used to improve the S/N ratio by the removal of charged-particle hits on the SDDs and selection of the reaction vertex. Charged decay particles from the target are detected by the CDS, which consists of a solenoid magnet, a cylindrical wire drift chamber (CDC), and a cylindrical detector hodoscope (CDH) with a solid angle coverage of 59% [14]. Figure 18 shows a schematic illustration of the CDS for the E57 setup. Tracking information of charged particles is obtained from the CDC, which operates in a solenoidal magnetic field of 0.7 T, and particle identification is performed using ToF together with a beamline trigger counter.

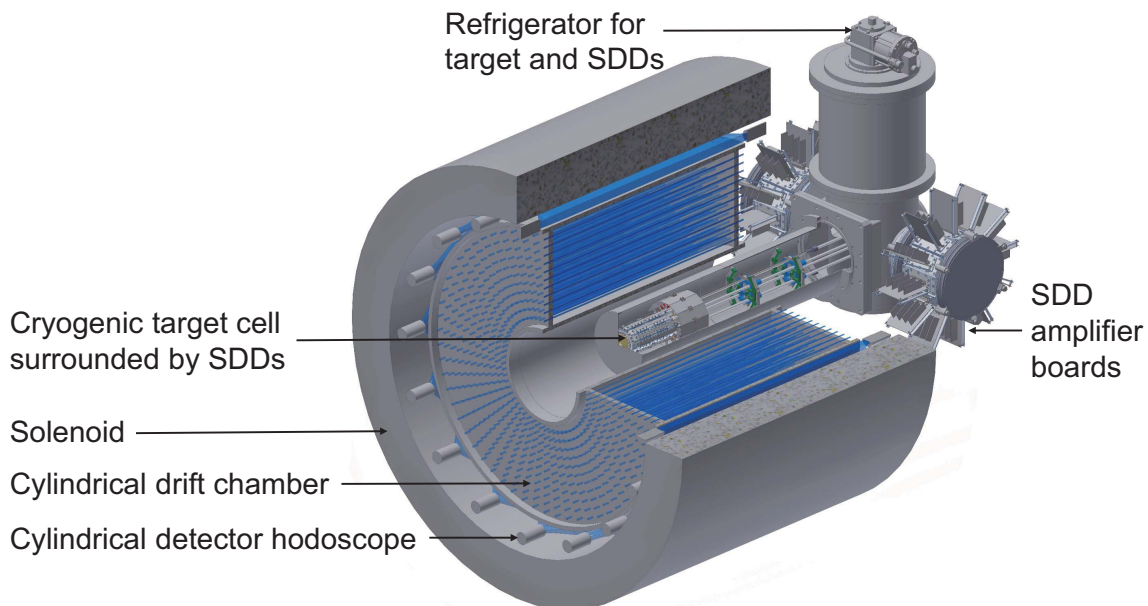


Figure 18: Schematic illustration of the CDS layout for the E57 setup.

In the experiment, negatively-charged kaons incident with a momentum of  $\sim 700$  MeV/c are degraded in carbon and copper degraders and are finally stopped inside the gaseous deuterium target. The kaonic deuterium atoms are produced via the stopped- $K^-$  reaction in the deuterium target, of which the target cell is cylindrical with a length of 19 cm and a 6 cm diameter. The  $2p \rightarrow 1s$  X-ray transition of the kaonic deuterium atom is measured with SDDs surrounding the target cell to give a total area of 246 cm<sup>2</sup>. Each monolithic SDD array that has been developed for the study of kaonic

deuterium at DAΦNF (SIDDHARTA-2) and J-PARC (E57) has 8 square cells with a total active area of 5.12 cm<sup>2</sup> [102], and in total 48 SDDs are used for the experiment. The read-out of the SDD is based on a CMOS charge sensitive preamplifier (CUBE) [112]. The performance of the SDDs has been confirmed to achieve an energy resolution of 130 eV at 6 keV with the temperature at 120 K. The cryogenic target cell surrounded by the SDDs is placed in the center of the CDS, as shown in Fig. 18.

Following a pilot experiment with a hydrogen target in the near future, the kaonic deuterium measurement will be performed.

### 3.2.2 Precise measurement of kaonic-helium $3d \rightarrow 2p$ X-rays

Kaonic atoms with  $Z \geq 2$  have been studied in terms of nuclear medium effects for the strong interaction at the threshold energy to derive information on the possible appearance of kaon condensation and the evolution of strangeness in high-density stars, such as neutron stars. Many experimental measurements of kaonic atom X-rays have been performed with various nuclear targets from helium (He) to uranium (U), and the  $\bar{K}$ -nucleus potential has been theoretically obtained using the density dependent optical potentials. The depth of the real-part potential obtained with the phenomenologically well known  $t\rho$  potential is typically 180 MeV [113, 114, 115, 116]. Such substantial attractive potentials have led to the possible existence of ‘deeply’ bound kaonic nuclear systems, which will be discussed in Sec. 3.2.4. The potential has also been constructed from the effective  $\bar{K}N$  interaction obtained from a coupled channel chiral unitary approach to the low-energy  $\bar{K}N$  data. The depth of the chiral based potential is typically 50 MeV [117, 118, 119], which is shallower than the potential obtained with the phenomenological models. However, the existing data is not sufficient to discriminate between the conflicting interpretations; both of the calculated results using the different potentials agree well with the experimental data within the uncertainties.

In such a situation, a possible breakthrough has been specifically pointed out; a high-precision measurement of the isotope shift between the kaonic-<sup>3</sup>He and kaonic-<sup>4</sup>He  $2p$  states could resolve the question of whether the potential is deep or shallow. Table 3 shows preliminary results for the calculated strong-interaction shifts of the kaonic-<sup>3</sup>He and kaonic-<sup>4</sup>He  $2p$  states [120]. The difference in the isotope shift between the two models has been predicted to be  $\sim 0.6$  eV.

Table 3: Preliminary results for the calculated shifts of the kaonic-<sup>3</sup>He and <sup>4</sup>He  $2p$  states [120]. The two different optical potentials of the phenomenological model [121] and the chiral unitary model [117] are assumed, where a Gaussian expansion method is used for the charge density distributions of <sup>3</sup>He and <sup>4</sup>He [122].

	Phenomenological [ $V_{optical} \sim -180 + i73$ MeV]	Chiral unitary [ $V_{optical} \sim -40 + i55$ MeV]
$K^-$ <sup>4</sup> He	-0.41 eV	-0.09 eV
$K^-$ <sup>3</sup> He	+0.23 eV	-0.10 eV
Isotope shift ( $K^-$ <sup>4</sup> He - $K^-$ <sup>3</sup> He)	-0.64 eV	+0.01 eV

However, the most precise experimental measurement was achieved by the KEK-PS E570 experiment using a liquid helium target and SDDs [123]:

$$\epsilon_{2p}(K^-{}^4\text{He}) = +2 \pm 2(\text{stat.}) \pm 2(\text{syst.}) \text{ eV.} \quad (10)$$

The SIDDHARTA experiment also measured the isospin dependence of the level shift by the strong interaction using gaseous helium targets and SDDs [124, 125]:

$$\epsilon_{2p}(K^-{}^4\text{He}) = +5 \pm 3(\text{stat.}) \pm 4(\text{syst.}) \text{ eV,} \quad (11)$$

$$\epsilon_{2p}(K^{-3}\text{He}) = -2 \pm 2(\text{stat.}) \pm 4(\text{syst.}) \text{ eV}. \quad (12)$$

Therefore, the experimental accuracy obtained to date has been an order of magnitude worse compared to the expected shifts obtained by theoretical calculations. The required precision of the kaonic-helium isotope measurements is in the order of  $\sim 0.2$  eV, which also makes it possible to determine the sign of the level shift for each isotope.

To realize high-resolution and high-accuracy measurements of kaonic-helium atoms X-rays, the J-PARC E62 experiment utilized a superconducting transition-edge-sensor (TES) microcalorimeter. The TES is a highly sensitive thermal sensor that measures energy deposition by measurement of the increase in the resistance of a superconducting material biased within the sharp phase transition between the normal and superconducting phases [126, 127]. The energy resolution of the TES microcalorimeter is  $\sim 5$  eV (FWHM) at 6 keV, which enables determination of the level shift to as good as 0.2 eV, which is one order of magnitude better than the precision of a semiconductor detector such as the SDD. Recent technological advances in the multiplexed readout of a TES multi-pixel array has enabled the use of the TES detector in measurements of kaonic-helium X-rays with reasonably large acceptance.

The experiment employed a 240 pixel TES array (effective area of  $23 \text{ mm}^2$ ) designed for hard X-ray measurements developed by the National Institute of Standards and Technology (NIST). As a demonstration of the feasibility of the TES-based detector to perform hadronic atom X-ray measurements, a precedence experiment was carried out at the PSI  $\pi$ M1 beamline in 2014, with the same type of TES spectrometer as that used in the E62 experiment [128, 129]. In this experiment, the *in situ* energy calibration method was demonstrated by shining characteristic X-rays on the TES, excited by an X-ray tube source during data acquisition. The FWHM energy resolution obtained was 6.8 eV at 6.4 keV (Fe  $K_{\alpha 1}$ ), and the uncertainty of the absolute energy calibration was achieved to 0.1 eV under a high-rate hadron beam condition of 1.45 MHz, which matches the E62 goal of the kaonic-helium measurement.

After a commissioning experiment at the secondary K1.8BR beamline in 2016 [130], the E62 experiment was performed in 2018. Figure 19 shows the experimental setup. Incident kaons extracted with a momentum of 900 MeV/c were counted with beamline counters, degraded, and stopped inside the liquid-helium target. X-rays emitted from the kaonic-helium atoms were detected by the TES spectrometer. An X-ray generator and secondary target metals were also installed to perform the absolute energy calibration for every single readout channel, as demonstrated in the precedence experiment.

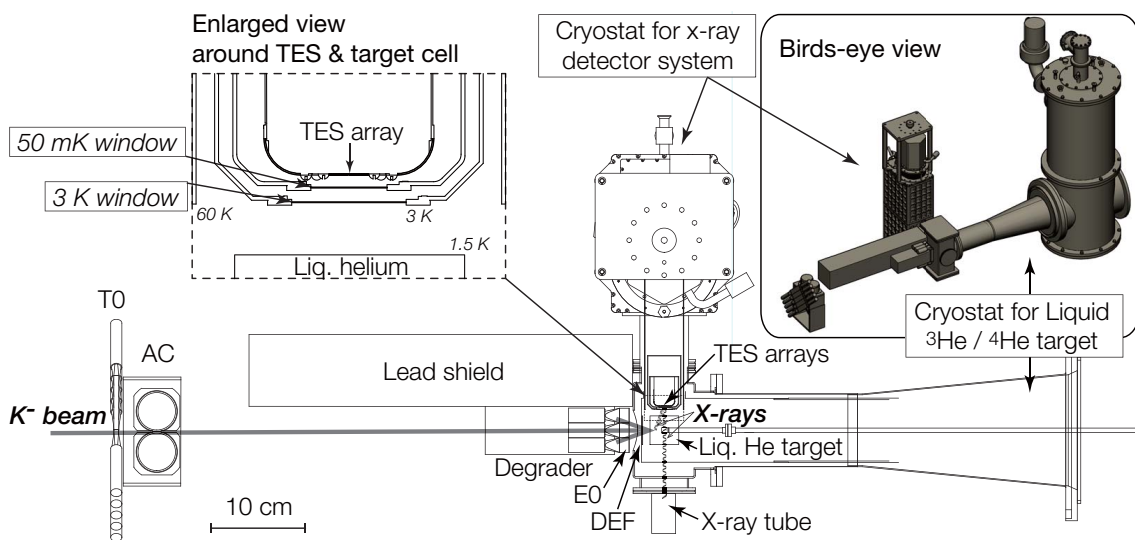


Figure 19: Schematic diagram of the E62 experimental setup around the experimental target. The insets show a birds-eye view and an enlarged view around the TES and the helium target cell. The figure is taken from the E62 proposal [131].

During the  $\sim 20$  days beam time, more than 100 X-ray counts from both kaonic- ${}^3\text{He}$  and  ${}^4\text{He}$   $3d \rightarrow 2p$  transitions were accumulated [132]. The energy resolutions achieved were  $\sim 7$  eV (FWHM) at 6 keV. The expected statistical precisions of the kaonic-helium X-ray energies were 0.35 and 0.2 eV for  $K^- {}^3\text{He}$  and  $K^- {}^4\text{He}$ , respectively, with a systematic uncertainty of 0.1 eV.

### 3.2.3 Investigation of the $\Lambda(1405)$ line shape

Extensive measurements of the  $K^-p$  scatterings has also led to a theoretical prediction of the existence of the  $\Lambda(1405)$  state below the  $K^- + p$  mass threshold [133]. After the first observation of the  $\Lambda(1405)$  state using a hydrogen bubble chamber [134], the  $\Lambda(1405)$  state has been well established today and is listed in the table of the Particle Data Group as a four-star state [45]. The  $\Lambda(1405)$  state is known to have strangeness  $S = -1$  and isospin  $I = 0$ , which is located slightly below the  $K^- + p$  mass threshold (Fig. 17) and decays into the  $\pi\Sigma$  channels with a 100% branching ratio. The quantum number  $J^P = 1/2^-$  was recently derived by the CLAS collaboration at Jefferson Lab (JLab) using the reaction  $\gamma p \rightarrow K^+\Lambda(1405)$  [135].

It is well known that there is a difficulty in describing the  $\Lambda(1405)$  state as an ordinary three-quark state in simple constituent quark models because its mass is lower than any other excited spin  $1/2$  baryons [1]. Thus, the  $\Lambda(1405)$  state has been widely interpreted as a dynamically generated resonance through a  $\bar{K}N-\pi\Sigma$  coupled channel system [78]. A recent lattice QCD calculation also strongly suggested that the structure of the  $\Lambda(1405)$  state is dominated by a bound  $\bar{K}N$  component [136].

During the past decade, many new experimental results on the  $\Lambda(1405)$  state have been reported; photoproduction at the LEPS (SPring-8) [137] and the CLAS (JLab) [138], electroproduction at the CLAS (JLab) [139], and proton-proton collision at the ANKE (COSY) [140] and the HADES (GSI) [141]. Using these precise  $\pi\Sigma$  spectra, detailed theoretical studies on the  $\Lambda(1405)$  line shape have also been performed. However, despite many such experimental attempts and theoretical analyses, the most fundamental unsettled question still remains: whether the  $\Lambda(1405)$  state is located at 1405 MeV/ $c^2$  or at 1420 MeV/ $c^2$ , which correspond to the respective single- or double-pole nature of the  $\Lambda(1405)$  state.

The phenomenological models are based on theoretical fits of the  $\pi\Sigma$  invariant mass spectra with a single pole energy independent structure, which shows the  $\Lambda(1405)$  mass pole is around 1405 MeV with a deep  $\bar{K}N$  potential [81, 82]. In contrast, the chiral unitary approaches are based on an effective Lagrangian of the chiral perturbation theory, and are thus energy dependent. The potential is constructed by combining the experimental data of the low-energy  $\bar{K}N$  scatterings and the kaonic hydrogen, the result of which gives a shallow potential. In the chiral unitary approaches, the  $\Lambda(1405)$  state is predicted to have a double pole structure, and consequently the line shape has a single-like peak structure around 1420 MeV; the first and main pole coupled to the  $\bar{K}N$  channel is located near the  $\bar{K}N$  mass threshold ( $\sim 1432$  MeV) with a relatively small width, and the second pole coupled to the  $\pi\Sigma$  channel appears near the  $\pi\Sigma$  threshold ( $\sim 1328$  MeV) with a large width [83, 84, 85, 86].

The Review of Particle Physics by the Particle Data Group (PDG) [45] has adopted the values obtained by the phenomenological analyses based on the single-pole nature of  $\Lambda(1405)$ ; a mass of  $1405.1^{+1.3}_{-1.0}$  MeV/ $c^2$  and a width of  $50.5 \pm 2.0$  MeV/ $c^2$ . These values were obtained from the theoretical fits to the  $\pi\Sigma$  invariant mass spectra from the reaction  $K^-p \rightarrow \Sigma^+\pi^-\pi^+\pi^-$  at 4.2 GeV/ $c$  measured by a hydrogen bubble chamber experiment [142, 81], the stopped  $K^-$  reaction in  ${}^4\text{He}$  measured by a helium bubble chamber experiment [143, 144], and the reaction  $pp \rightarrow \Sigma^\pm\pi^\mp K^+p$  at 3.5 GeV from the HADES experiment [141, 145].

On the other hand, the precise  $\pi\Sigma$  spectra obtained from the  $\gamma$ -induced reaction at the CLAS experiment were also theoretically analyzed using the chiral motivated models, *i.e.* based on the double-pole nature of  $\Lambda(1405)$  [146, 147, 148]. The CLAS data have been well reproduced by the theoretical models, the obtained pole positions of which are summarized in the review “*Pole structure of the  $\Lambda(1405)$  region*” (U.-G. Meissner and T. Hyodo, 2015) [45]. However, a recent phenomenological analysis of the CLAS

data has also extracted the pole of the  $\Lambda(1405)$  state based on a single pole model, and claimed that the pole is consistent with the PDG value [149]. Also, a recent partial wave analysis has shown the good description of experimental data with a single pole model having the pole of  $(1422 \pm 3, -i(21 \pm 3))$  MeV [150]; photoproduction data from the CLAS experiment and  $K^-$  induced reaction data obtained with the Crystal Ball multiphoton spectrometer at BNL [151] and old bubble chambers were utilized.

Therefore the situation is still controversial in terms of the theoretical analysis of the  $\Lambda(1405)$  line shape. To clarify which scenario is valid, decomposition of the  $\Lambda(1405)$  state coupled to  $\bar{K}N$  is of essential importance;  $\Lambda(1405)$  lies below the  $\bar{K}N$  threshold and thus has no decay channel into  $\bar{K}N$ ; therefore, investigation of the  $\bar{K}N$  collision process in a virtual state is required.

The J-PARC E31 experiment aims to exclusively show the  $\Lambda(1405)$  line shape via the  $\bar{K}N \rightarrow \pi\Sigma$  channels using the  $(K^-, n)$  reaction on a deuterium target.  $\Lambda(1405)$  production initiated by virtual  $\bar{K}N$  scattering is theoretically expected to be enhanced in the  $K^-d \rightarrow \Lambda(1405)n$  process [152]; therefore, this process is important to investigate the  $\Lambda(1405)$  properties via the sub-threshold  $\bar{K}N \rightarrow \pi\Sigma$  channels. In the experiment, the missing-mass spectra of the  $d(K^-, n)$  reaction are measured in coincidence with decay particles from the  $\Lambda(1405)$  state. To decompose the isospin amplitudes of  $I = 0, 1$  and their interference term in the  $\pi\Sigma$  spectrum, all of the  $\pi^+\Sigma^-, \pi^-\Sigma^+$ , and  $\pi^0\Sigma^0$  final states are identified. An exclusive measurement is realized by the detection of a neutron from the  $(K^-, n)$  reaction and two charged particles from the  $\pi\Sigma$  decays, where the missing neutral particle(s) is identified by the missing mass of the reaction:

$$\begin{aligned} \Lambda(1405) &\rightarrow \pi^+\Sigma^- \rightarrow \pi^+\pi^-n \text{ (33\%),} \\ &\rightarrow \pi^-\Sigma^+ \rightarrow \pi^+\pi^-n \text{ (16\%)} / \pi^0\pi^-p \text{ (17\%),} \\ &\rightarrow \pi^0\Sigma^0 \rightarrow \gamma\pi^0\pi^-p \text{ (21\%),} \end{aligned} \quad (13)$$

where the numbers in parentheses show the branching ratio in each reaction with the assumption of a branching ratio of 33.3% for each decay channel of  $\Lambda(1405) \rightarrow \pi^{\pm 0}\Sigma^{\mp 0}$ . The  $\Sigma(1385)^0$  resonance ( $I = 1$ ) is a significant background to isolate the  $\Lambda(1405)$  state ( $I = 0$ ) in the  $\pi^{\pm}\Sigma^{\mp}$  channels:

$$\begin{aligned} \Sigma(1385)^0 &\rightarrow \pi^+\Sigma^- \rightarrow \pi^+\pi^-n \text{ (6\%),} \\ &\rightarrow \pi^-\Sigma^+ \rightarrow \pi^+\pi^-n \text{ (3\%)} / \pi^0\pi^-p \text{ (3\%),} \\ &\rightarrow \pi^0\Lambda \rightarrow \pi^0\pi^-p \text{ (56\%).} \end{aligned} \quad (14)$$

The measurement was performed using the K1.8BR spectrometer. The incident  $K^-$  momentum of 1.0 GeV/c was selected to maximize the  $(K^-, n)$  reaction rate [153]. The scattered neutrons from the  $(K^-, n)$  reaction were measured by a neutron counter (NC) located  $\sim 15$  m downstream from the target position, with a missing-mass resolution of  $\sim 10$  MeV/c<sup>2</sup> ( $\sigma$ ) for the region of interest. The decay charged particles associated with the reaction were detected by the CDS surrounding a liquid deuterium target system. To detect a backward boosted proton from the sequential decay of the  $\Lambda(1405) \rightarrow \pi^0\Sigma^0 \rightarrow \gamma\pi^0\pi^-p$  decay, the E31 experiment used backward-proton detectors installed just upstream of the target system in the CDS [14].

In 2016 and 2018, the first (E31-1st) and second (E31-2nd) experiments were conducted with respectively  $1.5 \times 10^{10}$  and  $3.9 \times 10^{10}$  kaons on a deuteron target. Figure 20 shows results of the  $d(K^-, n)\pi^{\pm}\Sigma^{\mp}$  missing-mass spectra [154]. In the analysis, a neutron from the  $\Sigma^{\pm}$  decay was identified using the missing-mass of  $d(K^-, n\pi^{\mp})X$  as  $X = n$ , and the  $\Sigma^{\pm}$  were then obtained from the missing-mass of  $d(K^-, n\pi^{\mp})X$  as  $X = \Sigma^{\pm}$ . The ratio of the  $\pi^+\Sigma^-$  to  $\pi^-\Sigma^+$  states was evaluated with a Monte Carlo template fitting in each 10 MeV/c<sup>2</sup> bin.

The difference of the spectral shape and strength between the  $\pi^+\Sigma^-$  and  $\pi^-\Sigma^+$  spectra is clearly evident in Fig. 20. This is strong evidence of the interference between the  $I = 0$  and  $I = 1$  channels in

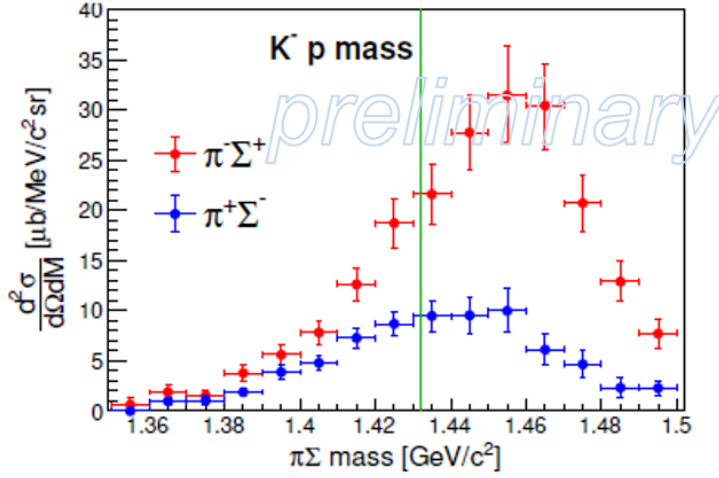


Figure 20: Results of the  $d(K^-, n)\pi^\pm\Sigma^\mp$  missing-mass spectra obtained with the E31-1st data. Reproduced from Ref. [154], with the permission of AIP Publishing.

the  $\pi^\pm\Sigma^\mp$  states, which can be given as [155]:

$$\frac{d\sigma}{d\Omega}(\pi^+\Sigma^-) \propto \frac{1}{3}|f_{I=0}|^2 + \frac{1}{2}|f_{I=1}|^2 + \frac{\sqrt{6}}{3}\text{Re}(f_{I=0}f_{I=1}^*), \quad (15)$$

$$\frac{d\sigma}{d\Omega}(\pi^-\Sigma^+) \propto \frac{1}{3}|f_{I=0}|^2 + \frac{1}{2}|f_{I=1}|^2 - \frac{\sqrt{6}}{3}\text{Re}(f_{I=0}f_{I=1}^*), \quad (16)$$

$$\frac{d\sigma}{d\Omega}(\pi^0\Sigma^0) \propto \frac{1}{3}|f_{I=0}|^2, \quad (17)$$

where  $f_{I=0}$  and  $f_{I=1}$  denote the  $I = 0$  and  $I = 1$  amplitudes, respectively. To cancel out the interference between the  $I = 0$  and  $I = 1$  components, the  $\pi^\pm\Sigma^\mp$  spectra are averaged, as shown in Fig. 21. In addition, the pure  $I = 1$  component of the  $d(K^-p)\pi^-\Sigma^0$  reaction was obtained with the same data set using a forward proton ToF counter array located alongside the NC. The missing-mass spectrum of  $d(K^-, p)\pi^-\Sigma^0$  is plotted in Fig. 21 together with the averaged  $\pi^\pm\Sigma^\mp$  spectra. Under an assumption of the similarity of the  $d(K^-, n)$  and  $d(K^-, p)$  reaction mechanisms, these two amplitudes can be written as:

$$\frac{1}{2} \left( \frac{d\sigma}{d\Omega}(\pi^+\Sigma^-) + \frac{d\sigma}{d\Omega}(\pi^-\Sigma^+) \right) \propto \frac{1}{3}|f_{I=0}|^2 + \frac{1}{2}|f_{I=1}|^2, \quad (18)$$

$$\frac{1}{2} \frac{d\sigma}{d\Omega}(\pi^-\Sigma^0) \propto \frac{1}{2}|f_{I=1}|^2. \quad (19)$$

Therefore, the results strongly indicate that the amplitude of the  $I = 0$  component is dominated at the forward direction, in particular, below the  $\bar{K}N$  threshold.

Figure 22 shows the result of the  $d(K^-, n)\pi^0\Sigma^0$  missing-mass spectrum without the acceptance correction. In the analysis, a negative pion and a backward-going proton in the decay chain of  $\pi^0\Sigma^0 \rightarrow \gamma\pi^0\Lambda \rightarrow \gamma\pi^0\pi^-p$  were identified by the CDS and the backward-proton detectors, respectively. The  $\Lambda \rightarrow \pi^-p$  decay was then identified in the  $\pi^-p$  invariant mass spectrum, and the  $K^-d \rightarrow \pi^0\Sigma^0n$  event was selected using the missing-mass spectrum of  $d(K^-, n\Lambda)X$  as  $X = \gamma\pi^0$ . In the figure, the background from the  $K^-d \rightarrow \pi^-\Sigma^+n/\pi^0\Lambda n \rightarrow \pi^0\pi^-pn$  reactions is also plotted. The significant yield below the  $\bar{K}N$  threshold is evident, where the  $\pi^-\Sigma^+/\pi^0\Lambda$  background is negligibly small.

The results obtained can be compared with theoretical calculations, taking into account the kinematics of the E31 experiment; the  $(K^-, n)$  measurement at  $0^\circ$  with a kaon momentum of 1.0 GeV/c.

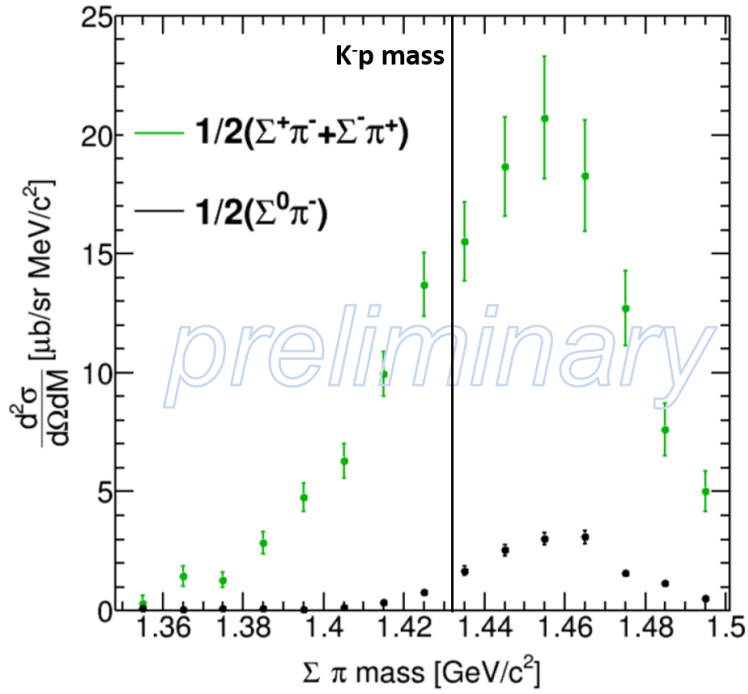


Figure 21: Result of the average of the  $d(K^-, n)\pi^\pm\Sigma^\mp$  missing-mass spectra obtained with the E31-1st data. The  $d(K^-, p)\pi^-\Sigma^0$  missing-mass spectrum divided by two is also shown. Reproduced from Ref. [154], with the permission of AIP Publishing.

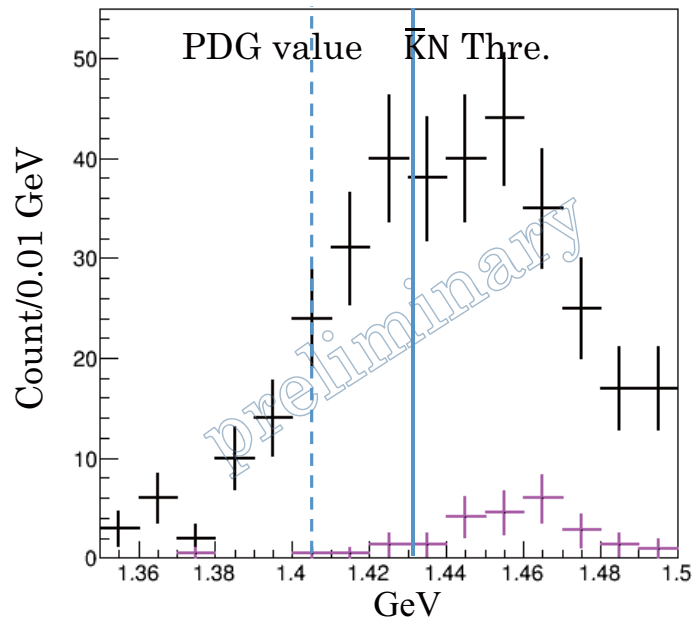


Figure 22: Result of the  $d(K^-, n)\pi^0\Sigma^0$  missing-mass spectrum without the acceptance correction. The background contribution (magenta) from the  $K^-d \rightarrow \pi^-\Sigma^+n/\pi^0\Lambda n \rightarrow \pi^0\pi^-pn$  reactions is also plotted. The figure is taken from Ref. [156].

In Ref. [157], a model of the  $K^-d \rightarrow \pi\Sigma N$  reactions was developed with the off-shell amplitudes of the  $\bar{K}N \rightarrow \bar{K}N$  and  $\bar{K}N \rightarrow \pi Y$  reactions generated from a dynamical coupled-channels (DCC) model that was constructed by fitting the existing data of the  $K^-p \rightarrow \bar{K}N, \pi\Sigma, \pi\Lambda, \eta\Lambda$ , and  $K\Xi$  reactions [47]. The model indicates the appearance of the two-pole structure of the  $\Lambda(1405)$  state, similar to the structure obtained in the chiral unitary models. Furthermore, in Ref. [158], the reaction  $K^-d \rightarrow \pi\Sigma N$  has been studied within a Faddeev-type approach using the  $\bar{K}N \rightarrow \bar{K}N$  amplitude obtained by a partial wave analysis [159] and chiral unitary models of the  $\bar{K}N \rightarrow \pi\Sigma$  interaction [160, 77, 161]. Both of the calculated  $K^-d \rightarrow \pi\Sigma N$  spectra in Ref. [157] and Ref. [158] show reasonable agreement with the E31 results. Therefore, the E31 results show significant potential to reveal the details of the  $\bar{K}N \rightarrow \pi\Sigma$  amplitude and to provide substantial constraints on the line shape of the  $\Lambda(1405)$  state in conjunction with various theoretical calculations.

### 3.2.4 Search for kaonic nuclei

The  $\Lambda(1405)$  state can be inherently interpreted as the  $\bar{K}N$  quasi-bound state due to the strongly attractive  $\bar{K}N$  interaction in the  $I = 0$  channel; therefore, the existence of the  $\bar{K}$ -nuclear quasi-bound state has been widely discussed [162, 82, 163] and various interesting phenomena have been suggested. The most significant interest of these exotic states is that they could form high-density cold nuclear matter, such as the inner core of neutron stars, where the chiral symmetry is expected to be restored [164, 165]. Therefore, investigation of the  $\bar{K}$ -nuclear quasi-bound states is expected to provide new insights, not only on meson-baryon interactions in the low-energy QCD, but also on the change of the meson properties in nuclear media.

The lightest predicted  $S = -1$   $\bar{K}$  nucleus is the  $\bar{K}NN$  system (symbolically denoted as “ $K^-pp$ ”), which is expected to be a  $[\bar{K} \otimes NN_{I=0, S=0}]_{I=1/2}$  with  $J^P = 0^-$  state. The existence of the  $\bar{K}NN$  quasi-bound state is supported by many theoretical predictions based on few-body calculations using the  $\bar{K}NN$ - $\pi\Sigma N$ - $\pi\Lambda N$  coupled formalism. However, the calculated properties, such as the binding energy ( $B$ ) and the width ( $\Gamma$ ), are scattered due to the large dependence of the model on the  $\bar{K}N$  interaction. Table 4 summarizes the calculated binding energies and widths obtained from various theoretical works. Calculations based on the energy independent models (phenomenological models) show rather large binding energies of  $\sim 40$ – $90$  MeV [163, 166, 167, 168, 169, 170, 171, 172, 173], whereas this becomes as small as  $\sim 10$ – $50$  MeV with the energy dependent models (chiral unitary models) [174, 175, 176, 177, 178, 171, 173, 179]. With regard to the widths, the predicted values are widely spread ( $\sim 20$ – $110$  MeV) and independent of the  $\bar{K}N$  interaction models. In the framework of the chiral model, a double pole structure of the  $\bar{K}NN$  has also been proposed in relation to the  $\Lambda(1405)$  state [176, 180].

There are several reports on the experimental observation of a “ $K^-pp$ ” candidate with a binding energy of around 100 MeV, which were measured with non-mesonic decay branches of  $\Lambda p$  and/or  $\Sigma^0 p$  in different reactions. The FINUDA collaboration measured back-to-back  $\Lambda p$  pairs in stopped  $K^-$  reactions on light nuclear targets [181], and the DISTO collaboration analyzed the  $pp \rightarrow \Lambda p K^+$  channel at a proton energy of 2.85 GeV [182]. However, the obtained spectra can also be understood without the inclusion of a bound state; the AMADEUS collaboration reported that the spectra in the stopped  $K^-$  reactions can be well described by  $K^-$  multi-nucleon absorption processes without the need for the “ $K^-pp$ ” component [183, 184], and the  $K^+\Lambda p$  final state in the  $p + p$  collision can be explained with resonant and non-resonant intermediate states that decay into a  $K^+\Lambda$  pair, as reported by the HADES collaboration [185]. The LEPS collaboration also reported only upper limits on the cross section for the “ $K^-pp$ ” bound state in  $\gamma$ -induced reactions [186].

Thus, the experimental situation to search for the “ $K^-pp$ ” bound state was also controversial. To clarify whether or not the “ $K^-pp$ ” bound state exists, the key to the experimental search is to adopt a simple reaction and to measure it exclusively. Simple reactions, such as in-flight  $\bar{K}$  induced reactions

Table 4: Calculated binding energy ( $B$ ) and width ( $\Gamma$ ) of the  $\bar{K}NN$  quasi-bound state from various theoretical works.

Energy independent $\bar{K}N$ interactions (Phenomenological model)							
	Variational			Faddeev			Complex-scaling
B (MeV)	48	40–80	49	50–70	60–95	47–53	51
$\Gamma$ (MeV)	61	40–85	62	90–110	45–80	50–65	32
Ref.	[163]	[170]	[173]	[166, 167]	[168, 169]	[171]	[172]

Energy dependent $\bar{K}N$ interactions (Chiral unitary model)							
	Variational			Faddeev			Complex-scaling
B (MeV)	17–23	16	26–28	9–16	15–30	32	14–50
$\Gamma$ (MeV)	40–70	41	31–59	34–46	75–80	49	16–38
Ref.	[174, 175]	[177]	[173]	[176]	[178]	[171]	[179]

with light target nuclei, would make the “ $K^-pp$ ” production mechanism clear. Exclusive measurement is thus crucial to distinguish a small and broad signal from largely and widely distributed quasi-free backgrounds.

At J-PARC, two experimental searches for the “ $K^-pp$ ” bound state were conducted. The J-PARC E27 experiment aimed to search for the “ $K^-pp$ ” bound state in the  $\pi^+ + d \rightarrow K^+ + X$  reaction at 1.69 GeV/ $c$ . In this reaction, a possible “ $K^-pp$ ” production mechanism has been suggested to produce the “ $K^-pp$ ” state via the  $\Lambda(1405) + p$  collision as a doorway process; the off-shell  $\Lambda(1405)$  ( $\Lambda(1405)'$ ) is produced by the  $\pi^+ + n \rightarrow K^+ + \Lambda(1405)'$  reaction followed by the  $\Lambda(1405)' + p \rightarrow \text{“}K^-pp\text{”}$  reaction [187]. However, due to the large recoil momentum of the  $\Lambda(1405)$  state in the reaction, a small sticking probability of the  $\Lambda(1405)' + p \rightarrow \text{“}K^-pp\text{”}$  reaction is expected.

The E27 experiment was conducted at the K1.8 beamline in 2012 with  $3.3 \times 10^{11}$  incident pions. The details of the experimental setup are given in Ref. [188]. The incident  $\pi^+$  and outgoing  $K^+$  momenta were reconstructed with the K1.8 beamline spectrometer and the SKS covering the scattering angle between  $2^\circ$  and  $16^\circ$  in the laboratory system, respectively. Figure 23 shows the inclusive missing-mass spectrum of the  $d(\pi^+, K^+)$  reaction at 1.69 GeV/ $c$ , where quasi-free  $\Lambda$ , quasi-free  $\Sigma^+$  and  $\Sigma^0$ , and quasi-free  $Y^*$  ( $Y^* = \Lambda(1405)/\Sigma(1385)^+/\Sigma(1385)^0$ ) production is clearly evident. Although the overall structure of the spectrum is well reproduced by a full Monte-Carlo simulation, as shown by the solid line, a difference is observed at the  $\Sigma N$  mass threshold of 2.13 GeV/ $c^2$ , which is originated from the cusp effect. Furthermore, the peak position of the quasi-free  $Y^*$  production is shifted by approximately 30 MeV/ $c^2$  toward low-mass side, which may indicate that a strong attractive  $Y^*N$  interaction exists ( $\Lambda(1405)N$  and/or  $\Sigma(1385)N$ ) [188]. Note that the LEPS group reported a similar inclusive spectrum for the  $d(\gamma, K^+\pi^-)X$  reactions in the 1.5–2.4 GeV photon energy region, although no significant shift was observed in the  $Y^*N$  region [186]. This puzzling “shift” should be clarified theoretically by taking into account the final state interaction. Focusing below the  $K^- + p + p$  mass threshold of 2.37 GeV/ $c^2$ , a possible signal of the “ $K^-pp$ ” not readily visible in the inclusive spectrum.

To reconstruct the expected “ $K^-pp$ ”  $\rightarrow \Lambda/\Sigma^0 + p$  decays exclusively, a range counter array (RCA) was installed surrounding the target system. By requiring high-momentum proton(s) over 250 MeV/ $c$  at large emission angles ( $39^\circ < \theta_{lab} < 122^\circ$ ) with an RCA, a broad enhancement in the  $d(\pi^+, K^+)X$

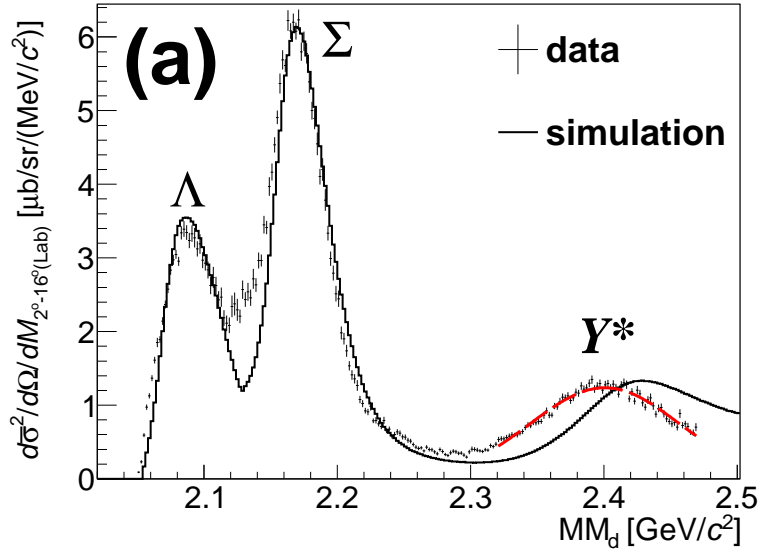


Figure 23: Inclusive missing-mass spectrum of the  $d(\pi^+, K^+)X$  reaction measured in the J-PARC E27 experiment. The crosses show the data and the solid line shows a simulated spectrum assuming quasi-free kinematics. The figure is taken from Ref. [188].

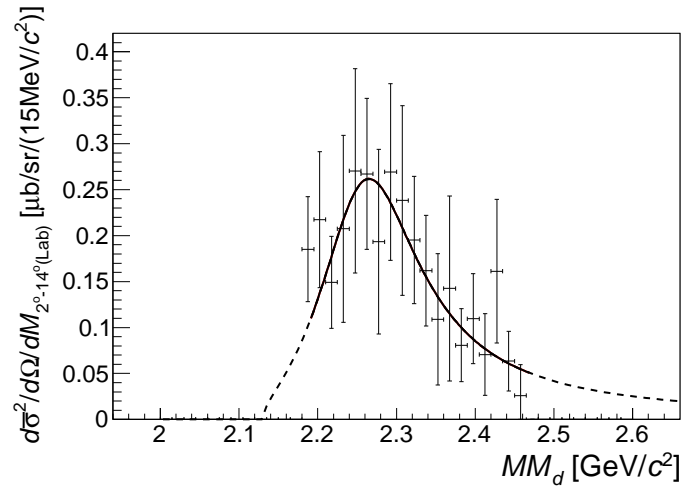


Figure 24: Exclusive missing-mass spectrum of the  $d(\pi^+, K^+)X$  reaction with the  $X \rightarrow \Sigma^0 p$  identification measured in the J-PARC E27 experiment. The spectrum is fitted with a relativistic Breit-Wigner function. The figure is taken from Ref. [189].

missing-mass spectrum was observed around 2.27 GeV/c<sup>2</sup> [189]. The decay branches of  $\Lambda p(\rightarrow \pi^- pp)$ ,  $\Sigma^0 p(\rightarrow \gamma \pi^- pp)$ , and  $\pi Y N(\rightarrow \pi \pi pp)$  were decomposed using the  $d(\pi^+, K^+ pp)X$  missing-mass spectra. Figure 24 shows the missing-mass spectrum of the  $d(\pi^+, K^+)$  reaction for the  $\Sigma^0 p$  decay-branch events, where the spectrum is fitted with a relativistic Breit-Wigner function. The obtained binding energy and width are  $95_{-17}^{+18}(\text{stat.})_{-21}^{+30}(\text{syst.})$  MeV and  $162_{-45}^{+87}(\text{stat.})_{-78}^{+66}(\text{syst.})$  MeV, respectively [189], both of which are significantly larger than those of the theoretical calculations for the “ $K^- pp$ ” bound state. The obtained production cross section  $d\sigma/d\Omega_{\Sigma^0 p\text{-decay}}$  is  $3.0 \pm 0.31(\text{stat.})_{-1.1}^{+0.7}(\text{syst.})$   $\mu\text{b/sr}$ . The cross section of the peak structure in the  $\Lambda p$  decay branch was also evaluated from the fitting by assuming the same distribution of the structure in the missing-mass spectrum of  $d(\pi^+, K^+)X$ . The obtained branching fraction between the  $\Sigma^0 p$  and  $\Lambda p$  decay modes is  $\Gamma_{\Lambda p}/\Gamma_{\Sigma^0 p} = 0.92_{-0.14}^{+0.16}(\text{stat.})_{-0.42}^{+0.60}(\text{syst.})$ , which is consistent with the theoretically calculated ratio of 1.2 [190]. Such a branching ratio gives important information to investigate the properties of the observed structure.

A comparison with the  $\Lambda(1405)$  cross section was performed to reveal the production mechanism related to the  $\Lambda(1405) + p \rightarrow$  “ $K^- pp$ ” doorway process. By comparing with a past measurement of the  $\Lambda(1405)$  production in the  $p(\pi^-, K^0)$  reaction at 1.69 GeV/c [191], a production ratio ( $d\sigma/d\Omega_{Y p\text{-decay}} / (d\sigma/d\Omega_{\Lambda(1405)})$ ) of  $7 \sim 8\%$  was obtained [192], which is much larger than the theoretical expectation in the order of 0.1–1.0% evaluated with a naive coalescence mechanism of  $\Lambda(1405) + p \rightarrow$  “ $K^- pp$ ” [187].

These discrepancies between the experimental and theoretical binding energies, widths, and production ratios could be explained not by the *usually* expected  $\bar{K} NN$  bound state with the quantum number of ( $Y = 1, I = 1/2, J^P = 0^-$ ), but by a  $\pi \Sigma N - \pi \Lambda N$  bound state with ( $Y = 1, I = 3/2, J^P = 2^+$ ) [193]. However, further measurement with high statistics and a larger acceptance detector system is required to identify the origin of the structure. One possible detector system to conduct further ( $\pi^+, K^+$ ) experiment is the Hyperon Spectrometer. A successor experiment to E27 with the new spectrometer system is now under discussion.

The other experiment, J-PARC E15, measured the  $K^- + {}^3\text{He}$  reaction at 1.0 GeV/c. In the reaction, “ $K^- pp$ ” can be produced via the  $(K^-, n)$  reaction; a recoiled virtual kaon (‘ $\bar{K}$ ’) generated by  $K^- N \rightarrow$  ‘ $\bar{K}$ ’  $n$  processes can be directly induced into two residual nucleons within the strong interaction range. The momentum of the ‘ $\bar{K}$ ’ is described as the momentum difference of the incident kaon and the outgoing neutron,  $q = |\mathbf{p}_{K^-}^{\text{lab}} - \mathbf{n}_n^{\text{lab}}|$ . When the backscattered ‘ $\bar{K}$ ’ is realized,  $q$  is as small as  $\sim 200$  MeV/c, which makes the probability for the formation of “ $K^- pp$ ” large.

The E15 experiment was performed at the K1.8BR beamline. The first (E15-1st) and second (E15-2nd) physics runs were performed in 2013 with  $5.3 \times 10^9$  kaons [194, 195] and in 2015 with  $32.5 \times 10^9$  kaons [196] on a liquid  ${}^3\text{He}$  target, respectively. In the semi-inclusive  ${}^3\text{He}(K^-, n)X$  analysis, a forward-going neutron produced from the  ${}^3\text{He}(K^-, n)$  reaction was detected by the forward NC array at  $\theta_n^{\text{lab}} = 0^\circ$ , where at least one charged track in the CDS was required to reconstruct the reaction vertex. Figure 25 shows the obtained  ${}^3\text{He}(K^-, n)X$  missing-mass spectrum and a simulated spectrum [194]. The quasi-elastic scattering ( $K^- n \rightarrow K^- n$ ) and the charge-exchange reaction ( $K^- p \rightarrow K^0 n$ ) are clearly evident, of which the cross sections were evaluated to be  $\sim 6$  and  $\sim 11$  mb/sr, respectively.

In the  $(K^-, n)$  spectrum, a definitive excess of the yield is observed in the bound region, whereas the global spectrum in the unbound region is well reproduced by elementary reactions. Figure 26 shows a close-up view of the region below the  $K^- + p + p$  mass threshold. The excess that reaches to  $\sim 100$  MeV below the  $K^- + p + p$  mass threshold cannot be explained by any simulation result with the elementary reactions. Therefore, the excess will be attributed not only to the attractive  $\bar{K} N$  interaction, but also to two-nucleon absorption processes such as  $K^- N \rightarrow$  ‘ $\bar{K}$ ’  $N$  followed by ‘ $\bar{K}$ ’  $+ NN \rightarrow Y^* N$  and/or ‘ $\bar{K}$ ’  $+ NN \rightarrow$  “ $K^- pp$ ” reactions. However, no significant peak structure was found in the deeply bound region around the binding energy of  $\sim 100$  MeV/c<sup>2</sup>, where the FINUDA, DISTO and E27 collaborations reported the peak structure in different production reactions. The upper limits of the deeply bound “ $K^- pp$ ” state obtained are  $30 - 270$   $\mu\text{b/sr}$  for natural widths of  $20 - 100$  MeV at a 95% confidence level [194]. These values correspond to (0.5 – 5)% and (0.3 – 3)% of the quasi-elastic and the charge-

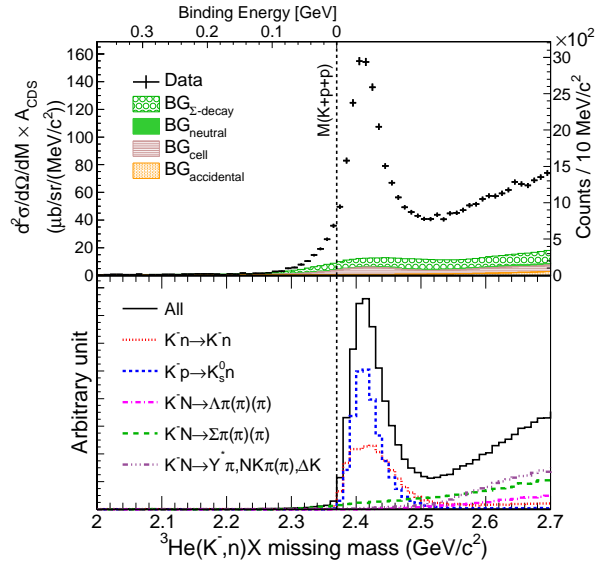


Figure 25:  ${}^3\text{He}(K^-, n)X$  semi-inclusive missing-mass spectra obtained in the E15-1st experiment (top) and by simulation (bottom). The  $K^- + p + p$  binding threshold ( $2.37 \text{ GeV}/c^2$ ) is shown as a dotted line. The figure is taken from Ref. [194].

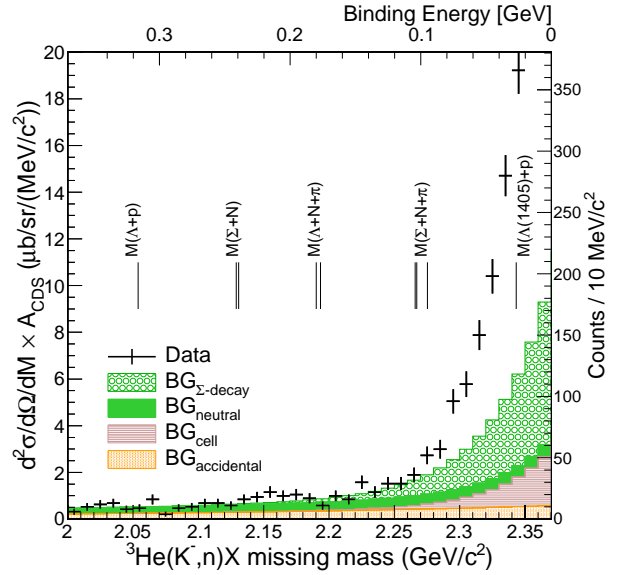


Figure 26: Close-up view of the  ${}^3\text{He}(K^-, n)X$  semi-inclusive missing-mass spectrum on the “ $K^-pp$ ” bound region in Fig. 25 (top). The figure is taken from Ref. [194].

exchange reaction cross sections, respectively.

To kinematically discriminate the “ $K^-pp$ ” signal from the two-nucleon absorption processes, an exclusive  ${}^3\text{He}(K^-, \Lambda p)n$  analysis was conducted. Two protons and one negative pion were detected with the CDS, and a missing neutron was identified by the missing-mass of  ${}^3\text{He}(K^-, pp\pi^-)X$  as  $X = n$ . In the E15-1st experiment, a peak structure was identified below the mass threshold in the  $\Lambda p$  invariant mass spectrum, which is concentrated in the low momentum-transfer region of the  $(K^-, n)$  reaction, as expected [195].

The peak structure observed in the  $\Lambda p$  spectrum was confirmed with  $\sim 30$  times more data on the  $\Lambda pn$  final state by focusing on the  $\Lambda pn$  event accumulation in the E15-2nd experiment. Figure 27 shows the event distribution of the momentum transfer  $q$ , and the  $\Lambda p$  invariant mass  $IM(\Lambda p)$  [196], where the reaction of  $K^- + {}^3\text{He} \rightarrow “K^-pp” + n \rightarrow \Lambda + p + n$  can be uniquely described by these two parameters,  $q$  and  $IM(\Lambda p)$ . Figure 27(a) shows a strong event concentration near the mass threshold of  $K^- + p + p$  in the lower  $q$  region, as previously reported in Ref. [195]. The structure near the threshold is composed of two structures that cannot be represented as a single Breit-Wigner function as assumed in the previous analysis. The centroid of the structure just below the mass threshold does not depend on  $q$  within the statistical uncertainty. This behavior is strong evidence of the existence of a bound state. On the other hand, the distribution centroid above the mass threshold is dependent on  $q$ , *i.e.*, the centroid shifts to heavier mass for larger  $q$ . A natural interpretation of the structure above the threshold is non-resonant absorption of the backward quasi-free ‘ $\bar{K}$ ’ by the  $NN$  spectator, where the ‘ $\bar{K}$ ’ propagates as an on-shell particle; the  $\Lambda p$  final state is generated by the ‘ $\bar{K}$ ’ +  $NN \rightarrow \Lambda p$  conversion due to the final state interaction. The structure below the threshold cannot be reproduced by  $Y^{(*)}$  productions in two nucleon absorption process followed by  $\Lambda p$  conversion, which also have the  $q$ -dependence:  $K^- {}^3\text{He} \rightarrow Y^{(*)} NN_R \rightarrow \Lambda pn$ , where  $N_R$  denotes a residual nucleon.

The simplest model fitting that takes into account the bound state, the quasi-free process, and a broad background reproduces the event distribution, and the results are shown as colored curves

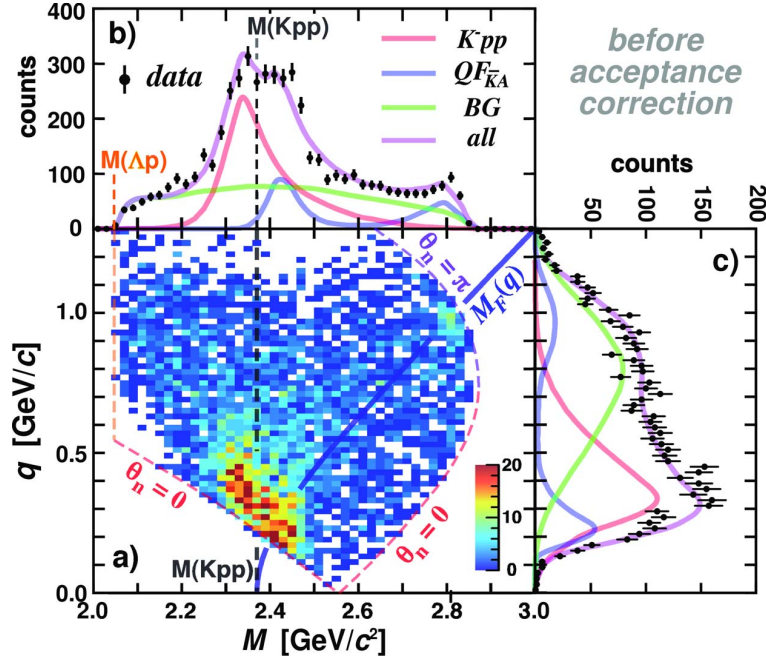


Figure 27: Event distribution on  $M$  ( $= IM(\Lambda p)$ ) and the momentum transfer  $q$ , for the  $\Lambda p n$  final state (a). Histograms projected onto the  $M$  axis (b) and  $q$  axis (c). The fitting results with the simple model are also plotted as colored curves. The figure is taken from Ref. [196].

in Figs. 27(b) and (c). The details of the fitting are given in Ref. [196]. Figure 28 shows the  $\Lambda p$  invariant mass spectrum corrected by the detector acceptance and the experimental efficiency in the momentum transfer window of  $350 < q < 650$  MeV/c, where the signal from the bound state and the quasi-free contribution are clearly separated; the interference between the bound state formation and the quasi-free process will occur near the kinematical boundary. The yields of other processes are largely suppressed in contrast to the bound state, and the quasi-free distribution is also clearly separated from the peak of the bound state. The fitting result provides the Breit-Wigner pole position at  $M = 2324 \pm 3(stat.)_{-3}^{+6}(syst.)$  MeV/c<sup>2</sup>, (*i.e.*, a binding energy of  $B = 47 \pm 3(stat.)_{-3}^{+6}(syst.)$  MeV/c<sup>2</sup>) with a width of  $\Gamma = 115 \pm 7(stat.)_{-20}^{+10}(syst.)$  MeV/c<sup>2</sup>, and the  $S$ -wave Gaussian form factor parameter  $Q = 381 \pm 14(stat.)_{-0}^{+57}(syst.)$  MeV/c<sup>2</sup> [196]. The  $q$ -integrated “ $K^-pp$ ” formation yield going to the  $\Lambda p$  decay channel evaluated is  $\sigma_{Kpp} \cdot Br_{\Lambda p} = 11.8 \pm 0.4(stat.)_{-1.7}^{+0.2}(syst.)$   $\mu b$ .

In Ref. [196], the E15 collaboration has concluded that “the simplest and natural interpretation is a kaonic nuclear bound state “ $K^-pp$ ””. The binding energy and width obtained in the experiments are summarized in Fig. 29 together with those taken from the theoretical calculations of the “ $K^-pp$ ”. The binding energy of  $\sim 50$  MeV obtained in the E15 experiment is deeper than those obtained by the chiral motivated calculations, while rather consistent with those obtained by the phenomenological based calculations. The width of  $\sim 100$  MeV is wide, meaning very absorptive. It should be similar to that of  $\Lambda(1405) \rightarrow \pi\Sigma$  ( $\Gamma \sim 50$  MeV) if the “ $K^-pp$ ” decays like ‘ $\Lambda(1405)$ ’ + ‘ $p$ ’  $\rightarrow \pi\Sigma p$ , as theoretical calculations taken into account only mesonic decay channels show. Thus the observed large width indicates that the non-mesonic  $YN$  channels would be the major decay mode of the “ $K^-pp$ ”. The observed values of the large form factor of  $\sim 400$  MeV/c and the large binding energy of  $\sim 50$  MeV imply the formation of a compact system, although the static form-factor parameter of the “ $K^-pp$ ” should be studied more quantitatively. The structure below the mass threshold in the  $\Lambda p$  spectrum obtained has also been theoretically interpreted as the  $\bar{K}NN$  quasi-bound system [197, 198], in which the experimental spectrum can be reproduced with the  $\bar{K}NN$  quasi-bound system and the quasi-free processes based on theoretical treatment of the  ${}^3\text{He}(K^-, \Lambda p)n$  reaction.

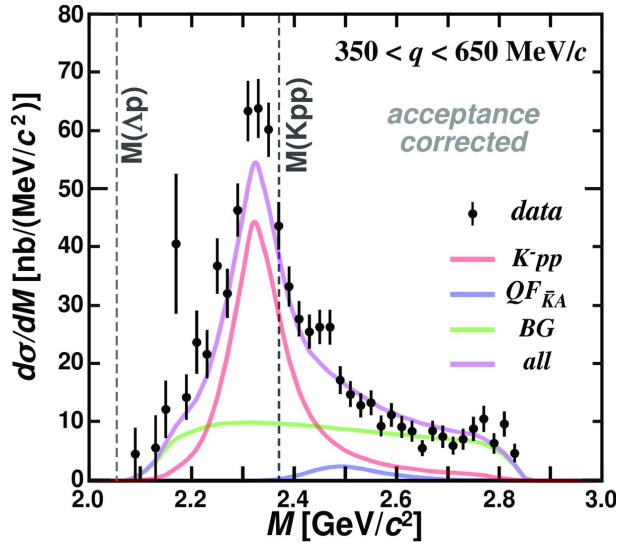


Figure 28: Efficiency and acceptance corrected  $\Lambda p$  invariant mass in the region of  $0.35 < q < 0.65$  GeV/c. The figure is taken from Ref. [196].

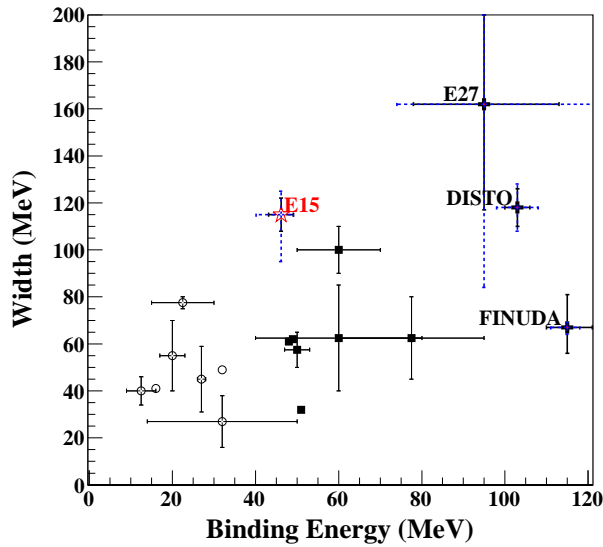


Figure 29: Summary of binding energies and widths for the “ $K^-pp$ ” bound state. The open star shows the values obtained in the E15 experiment [196], and closed crosses show those obtained in the FINUDA [181], DISTO [182], and E27 [189] experiments. Closed squares and open circles denote those from theoretical calculations based on energy independent (phenomenological) [163, 166, 167, 168, 169, 170, 171, 172, 173] and energy dependent (chiral unitary) [174, 175, 176, 177, 178, 171, 173, 179]  $\bar{K}N$  interaction models, respectively.

To confirm that the observed structure is the theoretically predicted  $\bar{K}NN$  quasi-bound state, the question whether or not the “ $K^-p$ ” bound state is also produced in the same  $K^- + {}^3\text{He}$  reaction must be answered. The  $\Lambda(1405)$  state is theoretically considered as a quasi-bound state of  $\bar{K}N$  in the  $I = 0$  channel, as discussed in Sec 3.2.3. Therefore, not only the “ $K^-pp$ ” bound state should be observed, but also the  $\Lambda(1405)$  state in the same  $K^- + {}^3\text{He}$  reaction. Furthermore, from a theoretical perspective, the  $\bar{K}NN$  is a resonant state in the  $\bar{K}NN$ - $\pi\Sigma N$ - $\pi\Lambda N$  coupled-channel system, and the mesonic  $\pi\Sigma N$  decays are expected to be dominant compared to the non-mesonic  $YN$  decays [199]. Measurements of the mesonic  $\pi\Sigma N$  channels originated from the “ $K^-pp$ ” bound state and the  $\Lambda(1405)p$  final state are therefore necessary to obtain further information on the kaonic nuclei.

For this purpose, analysis on the  $K^- {}^3\text{He} \rightarrow \pi^\pm \Sigma^\mp pn$  reactions has been in progress.  $\pi^\pm \Sigma^\mp p \rightarrow \pi^+ \pi^- np$  decays were detected with the CDS, where *the neutron from the  $\Sigma^\pm$  decays* was identified using the CDH by requiring no charged track of the CDC in front of a CDH hit and no hit in both neighboring sides of the CDH segment. One neutron in the reaction was identified with the missing-mass method of the  ${}^3\text{He}(K^-, \pi^+ \pi^- np)X$  with  $X = n$ . With the E31 data set, *i.e.*, the  $K^- + d$  reactions, a similar analysis on  $\Sigma^\pm$  detection using the CDS has been conducted to measure the momentum transfer dependence of the  $\Lambda(1405)$  cross section and to discuss the reaction form factor. In both analyses, the preliminary results clearly show the  $\Lambda(1405)$  signal in the  $\pi^\pm \Sigma^\mp$  invariant-mass spectra (see Ref. [200] for instance).

The system size dependence provides effective information to obtain further understanding of the kaonic nuclei. As summarized in Table 5, there are several theoretical calculations of the mass number ( $A$ ) dependence of the light kaonic nuclei with the different  $\bar{K}N$  interaction models. In the calculations, the values are widely spread but all the results show larger binding energies with larger  $A$ . Therefore, a systematic study of the mass number dependence of the kaonic nuclei will provide significant information on the  $\bar{K}N$  interaction below the mass threshold, and will be a good touchstone to establish the few-body calculations including the three-body problem. Form factor and decay-branching ratio measurements will also shed light on the internal structure of the kaonic nuclei, which is predicted to be compact and thus to form high density matter due to the strong attraction of the  $\bar{K}N$  interaction. A few-body calculation recently indicated that the  $\bar{K}NNNN$  ( $A = 4$ ) system has the largest central density of approximately  $0.7 \text{ fm}^{-3}$  in light kaonic nuclei up to the  $\bar{K}NNNNNN$  ( $A = 6$ ) systems [173]. The spin and parity measurements are also crucial to understand whether or not the observed “kaonic nuclei” are the theoretically predicted objects. To these ends, a new experiment with a new large  $4\pi$  spectrometer equipped with neutral-particle detectors has been proposed to perform systematic measurements of light kaonic nuclei, from the most fundamental “ $\bar{K}N$ ” state (*i.e.*, the  $\Lambda(1405)$  state) to the “ $\bar{K}NNNN$ ” state via the  $(K^-, N)$  reactions [201].

Table 5: Summary of theoretical calculations on light kaonic nuclear states.

	Ref. [82, 163]		Ref. [170]		Ref. [177]		Ref. [173]	
	$B(\text{MeV})$	$\Gamma(\text{MeV})$	$B(\text{MeV})$	$\Gamma(\text{MeV})$	$B(\text{MeV})$	$\Gamma(\text{MeV})$	$B(\text{MeV})$	$\Gamma(\text{MeV})$
$K^-pp$	48	61	40–80	40–80	16	41	26–49	31–62
$K^-pn$	-	-					25–48	32–62
$K^-ppp$	97	$\sim 24$					-	-
$K^-ppn$	108	20	90–150	20–30	19–29	31–33	-	-
$K^-pnn$	-	-					45–73	26–79
$K^-pppn$	$\sim 105$	$\sim 26$					-	-
$K^-ppnn$	86	34	120–220	10–30	-	-	68–85	28–87
$K^-pnnn$	-	-					70–87	28–87

### 3.3 Baryon-Baryon Interaction

It is important to understand the interactions between baryons in a unified way, *i.e.*,  $B_8B_8$  interaction under  $SU(3)_f$ . The  $B_8B_8$  interactions are decomposed to the following six multiplets by  $SU(3)_f$ :

$$\mathbf{8} \otimes \mathbf{8} = \mathbf{27} \oplus \mathbf{8}_s \oplus \mathbf{1} \oplus \overline{\mathbf{10}} \oplus \mathbf{10} \oplus \mathbf{8}_a, \quad (20)$$

where  $\mathbf{27}$ ,  $\mathbf{8}_s$ , and  $\mathbf{1}$  are symmetric under the exchange of two baryons, and  $\overline{\mathbf{10}}$ ,  $\mathbf{10}$ , and  $\mathbf{8}_a$  are asymmetric under the exchange of two baryons or more (basically two flavors of quarks). Among these,  $\mathbf{27}$  and  $\overline{\mathbf{10}}$  include  $NN$  interactions and are well known, at least phenomenologically, from many scattering experiments. Other multiplets are hyperon-nucleon ( $YN$ ) and  $YY$  interactions with newly introduced strangeness added.

According to theoretical  $B_8B_8$  interaction models based on the quark-gluon picture, the Pauli effect on quarks (quark Pauli effect) as well as color-magnetic interactions between quarks are important to produce a repulsive core [202, 203, 204]. In these models, the quark Pauli effect is strongly shown in  $\mathbf{8}_s$  (termed the Pauli forbidden state) and  $\mathbf{10}$  (almost Pauli forbidden state). For example in  $\mathbf{10}$ , the  $\Sigma^+p$  channel, where four  $u$  quarks exist, is expected to have a large repulsive core. In the  $SU(3)_f$  singlet ( $\mathbf{1}$ ), which is a part of  $\Lambda\Lambda$ ,  $\Xi N$ , and  $\Sigma\Sigma$  interactions, an attractive core rather than a repulsive core is expected to exist because the quark Pauli effect does not act and color-magnetic interaction is attractive only in this channel. As predicted by R.L. Jaffe [34], the  $H$ -dibaryon, which consists of  $uuddss$  quarks, is expected in this channel, although it has yet to be experimentally observed. Thus, observation of the  $H$ -dibaryon would be direct evidence of the attractive core and confirmation of a quark-based scenario. Measurements of its mass and width will also provide important information on the interaction.

It is difficult to realize hyperon beams and to conduct hyperon scattering experiments at low energies due to its production rate and short lifetime. The scattering data obtained are very limited; bubble chamber data in the 1970s [205, 206, 207, 208, 209, 210, 211, 212] and data using scintillating fiber or scintillating image detectors at KEK 12-GeV PS in the 1990s [213, 214, 215, 216]. Therefore,  $YN$  and  $YY$  interactions have been understood by the construction of interaction models based on the limited  $YN$  scattering data with the guide of  $SU(3)_f$  symmetry and reference to the rich data on  $NN$  scattering. On the other hand, the structure of hypernuclei such as level energies has been calculated using the constructed interactions and compared with the experimental hypernuclear spectroscopic data. Interaction models have been subsequently refined so as to reproduce experimental data on hypernuclei. Therefore, the experimental studies on hypernuclei together with the development of accurate many-body calculations are essential to achieve an understanding of the  $B_8B_8$  interaction.

The nuclear many-body effect is another subject of hypernuclear physics at J-PARC. In hypernuclei, large mixing effects due to  $\Lambda N$ - $\Sigma N$  or  $\Lambda\Lambda$ - $\Xi N$  coupling are expected because the mass differences are small: 80 and 28 MeV for  $\Lambda$ - $\Sigma$  and  $\Lambda\Lambda$ - $\Xi N$ , respectively. These mixing effects affect the energies of levels of hypernuclei and change the effective interaction in a nucleus from that of a bare interaction. Small changes of structures and interactions are interesting from a nuclear physics perspective of the many-body problem. On the other hand, understanding these changes is also very important to obtain the bare  $B_8B_8$  interaction from hypernuclear data.

In-medium hadron properties are of interest with respect to the spontaneous breaking of chiral symmetry. The hypernucleus provides one such platform for investigation. A hyperon is a different particle from a nucleon; therefore, the hyperon in the hypernucleus can be placed deep inside a nucleus and be distinguishable from other nucleons in the hypernucleus. If the hyperon properties in a hypernucleus can be measured and compared with those in free space, then a possible change of the baryon properties in a nuclear medium can be investigated.

Detailed investigations on  $\Lambda$  hypernuclei with  $S = -1$  have become possible with high intensity beams, especially that of  $K^-$  at the HEP. In  $\gamma$ -ray spectroscopy experiments, hypernuclear  $\gamma$ -rays are measured by Ge-detectors in coincidence with the production of hypernuclei identified via the  $(K^-, \pi^-)$

reaction by magnetic spectrometers. From such detailed investigations of  $\Lambda$  hypernuclei, information not only on  $\Lambda N$  interactions including spin-dependence, but also on the nuclear many-body effects could be obtained. Full-scale investigations on the  $S = -2$  systems, *i.e.*, double- $\Lambda$  hypernuclei,  $\Xi$  hypernuclei, and  $S = -2$  exotic systems have begun. Studies on those systems produced and identified by the  $(K^-, K^+)$  reaction will provide important information on  $\Lambda\Lambda$ ,  $\Xi N$ , and  $\Xi N \rightarrow \Lambda\Lambda$  interactions, and  $H$ -dibaryons in  $SU(3)_f$  singlet channel.

Recent developments of experimental techniques, such as fine segmented detectors with high-rate abilities and high-speed data acquisition (DAQ) systems, enable direct hyperon scattering experiments to be performed. Scattering events are identified kinematically without treatment of the image data as with a bubble chamber; therefore, high statistics data can be obtained in such modern experiments. At J-PARC, the  $\Sigma^\pm$ -proton scattering experiment is currently in progress.

### 3.3.1 Neutron-rich $\Lambda$ hypernuclei

Neutron-rich  $\Lambda$  hypernuclei are one of main research objects of the  $S = -1$  hypernuclear system at J-PARC. For the  $\Lambda$  hypernuclei, the structure change of the core nucleus was already observed in the  ${}^7_\Lambda\text{Li}$  hypernucleus [217]. Such a change results from the attractive  $\Lambda N$  interaction (glue-like role of  $\Lambda$ ). In addition to the glue-like role of  $\Lambda$ , the effect of the  $\Lambda$ - $\Sigma$  mixing may be enhanced in neutron-rich  $\Lambda$  hypernuclei. Although  $\Lambda$  and  $\Sigma$  are not mixed in free space,  $\Sigma$  may appear in nuclei as an intermediate state of  $\Lambda N$ ,  $\Lambda NN$ , etc., through the  $\Sigma N$ - $\Lambda N$  coupling. However  $\Sigma$ -mixing in the  $\Lambda$  hypernuclear state with zero isospin ( $N = Z$ ) core nucleus is forbidden without exciting the core nucleus, and thus the mixing is largely suppressed. Conversely, in the case of a neutron-rich  $\Lambda$  hypernucleus, the mixing effect is expected to be enhanced because of the large isospin value of the core nucleus. Potential information in the neutron-rich environment is closely related to an equation of states (EOS) for high-density neutron matter, which could provide a deeper understanding of the inside of neutron stars.

Neutron-rich  $\Lambda$  hypernuclei can be produced by double charge exchange (DCX) reactions such as the  $(\pi^-, K^+)$  and  $(K^-, \pi^+)$ . In these reactions, two protons are converted to a  $\Lambda$  and a neutron. The  $(e, e'K^+)$  reaction, in which a proton is converted to a  $\Lambda$ , can also produce neutron-rich  $\Lambda$  hypernuclei. However the DCX reactions can produce  $\Lambda$  hypernuclei more far from  $N = Z$  nuclei than the  $(e, e'K^+)$  reaction. Reaction mechanism is also in discussion for the  $\Lambda$  hypernuclear production via the DCX reaction. Two different mechanisms have been proposed. One is a two-step process that consists of two sequential reactions of the  $\Lambda$  production and the charge exchange reaction;  $\pi^- + (pp) \rightarrow \pi^0 + (pn) \rightarrow K^+ + (\Lambda n)$  or  $\pi^- + (pp) \rightarrow K^0 + (\Lambda p) \rightarrow K^+ + (\Lambda n)$ . The other is a single-step process in which a  $\Sigma^-$  admixture in the  $\Lambda$  hypernuclear state appears due to  $\Sigma^- p$ - $\Lambda n$  coupling (the so-called  $\Sigma$ -doorway reaction). In the former case, the production cross section is expected to peak at 1.05 GeV/ $c$  based on the  $\Lambda$  production process. While it is expected to show the similar dependence with the  $\Sigma$  production in the latter case.

In the previous experiment at KEK (KEK-PS E521),  ${}^{10}_\Lambda\text{Li}$  was attempted to produce using the  ${}^{10}\text{B}(\pi^-, K^+)$  reaction [218]. Clear signal events were observed in the bound region, although its production cross section was obtained to be very small of  $11.3 \pm 0.3$  nb/sr at 1.2 GeV/ $c$ . This value is three-orders of magnitude smaller than that by the  $(\pi^+, K^+)$  reaction ( $\sim 10$   $\mu\text{b/sr}$ ). A comparison of the production cross sections at 1.05 and 1.2 GeV/ $c$ , suggested that the single-step process is favored which is consistent with theoretical calculations [219].

The J-PARC E10 experiment was planned to measure  ${}^6_\Lambda\text{H}$  and  ${}^9_\Lambda\text{He}$  hypernuclei using  ${}^6\text{Li}$  and  ${}^9\text{Be}$  targets, respectively, at an incident  $\pi^-$  momentum of 1.2 GeV/ $c$ . The  ${}^6_\Lambda\text{H}$  run was carried out in 2012 and 2013 at the K1.8 beamline [222, 223]. Khin Swe Myint and Y. Akaishi theoretically discussed the structure of  ${}^6_\Lambda\text{H}$  [220]. As shown in Fig. 30, unbound  ${}^5\text{H}$  ground state reported as a broad resonance state of  $1.7 \pm 0.3$  MeV [224] becomes to be bound by adding a  $\Lambda$  due to the glue-like role of  $\Lambda$ . Additional binding could occur by taking the effect of so-called “coherent  $\Sigma N$ - $\Lambda N$  coupling”, leading to  $B_\Lambda = 5.8$

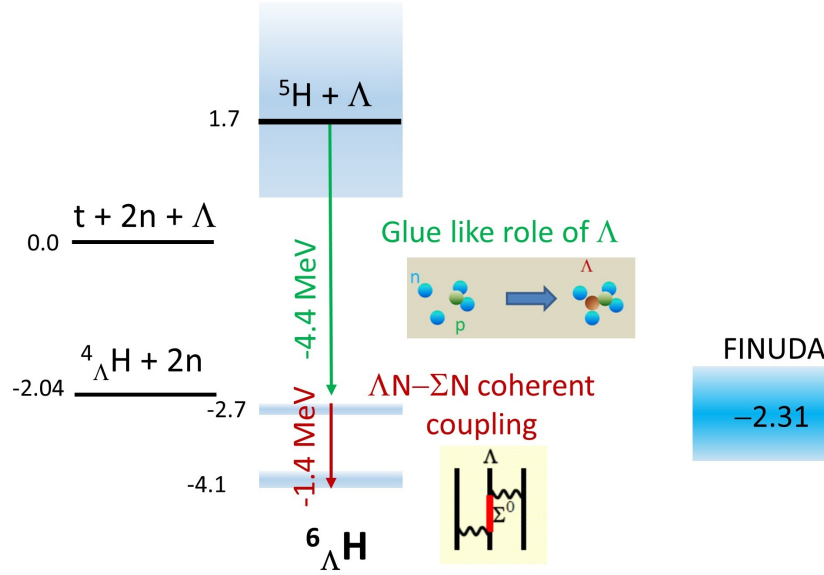


Figure 30: Expected level energy of  ${}^6_{\Lambda}\text{H}$ . Unbound  ${}^5\text{H}$  ground state becomes bound by adding a  $\Lambda$  hyperon due to glue-like role of  $\Lambda$ . Additional binding as a result of so-called “coherent  $\Sigma N$ - $\Lambda N$  coupling” is suggested by Khin Swe Myint and Y. Akaishi [220]. Result of the FINUDA experiment [221] is also drawn.

MeV with respect to the  ${}^5\text{H} + \Lambda$  system. A rather small  $B_{\Lambda}=3.83\pm 0.08\pm 0.22$  MeV was predicted by A. Gal and D. J. Millener based on shell-model calculations [225]. On the other hand, E. Hiyama *et al.* noted that the value of  $B_{\Lambda}$  is significantly affected by the spatial size of the core nucleus,  ${}^5\text{H}$ ; within the framework of the four-body cluster model that reproduce the energy and width of  ${}^5\text{H}$ , the ground state of  ${}^6_{\Lambda}\text{H}$  is obtained as a resonant state (0.87 MeV unbound above the  ${}^4_{\Lambda}\text{H} + 2n$  threshold) [226]. Therefore experimental confirmation of the existence of  ${}^6_{\Lambda}\text{H}$  and determination of its energy is important. Experimentally, the FINUDA group reported that 3 candidates of  ${}^6_{\Lambda}\text{H}$  had been observed in coincidence of the  $\pi^+$  from the  ${}^6\text{Li}(K_{\text{stopped}}^-, \pi^+){}^6_{\Lambda}\text{H}$  production with the  $\pi^-$  from  ${}^6_{\Lambda}\text{H} \rightarrow {}^6\text{He} + \pi^-$  decay [221]. The obtained averaged mass of 5801.43 MeV ( $-2.31$  MeV with respect to the  $t+2n+\Lambda$ ) indicates that the coherent  $\Sigma N$ - $\Lambda N$  coupling effect is small.

In the experiment, a high-intensity ( $1.2\text{--}1.4 \times 10^7/\text{spill}$ )  $\pi^-$  beam of 1.2 GeV/ $c$  was irradiated to the enriched  ${}^6\text{Li}$  (95.54%) target with 3.5 g/cm<sup>2</sup> in thickness. The beam  $\pi^-$ 's were measured by the K1.8 beam spectrometer, while the outgoing  $K^+$ 's were identified and analyzed by the SKS (superconducting kaon spectrometer) [12]. The missing-mass resolution was estimated to be 3.2 MeV(FWHM) from the  ${}^{12}\text{C}(\pi^+, K^+){}^{12}\text{C}$  spectrum measured with a 3.6 g/cm<sup>2</sup> graphite target. No peak was observed in the bound region of  $\Lambda$  and an upper limit of 1.2 nb/sr (90% CL) was reported in the initial paper [222]. In the improved analysis described in Ref. [223], no event was identified in the bound region or the near threshold region as shown in Fig. 31, and the upper limit was reduced to be 0.56 nb/sr (90% CL). Thus both bound and the resonance states seem not to exist, which contradicts the FINUDA result. Recently a new measurement on  ${}^5\text{H}$  resonance energy has been reported to be  $2.4\pm 0.3$  MeV [227], which is a larger value than the previously reported one of  $1.7\pm 0.3$  MeV [224]. This may lead no particle bound state of  ${}^6_{\Lambda}\text{H}$  in a naive estimation. Thus, the existence of  ${}^6_{\Lambda}\text{H}$  is still in discussion both experimentally and theoretically. Further studies on neutron-rich  $\Lambda$  hypernuclei will be carried out in future at the extended HEF.

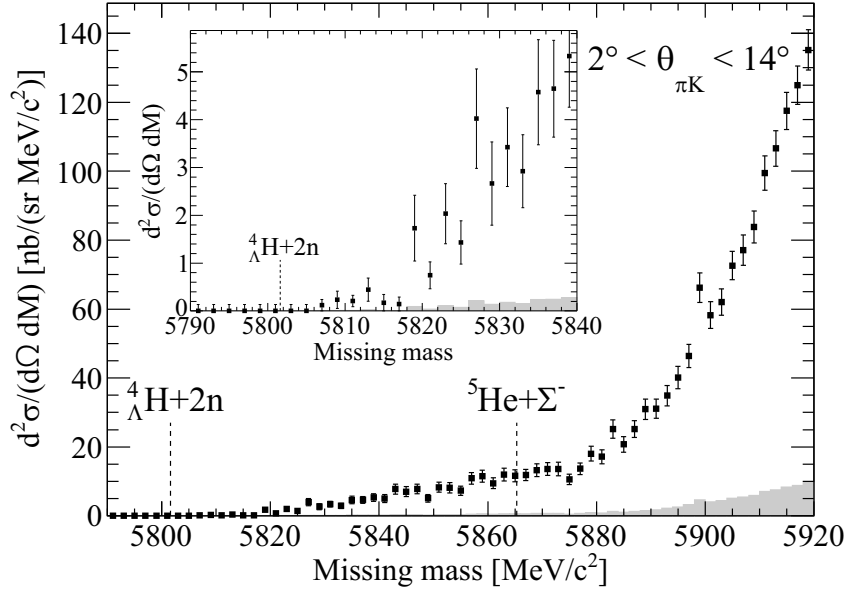


Figure 31: Missing-mass spectrum for the  ${}^6\text{Li}(\pi^-, K^+)$  reaction obtained from the improved analysis taken from Ref. [223]. No event was observed in the bound region or near the particle-bound threshold.

### 3.3.2 $\gamma$ -ray spectroscopy of $\Lambda$ hypernuclei for detailed studies on $\Lambda$ interactions

$\gamma$ -ray spectroscopy using Ge detectors is one of the most powerful methods to investigate fine structures of nuclei with a few keV or better resolution, and has revealed various many-body aspects of nuclei for many years. The first successful application of this spectroscopy method to hypernuclei have been performed at KEK-PS in 1998 [228]. Since then,  $p$ -shell  $\Lambda$  hypernuclei were intensively studied by this method at KEK-PS [228, 217, 229, 230, 231] and at BNL-AGS [232, 233, 234, 235] to obtain the spin-dependent  $\Lambda N$  effective interaction.

The  $\Lambda N$  effective interaction can be expressed as,

$$V_{\Lambda N}(r) = V_0(r) + V_\sigma(r)\mathbf{s}_N \cdot \mathbf{s}_\Lambda + V_\Lambda(r)\mathbf{l}_{N\Lambda} \cdot \mathbf{s}_\Lambda + V_N(r)\mathbf{l}_{N\Lambda} \cdot \mathbf{s}_N + V_T(r)[3(\sigma_\Lambda \cdot \hat{\mathbf{r}})(\sigma_N \cdot \hat{\mathbf{r}}) - \sigma_\Lambda \cdot \sigma_N], \quad (21)$$

where,  $\mathbf{s}_N(=\frac{1}{2}\sigma_N)$  and  $\mathbf{s}_\Lambda(=\frac{1}{2}\sigma_\Lambda)$  are the spins of a nucleon and a  $\Lambda$ , respectively, and  $\mathbf{l}_{N\Lambda}$  and  $\mathbf{r}$  are the relative angular momentum and the coordinate between a nucleon and a  $\Lambda$ , respectively. Level energies of low-laying states are primarily determined by strengths of the spin-dependent terms of Eq. 21. In the case of  $p$ -shell  $\Lambda$  hypernuclei with a  $\Lambda$  in the  $s$ -orbit and valence nucleons in the  $p$ -orbit in shell model picture, these strengths are parametrized as  $\Delta$  (spin-spin),  $S_\Lambda$  ( $\Lambda$  spin-orbit),  $S_N$  (nucleon spin-orbit), and  $T$  (tensor). These terms are defined as the radial integrals for the wave functions of a  $\Lambda$  in the  $s$ -orbit ( $s_\Lambda$ ) and a nucleon in the  $p$ -orbit ( $p_N$ ). From  $\gamma$ -ray data on  $p$ -shell  $\Lambda$  hypernuclei, these parameters were determined to be

$$\Delta = 0.43(A = 7) \text{ or } 0.33(A > 10) \text{ MeV}, \quad S_\Lambda = -0.01 \text{ MeV}, \quad S_N = -0.4 \text{ MeV}, \quad \text{and } T = 0.03 \text{ MeV},$$

although some inconsistent results were obtained for  ${}^{10}_\Lambda\text{B}$  and  ${}^{11}_\Lambda\text{B}$ . The ground state doublet spacing of  ${}^{11}_\Lambda\text{B}$  was determined to be 261 keV [230], while no  $\gamma$ -ray transition in  ${}^{10}_\Lambda\text{B}$  was observed, thus, suggesting the ground state doublet spacing of  ${}^{10}_\Lambda\text{B}$  is less than 100 keV [234]. This contradiction is thought to be due to the  $\Sigma N$ - $\Lambda N$  coupling [234, 236].

One of main goals of  $\gamma$ -ray spectroscopy of  $\Lambda$  hypernuclei at J-PARC is to extend prior studies on the effective  $\Lambda N$  spin-dependent interaction to cases other than  $p$ -shell hypernuclei. In these analysis, the strength parameters are radial integrals associated with the wave functions of  $s_\Lambda$  and the nucleons

in the outermost orbit. Thus a comparison of these parameters with those for hypernuclei of different sizes provides information on the radial dependence of each interaction term. This is also a unique test of our understanding of the  $\Lambda N$  interaction and hypernuclear structure. The  $\Sigma N$ - $\Lambda N$  coupling and the  $\Lambda NN$  three-body force are also important. The former gives rise to a mixture of  $\Lambda$  hypernuclear and  $\Sigma$  hypernuclear states and significantly affects the structure of hypernuclei. This effect is particularly important in terms of understanding the  $YN$  interaction in high-density matter. The two-body  $\Sigma N$ - $\Lambda N$  interaction can be incorporated into a two-body effective  $\Lambda N$  interaction, while the three-body  $\Lambda NN$  force due to  $\Sigma N$ - $\Lambda N$  coupling can not. Therefore it may not be possible to understand hypernuclear level energies based solely on the two-body effective interaction in Eq. 21, as suggested by the contradictory results on  ${}^{11}_{\Lambda}\text{B}$  and  ${}^{10}_{\Lambda}\text{B}$ . Thus investigations concerning the  $\Lambda NN$  three-body force are important not only to examine the three-body force itself but also to determine the strengths of the reliable two-body  $\Lambda N$  spin-dependent interactions.

Charge symmetry breaking (CSB) in the  $\Lambda N$  interaction is another important research topics. Nuclear force based on the strong interaction and nuclear system are invariant under the exchange of protons and neutrons (charge symmetry) or more generally under any rotation in the isospin space (charge independence). This approximate but basic symmetry holds almost exactly in  $NN$  interaction and ordinary nuclei, and the CSB effects are very small. For example, the binding energy difference between  ${}^3\text{H}$  and  ${}^3\text{He}$  is only 70 keV after the correction of a large Coulomb effect. In contrast, there has been a long-standing puzzle of CSB in hypernuclei. The binding energies of  $\Lambda$  on mirror  $\Lambda$  hypernuclei  ${}^4_{\Lambda}\text{H}$  and  ${}^4_{\Lambda}\text{He}$  obtained by emulsion experiments [237] have a significant difference of  $0.35 \pm 0.05$  MeV. The  $1^+-0^+$  level spacing of these mirror  $\Lambda$  hypernuclei measured by the transition  $\gamma$ -rays gives additional information on CSB effect. The  ${}^4_{\Lambda}\text{H}$   $\gamma$ -ray was measured three times [238, 239, 240] and its weighted average is  $1.09 \pm 0.02$  MeV. On the other hand, the  ${}^4_{\Lambda}\text{He}$   $\gamma$ -ray was reported only once to be  $1.15 \pm 0.04$  MeV. However, the  ${}^4_{\Lambda}\text{He}$   $\gamma$ -ray spectrum is statistically insufficient and it is claimed that the identification of the  ${}^4_{\Lambda}\text{He}$  events seems to be ambiguous. In order to confirm the reported data and to resolve the puzzle, new measurements of the  $1^+-0^+$  level spacing of  $A=4$   $\Lambda$  hypernuclei, especially for  ${}^4_{\Lambda}\text{He}$ , are both necessary and important.

The J-PARC E13 experiment was proposed to measure hypernuclear  $\gamma$ -rays from  ${}^4_{\Lambda}\text{He}$ ,  ${}^7_{\Lambda}\text{Li}$ ,  ${}^{10}_{\Lambda}\text{B}$ ,  ${}^{11}_{\Lambda}\text{B}$ , and  ${}^{19}_{\Lambda}\text{F}$ . Data on the  $s$ -shell hypernucleus,  ${}^4_{\Lambda}\text{He}$  [241], and the  $sd$ -shell hypernucleus,  ${}^{19}_{\Lambda}\text{F}$  [242], were obtained at the K1.8 beamline in 2015.

The  ${}^{19}_{\Lambda}\text{F}$  hypernucleus was produced by the  ${}^{19}\text{F}(K^-, \pi^-)$  reaction at 1.8 GeV/ $c$  with a 20 g/cm<sup>2</sup>-thick liquid CF<sub>4</sub> target. The hypernuclear states were identified by the missing mass for the reaction by analyzing the incident  $K^-$  and outgoing  $\pi^-$  using the K1.8 beam spectrometer and the SKS, respectively. The missing-mass resolution was 8.7 MeV (FWHM), which was sufficient to reject the contributions from highly excited states of  ${}^{19}_{\Lambda}\text{F}$  and background  ${}^{12}_{\Lambda}\text{C}$ . The  $\gamma$ -rays were measured in coincidence using Hyperball-J detectors [243], comprising 27 coaxial-type Ge detectors each having a crystal size of 70mm ( $\phi$ )  $\times$  70mm (length) and PWO counters for background suppression from Compton scattering in the Ge crystals and  $\pi^0 \rightarrow 2\gamma$ . After the in-beam energy calibration of the Ge detectors using a  ${}^{232}\text{Th}$  source and known  $\gamma$ -rays from the target or surrounding materials, an accuracy of 0.5 keV was achieved over the range from 0.1 to 2.5 MeV, while the energy resolution was measured to be 4.5 keV (FWHM) for 1 MeV  $\gamma$ -rays.

Figure 32 (left) presents the  $\gamma$ -ray spectrum after selecting the region associated with low-lying states of  ${}^{19}_{\Lambda}\text{F}$ . In addition to the  $\gamma$ -rays known to be emitted from ordinary nuclei, four additional  $\gamma$ -rays can be identified with energies of  $315.5 \pm 0.4$  (stat.)  ${}^{+0.6}_{-0.5}$  (syst.),  $895.2 \pm 0.3$  (stat.)  $\pm 0.5$  (syst.),  $952.8 \pm 1.2$  (stat.)  ${}^{+0.5}_{-0.6}$  (syst.), and  $1265.6 \pm 1.2$  (stat.)  ${}^{+0.7}_{-0.5}$  (syst.) keV. Assuming a weak-coupling between a  $\Lambda$  and a core nucleus and taking into account the expected cross sections of the excited states, a level structure of  ${}^{19}_{\Lambda}\text{F}$  is reconstructed and  $\gamma$ -ray transitions are assigned as shown in Fig. 32 (right).

The energy spacing of the ground-state doublet is primarily determined by the  $\Lambda N$  spin-spin interaction and is of great interest as discussed. The obtained spacing value of 316 keV is in good agreement

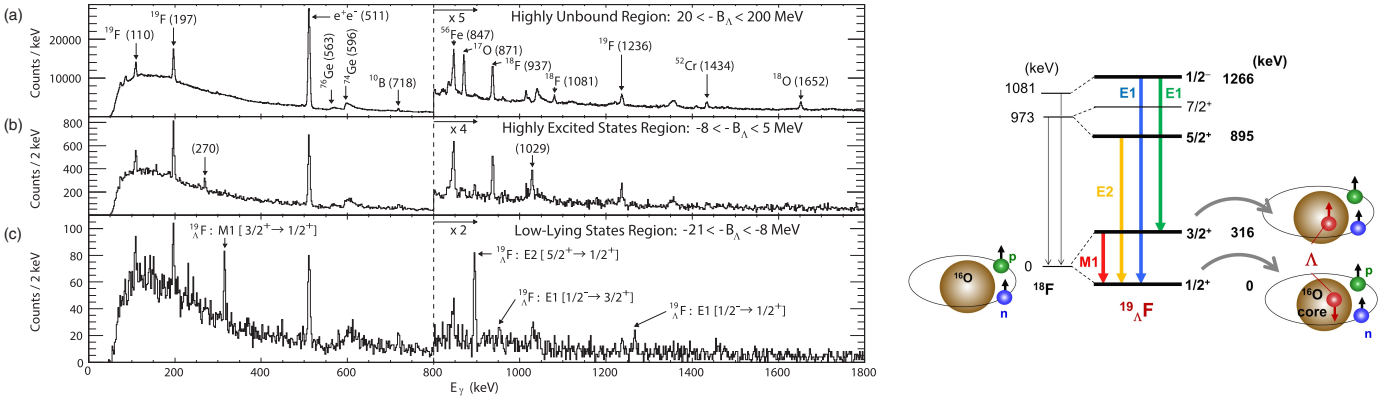


Figure 32:  $\gamma$ -ray spectra gated by  $\Lambda$  binding energy ranges in the missing mass of the  $^{19}\text{F}(K^-, \pi^-)$  reaction, showing (a) the highly unbound region ( $20 < -B_\Lambda < 200$  MeV), (b) the region associated with highly excited states ( $-8 < -B_\Lambda < 5$  MeV), (c) the region associated with low-lying states ( $-21 < -B_\Lambda < -8$  MeV). The figure is taken from Ref. [242] (left). A reconstructed level scheme of  $^{19}\Lambda\text{F}$  with the assigned  $\gamma$ -ray transitions (right).

with two independent shell-model calculations. D. J. Millner predicted value of 305 keV based on the phenomenological spin-dependent  $\Lambda N$  interaction strengths obtained from  $p$ -shell  $\Lambda$  hypernuclear data [244]. On the other hand, the shell model calculation by A. Umeya and T. Motoba using the effective  $\Lambda N$  interaction by G-matrix method based on Nijmegen SC97e and SC97f interactions [245] provides 419 and 245 keV, respectively [246]. A spacing of 346 keV is expected when the spin-spin interaction is adjusted by mixing the SC97e and SC97f interactions to reproduce the energy spacing of 692 keV for the  $p$ -shell hypernucleus,  $^7_\Lambda\text{Li}$ . The agreement between these values indicates that the theoretical framework and  $\Lambda N$  interaction as an input are good even for heavier hypernuclei.

The  $\gamma$ -ray from  $^4_\Lambda\text{He}$  was measured in a similar way as the  $\gamma$ -rays from  $^{19}\Lambda\text{F}$ . The  $^4_\Lambda\text{He}$  was produced and identified by the  $(K^-, \pi^-)$  reaction on a 2.8 g/cm<sup>2</sup>-thick liquid He target. An incident momentum of 1.5 GeV/ $c$  was chosen to populate the spin-flip  $1^+$  state as much as possible considering the spin-flip amplitude of the elementary  $K^+ + n \rightarrow \pi^- + \Lambda$  process and the beam intensity available at the K1.8 beamline. The  $^4\text{He}(K^-, \pi^-)$  missing-mass spectrum is shown in Fig. 33 (left), and exhibits a peak corresponding to the  $^4_\Lambda\text{He}$  bound states ( $0^+$  and  $1^+$ ). By selecting events in the  $\Lambda$  bound region,  $-4$  MeV  $<$  excitation energy  $<$  +6 MeV, the  $\gamma$ -ray spectra were obtained as shown in Fig. 33 (right top and bottom), for which an event-by-event Doppler-shift correction has and has not been applied, respectively. A 1406-keV peak is clearly visible after the Doppler-shift correction, which is consistent with M1 transition. Thus the excitation energy of the  $^4_\Lambda\text{He}$   $1^+$  state was precisely determined to be  $1.406 \pm 0.002$  (stat.)  $\pm 0.002$  (syst.) MeV, by taking the nuclear recoil effect of 0.2 keV into account.

This value for  $^4_\Lambda\text{He}$  is obviously larger than that for  $^4_\Lambda\text{H}$  ( $1.09 \pm 0.02$  MeV). This result clearly indicates the existence of a large CSB in the  $\Lambda N$  interaction. Combining this result with the  $\Lambda$  binding energies ( $B_\Lambda$ s) of the ground states from the past emulsion data [237], the  $B_\Lambda$  of the  $1^+$  state of  $^4_\Lambda\text{He}$  is  $0.98 \pm 0.03$  MeV as shown in Fig. 34. Comparing the present updated value for  $B_\Lambda$  and those reported for the  $1^+$  and  $0^+$  states of the mirror  $\Lambda$  hypernuclei, the  $B_\Lambda$  difference for the  $1^+$  states is  $0.03 \pm 0.05$  MeV, which is much smaller than that for the  $0^+$  state ( $0.35 \pm 0.05$  MeV). Therefore, the CSB effect is found to be strongly spin dependent. This fact would provide a key to resolve the puzzle for a large CSB in  $\Lambda$  hypernuclei and to elucidate the underlying  $\Lambda N$  interaction.

It should be noted that the efforts to confirm and improve the experimental data have been also performed at other facilities in order to clarify the CSB effect in  $\Lambda$  hypernuclei and to investigate its origin. The  $\pi^-$  momentum in the  $^4_\Lambda\text{H} \rightarrow ^4\text{He} + \pi^-$  weak decay was precisely measured at MAMI-C [247], and  $B_\Lambda$  of the  $0^+$  state of  $^4_\Lambda\text{H}$  was obtained to be  $2.12 \pm 0.01$  (stat.)  $\pm 0.09$  (syst.) MeV, which is consistent

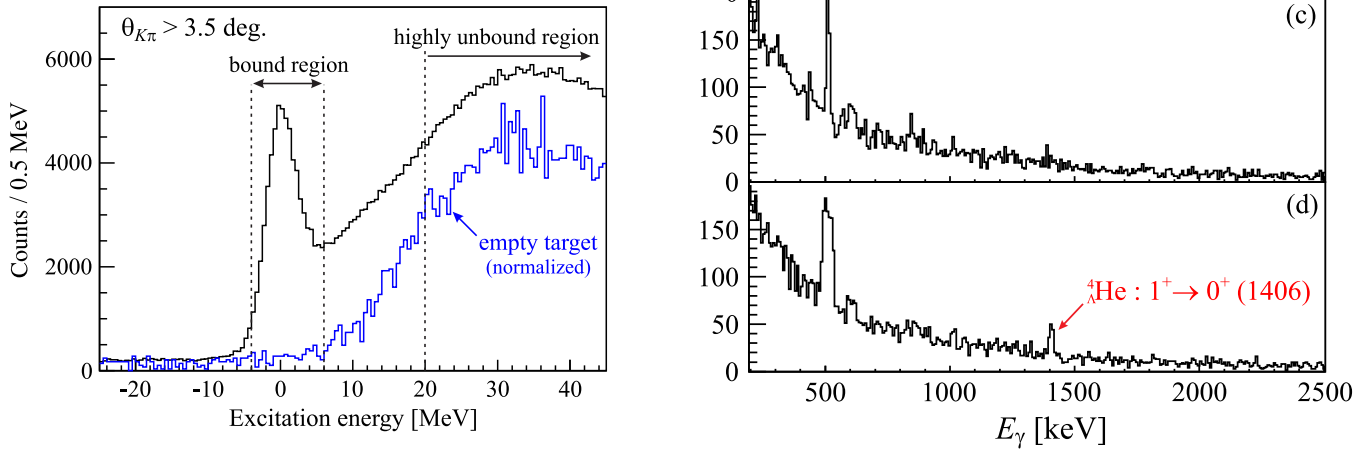


Figure 33: Missing-mass spectrum for the  ${}^4\text{He}(K^-, \pi^-)$  reaction (left). A peak shows the production of bound states for  ${}^4_{\Lambda}\text{He}$ . (black), while no peak exists in the empty target run (blue). The  $\gamma$ -ray spectra obtained by selecting events in the bound region in the left spectrum without (right top) and with (right bottom) a Doppler shift correction, respectively. The figures are taken from Ref. [241].

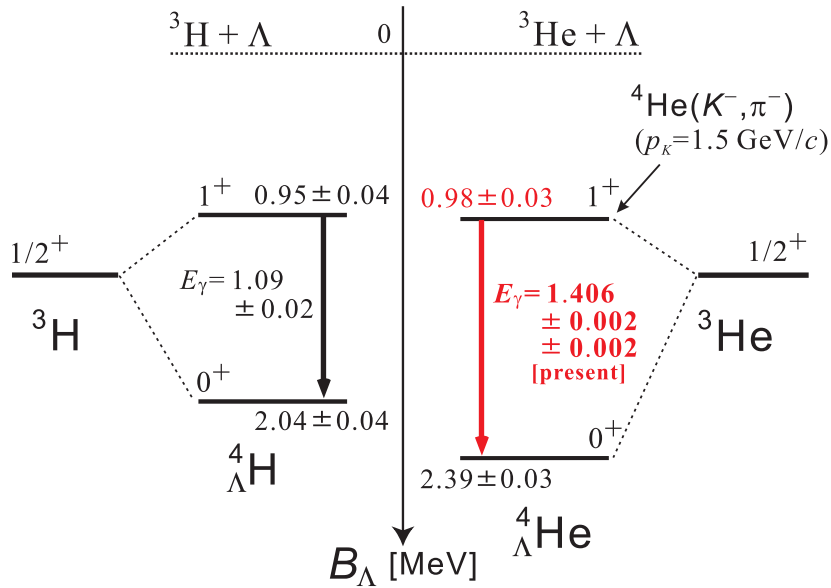


Figure 34: Level scheme for the mirror  $\Lambda$  hypernuclei,  ${}^4_{\Lambda}\text{H}$  and  ${}^4_{\Lambda}\text{He}$ .  $\Lambda$  binding energies ( $B_{\Lambda}$ ) for the ground states of  ${}^4_{\Lambda}\text{H}$  and  ${}^4_{\Lambda}\text{He}$  are taken from the emulsion data [237]. The  $B_{\Lambda}$  for the  $1^+$  state of  ${}^4_{\Lambda}\text{H}$  was obtained using  $B_{\Lambda}$  for the ground state of  ${}^4_{\Lambda}\text{H}$  and the weighted average of the  $\gamma$ -ray energies measured in past experiments [238, 239, 240]. The figure is taken from Ref. [241].

with the emulsion data. On the other hand, at Jefferson Lab, the  $B_\Lambda$  for the  ${}^7_\Lambda\text{He}$  ground state was measured by the  ${}^7\text{Li}(e, e'K^+)$  reaction and  $B_\Lambda$  values for the iso-triplet states of  $A = 7$   $\Lambda$  hypernuclei ( ${}^7_\Lambda\text{He}$ ,  ${}^7_\Lambda\text{Li}^*$ , and  ${}^7_\Lambda\text{Be}$ ) were compared [248]. Ref. [249] summarizes  $B_\Lambda$  values for  $A \leq 16$   $\Lambda$  hypernuclei iso-multiplets including the results from the FINUDA experiment. These results suggest very small CSB effects in the  $p$ -shell  $\Lambda$  hypernuclei.

At J-PARC, a measurement of  $\gamma$ -ray resulting from  $1^+ \rightarrow 0^+$  transition on  ${}^4_\Lambda\text{H}$  is planned as a new experiment, E63, which will be performed using the Hyperball-J and the SKS at the K1.1 beamline [250].  ${}^4_\Lambda\text{H}$  hypernuclei are produced by the  $(K^-, \pi^-)$  reaction on  ${}^7\text{Li}$  (or natural metal Li) target at 0.9 GeV/ $c$  as a fragment from the highly excited states of  ${}^7_\Lambda\text{Li}^*$ . In the previous experiment, a 1.1 MeV  $\gamma$ -ray peak was observed by selecting the highly unbound region (excitation energy  $E_x=22 - 33$  MeV) of  ${}^7_\Lambda\text{Li}$  produced by the  $(K^-, \pi^-)$  reaction at 0.83 GeV/ $c$  [251]. The fragment production process,  ${}^7_\Lambda\text{Li}^* \rightarrow {}^4_\Lambda\text{H} + {}^3\text{He}$ , gives a larger recoil velocity of  ${}^4_\Lambda\text{H}$  than that for  ${}^7_\Lambda\text{Li}^*$  produced via the  $(K^-, \pi^-)$  reaction, and the Doppler broadening can not be corrected for. However, this effect can be reduced by selecting  ${}^7_\Lambda\text{Li}^*$  events close to the  ${}^4_\Lambda\text{H}^* + {}^3\text{He}$  decay threshold in the missing-mass spectrum.

### 3.3.3 Investigation of in-medium $\Lambda$ properties by $\gamma$ -ray spectroscopy of $\Lambda$ hypernuclei

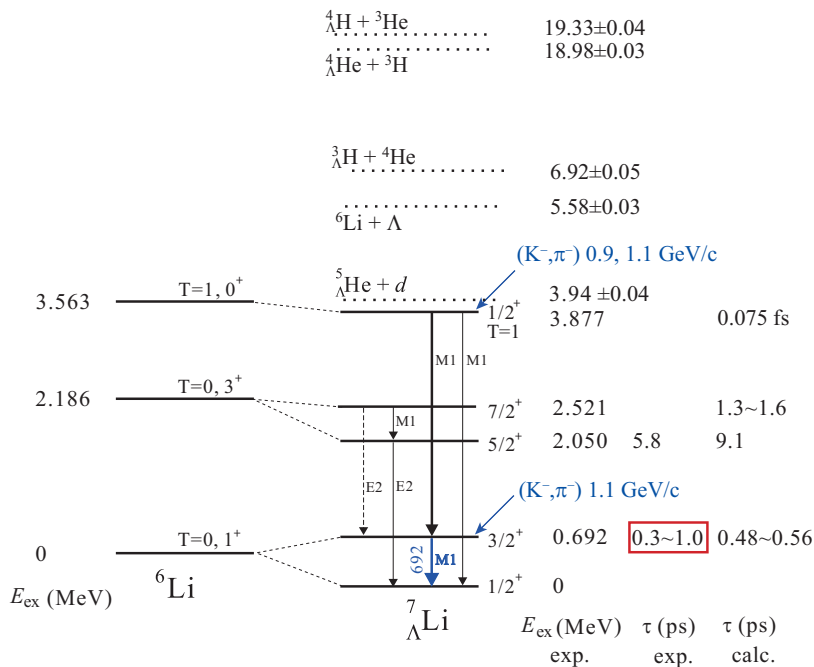


Figure 35: Level scheme of  ${}^7_\Lambda\text{Li}$  hypernucleus. The excitation energies of all bound states are experimentally determined [228, 233]. The lifetime of the  $3/2^+$  state shown in the red square will be precisely measured from the  $\gamma$ -ray peak shape for the  $M1(3/2^+ \rightarrow 1/2^+)$  transition shown in blue using the  $(K^-, \pi^-)$  reaction at 0.9 or 1.1 GeV/ $c$  [252]. The figure is taken from the E63 proposal [250].

In the E63 experiment which is a revised version of the E13 experiment,  $\gamma$ -rays from the  ${}^7_\Lambda\text{Li}$  ground state doublet transition will also be measured in order to derive the transition probability of a M1 transition ( $B(M1)$ ) and to examine the possible change of the  $g$ -factor of a  $\Lambda$  in a nucleus. In the picture of the constituent quark models, where the magnetic moment of baryons is well described as a sum of a magnetic moment of a Dirac particle with a constituent quark mass, the magnetic moment of the baryons may change, if the constituent mass is modified in a nucleus. A  $\Lambda$  hyperon in a  $\Lambda$  hypernucleus is the best probe to investigate whether such a change really occurs or not.

Instead of the direct measurement on the magnetic moment of a  $\Lambda$  hypernucleus, which is extremely difficult due to a short lifetime for spin precession, the  $g$ -factor of the  $\Lambda$  in the nucleus will be derived from the probability of a  $\Lambda$  spin-flip transition. Because the level scheme of  ${}^7_\Lambda\text{Li}$  has been well established experimentally as shown in Fig. 35 [228, 233], the best target is the ground-state doublet of  ${}^7_\Lambda\text{Li}$ . In the ground-state doublet of  ${}^7_\Lambda\text{Li}$ , spin directions of the  $\Lambda$  of two members are opposite each other to the spin direction of the core nucleus and the  $3/2^+ \rightarrow 1/2^+$  transition corresponds to a spin-flip of the  $\Lambda$ . In a weak coupling limit between the  $\Lambda$  and the core nucleus, the  $B(M1)$  value of such a transition can be expressed as [253],

$$\begin{aligned}
B(M1) &= (2J_{up} + 1)^{-1} |\langle \phi_{low} \| \boldsymbol{\mu} \| \phi_{up} \rangle|^2 \\
&= (2J_{up} + 1)^{-1} |\langle \phi_{low} \| g_c \mathbf{J}_c + g_\Lambda \mathbf{J}_\Lambda \| \phi_{up} \rangle|^2 \\
&= (2J_{up} + 1)^{-1} |\langle \phi_{low} \| g_c \mathbf{J} + (g_\Lambda - g_c) \mathbf{J}_\Lambda \| \phi_{up} \rangle|^2 \\
&= \frac{3}{8\pi} \frac{(2J_{low} + 1)}{(2J_c + 1)} (g_c - g_\Lambda)^2,
\end{aligned} \tag{22}$$

where  $g_c$  and  $g_\Lambda$  denote the effective  $g$ -factors of the core nucleus and the  $\Lambda$ , respectively.  $\mathbf{J}_c$  and  $\mathbf{J}_\Lambda$  denote their spins, and  $\mathbf{J} = \mathbf{J}_c + \mathbf{J}_\Lambda$  is the spin of the  $\Lambda$  hypernucleus. The spatial components of the wave functions for the lower and upper states of the doublet,  $\phi_{low}$  with spin  $J_{low}$  and  $\phi_{up}$  with spin  $J_{up}$ , are assumed to be identical. The reduced transition probability  $B(M1)$  can be derived from the lifetime  $\tau$  of the upper state as,

$$1/\tau = \frac{16\pi}{9} E_\gamma^3 B(M1), \tag{23}$$

where  $E_\gamma$  is the energy of transition  $\gamma$ -rays. The lifetime can be determined using Doppler shift attenuation method (DSAM) which was successfully applied to obtain  $B(E2)$  for the  $5/2^+ \rightarrow 1/2^+$  transition of  ${}^7_\Lambda\text{Li}$  in the previous experiment [217]. In order to apply the DSAM, the stopping time  $t_{stop}$  of the produced excited states of the  $\Lambda$  hypernucleus in the target material should be on the same order as its lifetime  $\tau$ . According to a simulation, this lifetime can be determined most precisely when the stopping time is 2 – 3 times longer than the lifetime. Barring any anomalous effects, the lifetime of the  $3/2^-$  state is estimated to be very short, on the order of  $\sim 0.5$  ps. Therefore a high-density  $\text{Li}_2\text{O}$  target of  $2.01 \text{ g/cm}^3$  will be used.

The  $3/2^+$  state of  ${}^7_\Lambda\text{Li}$  is produced by the  $(K^-, \pi^-)$  reaction at 1.1 or 0.9 GeV/ $c$ . The 1.1 GeV/ $c$  is the best suited to directly populate the spin-flip  $3/2^+$  state, due to the large spin-flip amplitude of the elementary process at finite angles. The highest  $K^-$  beam intensity can be also obtained at 1.1 GeV/ $c$ . Another option is the 0.9 GeV/ $c$ , at which the elementary process has the largest non-spin-flip amplitude to produce the  $1/2^+(T = 1)$  state and feeding process of  $1/2^+(T = 1) \rightarrow 3/2^+$ , although the  $K^-$  beam intensity is lower than that at 1.1 GeV/ $c$ . The beam momentum will be determined by taking pilot data to investigate yields and background levels.

### 3.3.4 Hyperon-Nucleon scattering

There had been long discussions on the existence of  $\Sigma$  hypernuclei and their widths. The BNL-AGS E905 experiment showed that a  $\Sigma$ -bound state exists in the isospin  $I = 1/2$  channel ( ${}^4_\Sigma\text{He}$ ), while no bound state exists in the  $I = 3/2$  channel for the  $A = 4$  system, by comparing the  ${}^4\text{He}(K^-, \pi^\pm)$  spectra [254]. Thus,  $\Sigma$ -nucleus potential turned out to have a large isospin dependence (Lane-term) and to be repulsive in isospin average. The spectra for quasi-free  $\Sigma$  production on medium-to-heavy nuclear targets also support a repulsive  $\Sigma$  potential [255, 256]. Therefore, quantitative information on  $\Sigma$  potential and  $\Sigma N$  interaction can not be extracted via the spectroscopic methods. Thus direct scattering experiments of  $\Sigma$  hyperons yielding high statistics data set have been desired.

The  $\Sigma^+ p$  channel can be simply described by two multiplets of **27** and **10** in Eq. 20. In the case of the S-wave interaction that is dominant in the low-energy region, the spin singlet state ( ${}^1S_0$ ) can be

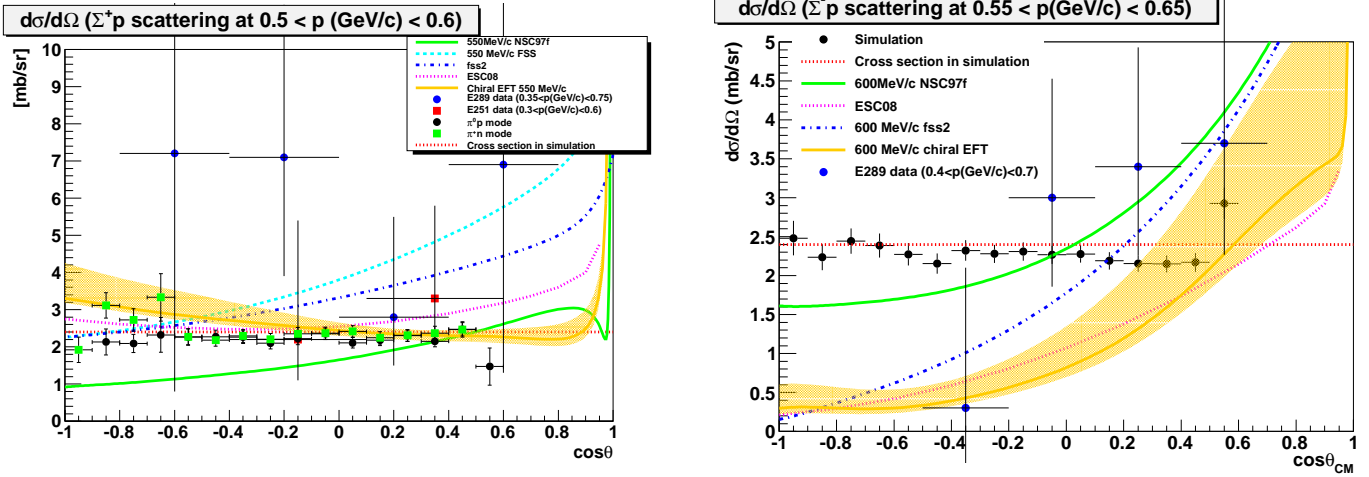


Figure 36: Simulated differential cross sections showing the expected experimental errors taken from the presentation by K. Miwa at HYP2015 [257]. (Left)  $\Sigma^+p$  elastic channel of the  $\Sigma^+$  momentum from 0.5 to 0.6 GeV/c for the  $55 \times 10^6$  tagged  $\Sigma^+$  beam. The black circles and green squares represent the results for the  $p\pi^0$  and  $n\pi^+$  decay modes, respectively, assuming the cross section with a flat angular distribution shown by a red dotted line. The blue circles and red squares are the experimental data obtained in the KEK-PS E289 [215] and the KEK-PS E251 [213], respectively. The additional curves present the theoretical predictions for meson exchange models, NSC97a (green solid) [245] and ESC08 (magenta dotted) [258], quark cluster models, FSS (light blue dotted) [259] and fss2 (blue dotted) [260]. The orange band indicates the prediction by chiral effective theory [261]. (Right)  $\Sigma^-p$  elastic channel of the  $\Sigma^-$  momentum from 0.45 to 0.55 GeV/c for the  $16 \times 10^6$  tagged  $\Sigma^-$  beam. The black circles show the results assuming the cross section with a flat angular distribution shown by the red dotted line. The blue circles show the experimental data obtained in the KEK-PS E289 [214]. The additional curves and the band present the same information as those in the left figure.

described by **27** which is the same multiplet as appeared in the  $NN(I = 1)$  channel, and is well known at least phenomenologically based on a substantial quantity of  $NN$  data. The spin triplet state ( ${}^3S_1$ ) can be described by **10** which is almost Pauli forbidden state. Considering the spin-weight factors, the  $\Sigma^+p$  channel is expected to be quite repulsive because of the almost Pauli forbidden state as previously discussed. As shown in Fig. 36 (left), theoretical models based on meson exchange (Nijmegen models NSC97f [245] and NSC08 [258]) and quark cluster models which include an explicit quark degree of freedom in the short range part (FSS [259] and fss2 [260]) predict very different cross sections. The  $\Sigma^+p$  data can be used to determine which model is superior and whether or not our current understanding of quark-based picture in the short range part is correct. In addition, a large core radius can also be confirmed from the energy dependence of the differential cross sections at  $90^\circ$ , as R. Jastrow applied to the  $pp$  scattering data and estimated a hard core radius of nuclear force [262].

Assuming isospin symmetry, the  $\Sigma^+p$  and  $\Sigma^-n$  interactions should be the equivalent except for the contribution of the electromagnetic interaction. Therefore the experimental measurements on the strength on the repulsive force between  $\Sigma^+$  and proton is essential information on constructing EOS for high density neutron star matter. In such a high-density neutron star matter, negatively charged particles can reduce the large Fermi energies of electrons (and neutrons) via the so-called hyperionization process. The  $\Sigma^-$  potential, the primary component of which is the  $\Sigma^-n$  interaction, determines whether  $\Sigma^-$  hyperons emerge in the core of a neutron star and, if so, at what density.

The J-PARC E40 experiment aims to measure  $\Sigma^\pm p$  elastic scattering and  $\Sigma^-p \rightarrow \Lambda n$  conversion with high statistics using the modern techniques. Figure 36 shows the expected statistical errors in the differential cross sections for  $\Sigma^+p$  (left) and  $\Sigma^-p$  (right) elastic scattering estimated by simulations assuming the cross section with a flat angular distribution shown by the red dotted lines. In this experiment,  $\Sigma^\pm$  hyperons are produced using high intensity  $\pi^\pm$  beams via the  $p(\pi^\pm, K^+)\Sigma^\pm$  reactions on a liquid hydrogen target at the incident momenta of 1.4 GeV/ $c$  for  $\pi^+$  and 1.32 GeV/ $c$  for  $\pi^-$  and identified by the K1.8 beam and KURAMA spectrometers. In these kinematics,  $\Sigma$  momentum ranges from 0.45 to 0.85 GeV/ $c$ .  $\Sigma$  hyperons are scattered by protons in the same liquid hydrogen target. Charged particles are produced by the reactions, then their decays are measured by a detector system surrounding the target which is called a cylindrical active tracker and calorimeter system for hyperon-proton scattering (CATCH) [263]. The CATCH detector consists of a cylindrical fiber tracker with 6 straight and 6 spiral layers of scintillation fibers for trajectory measurements and BGO calorimeters for energy measurements, as shown in Fig. 37. Secondary reactions such as elastic scattering and conversion process are kinematically identified from  $\Sigma$  momentum vectors using magnetic spectrometers, the energy and direction of each charged particles measured using CATCH.

Commissioning of the beamline and the spectrometer system for the E40 experiment was carried out in February 2017. In total  $\sim 17 \times 10^6$  tagged  $\Sigma^-$  data for the  $\Sigma^-p$  mode were obtained using  $1.96 \times 10^7$   $\pi^-$  per spill beam in June 2018, February and March 2019. About a half of the  $\Sigma^+p$  data ( $\sim 40 \times 10^6$  tagged  $\Sigma^+$ ) were also taken using  $1.9 \times 10^7$   $\pi^+$  per spill beam in April 2019, while the remaining  $\Sigma^+p$  data will be taken in March 2020. The analysis of the scattering events is in progress. Thus high-statistic cross section data including their angular distributions will be reported in the near future.

### 3.3.5 Double- $\Lambda$ hypernuclei

To date, there has been only limited information available regarding the  $B_8B_8$  interaction and the hadron system with  $S = -2$ . The  $\Lambda\Lambda$  and  $\Xi N$  interactions as well as  $\Xi N \rightarrow \Lambda\Lambda$  conversion interaction must be determined experimentally including the spin and/or isospin dependence. Five experiments aiming to investigate the  $S = -2$  system and to obtain these  $B_8B_8$  interactions in the  $S = -2$  channel have been approved at J-PARC; a photographic emulsion experiment (E07), missing-mass spectroscopy of the  ${}^{12}_{\Xi}\text{Be}$  hypernucleus (E05 and E70), X-ray spectroscopy of  $\Xi^-$ -Fe atom (E03), and a search for the  $H$ -dibaryon (E42) (as already discussed in Sec. 3.1.2). Each of these experiments requires a high-

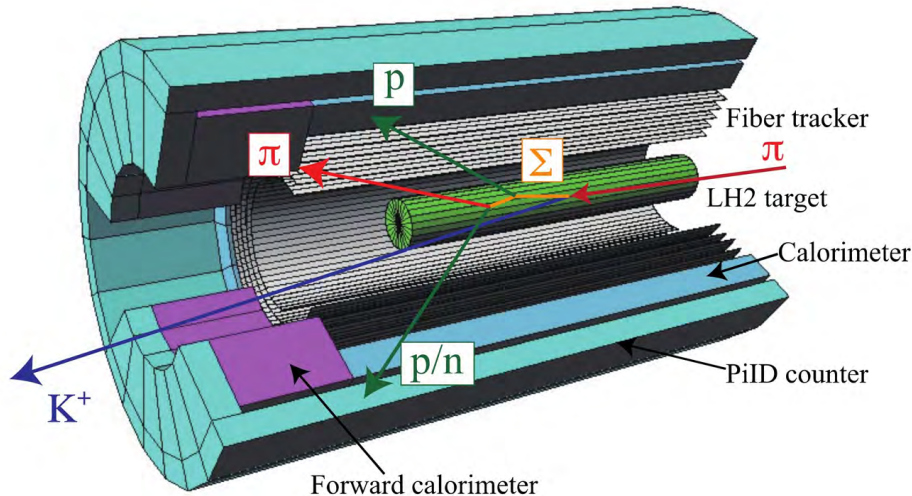


Figure 37: Schematic drawing of CATCH detector for the  $\Sigma^\pm p$  scattering experiment.

intensity 1.8 GeV/c  $K^-$  beam at the K1.8 beamline to produce the  $S = -2$  system via the  $(K^-, K^+)$  reaction. Some of these have already been carried out.

Since a  $\Lambda$  hyperon can not be used as a fixed target due to its very short lifetime, a direct  $\Lambda\Lambda$  scattering experiment can not be carried out. Therefore, spectroscopic studies on double- $\Lambda$  hypernuclei, in which two  $\Lambda$  hyperons are embedded in nuclei, are possible ways to investigate the  $\Lambda\Lambda$  interaction except for using final state interaction (FSI) or the measurements of the  $\Lambda\Lambda$  momentum-correlation in heavy ion collision which was successfully done recently [264]. The  $\Lambda\Lambda$  interaction strength in the double- $\Lambda$  hypernucleus  ${}_{\Lambda\Lambda}^AZ$  is often expressed in terms of  $\Delta B_{\Lambda\Lambda}({}_{\Lambda\Lambda}^AZ)$ . This can be deduced from the masses of the double- $\Lambda$  and single- $\Lambda$  hypernuclei, and is defined as

$$\Delta B_{\Lambda\Lambda}({}_{\Lambda\Lambda}^AZ) = B_{\Lambda\Lambda}({}_{\Lambda\Lambda}^AZ) - 2B_{\Lambda}({}_{\Lambda}^{A-1}Z), \quad (24)$$

where  $B_{\Lambda\Lambda}$  and  $B_{\Lambda}$  are the binding energies of two  $\Lambda$  hyperons in the double- $\Lambda$  hypernucleus and a  $\Lambda$  hyperon in the single- $\Lambda$  hypernucleus, respectively.

The double- $\Lambda$  hypernucleus was first reported by M. Danysz *et al.* as an event with a topology of sequential weak decays in the nuclear emulsion [265]. This event was interpreted as a  ${}_{\Lambda\Lambda}^{10}\text{Be}$  or  ${}_{\Lambda\Lambda}^{11}\text{Be}$ , indicating a relatively strong attractive force between  $\Lambda$  hyperons of  $\Delta B_{\Lambda\Lambda} = 4.5 \pm 0.4$  or  $3.2 \pm 0.6$  MeV, respectively. Among the several double- $\Lambda$  hypernuclear events so far reported in the emulsion experiments [265, 266, 267, 268, 269], the most impressive one is the *NAGARA* event discovered in the KEK-PS E373 experiment using a counter-emulsion hybrid method. This event was uniquely identified as a  ${}_{\Lambda\Lambda}^6\text{He}$  without any ambiguity such as a possible excited state of daughter (hyper)nucleus [268, 269]. From this result, the  $\Lambda\Lambda$  interaction was determined to be weakly attractive, *i.e.*  $\Delta B_{\Lambda\Lambda} = 0.67 \pm 0.17$  MeV by assuming  $\Xi^-$  capture from an atomic 3D state of  ${}^{12}\text{C}$  with a binding energy of 0.13 MeV. Based on this result, the event reported by M. Danysz *et al.* can be consistently interpreted as a  ${}_{\Lambda\Lambda}^{10}\text{Be}$ , the decayed daughter of which ( ${}^9\text{Be}$ ) was in an excited state.

There have been discussions that  $\Delta B_{\Lambda\Lambda}$  is not a good measure of the  $\Lambda\Lambda$  interaction, since the mass or  $B_{\Lambda}$  of a single- $\Lambda$  hypernucleus is greatly affected by the structure of the core nucleus [270, 271]. As an example, if the core nucleus is not spin-less,  $B_{\Lambda}$  has an effect based in the  $\Lambda N$  spin-dependent interactions, which are canceled in the case of double- $\Lambda$  hypernucleus in the ground state. Change of the nuclear size by adding a  $\Lambda$  ( ${}^7_{\Lambda}\text{Li}$  [217]) is another example. Because the core nucleus ( ${}^4\text{He}$ ) is spin-less and stiff in the case of  ${}_{\Lambda\Lambda}^6\text{He}$ , the obtained  $\Delta B_{\Lambda\Lambda}$  is thought to present a pure  ${}^1S_0$  interaction between  $\Lambda$  hyperons. In order to confirm this and to obtain a bare  $\Lambda\Lambda$  interaction taking into account nuclear

structure effects, systematic studies on double- $\Lambda$  hypernuclei, especially  $p$ -shell ones, are necessary. The P-wave  $\Lambda\Lambda$  interaction is also of interest in the context to the hyperon puzzle [272]. The P-wave interaction can be extracted by observing “ $\Lambda$ -excited” double- $\Lambda$  hypernuclear states where one  $\Lambda$  is in the  $s$ -state and the other is in the  $p$ -state, although such states may not be bound.

The  $\Xi N \rightarrow \Lambda\Lambda$  conversion interaction can be obtained from the strength of the imaginary part of the  $\Xi$ -nucleus potential or the widths of  $\Xi$  hypernuclear states as described in the following sections. However, in case that the level spacing is similar to the width or the width is much smaller than the experimental resolution, it may be difficult to obtain this interaction by those methods. Another possible approach is to measure masses of the  $A = 4$  and 5 double- $\Lambda$  hypernuclei,  ${}_{\Lambda\Lambda}^4\text{H}$ ,  ${}_{\Lambda\Lambda}^5\text{H}$ , and  ${}_{\Lambda\Lambda}^5\text{He}$ . A large mixing effect due to the  $\Xi N$ - $\Lambda\Lambda$  conversion interaction is expected in the  $S = -2$  system because of the small mass difference of 28 MeV. However, this mixing effect is suppressed in double- $\Lambda$  hypernuclei having a saturated core nucleus such as  ${}_{\Lambda\Lambda}^6\text{He}$ , because a nucleon associated with the  $\Lambda\Lambda \rightarrow \Xi^- p$  or  $\Xi^0 n$  process should be in a higher energy shell. However, in the case of the  $A = 4$  and 5 double- $\Lambda$  hypernuclei,  $s$ -shell nucleons are not fully occupied and this mixing is expect to significantly affect the mass.

The J-PARC E07 experiment is a third generation counter-emulsion hybrid experiment to study double-strangeness nuclei such as double- $\Lambda$  and  $\Xi$  hypernuclei. In the second generation counter-emulsion hybrid experiment, E373,  $\Xi^-$  hyperons produced via the quasi-free  $K^- + “p” \rightarrow K^+ + \Xi^-$  reaction on a diamond target were injected into the emulsion module, and the reaction was identified by a magnetic spectrometer system. Based on guidance of position and direction of the  $\Xi^-$  determined by scintillating-fiber detectors upstream of the emulsion module, the  $\Xi^-$  hyperons were followed through the emulsion until they stopped, decayed, or passed through. Among the  $\sim 650$   $\Xi^-$  stop events [273], 7 *double events* (that exhibit sequential decays of double- $\Lambda$  hypernuclei) and 2 *twin events* (showing that two single- $\Lambda$  hypernuclei are emitted from the  $\Xi^-$  capture point) were found [269]. The goal of the E07 experiment is to obtain ten times the double-strangeness nuclear events compared to the E373 experiment (that is,  $\sim 100$  double-strangeness nuclei among  $\sim 10^4$   $\Xi^-$  stop events). The physics runs were carried out separately in 2016 and 2017. Prior to the E07 runs, the SKS located in the K1.8 area was moved to the K1.1 beamline area and the KURAMA spectrometer used to measure the outgoing  $K^+$  was installed in the K1.8 area instead of the SKS. In order to accumulate ten times the data, a number of improvements and upgrades were essential. These are itemized below.

- A high-intensity, high-purity  $K^-$  beam.  
 Since the total number of the irradiated beam particles is limited so as to maintain suitable efficiency in the scanning and analysis of the emulsions, the purity of  $K^-$  in the beam is essential to enhance the statistics. During the beam exposure, a  $K^-$  beam with an intensity of  $2.8 \times 10^5$  particles per spill of 2.0 s duration in every 5.52 s with the purity of 82% was used. The purity and intensity were increased by factors of  $\sim 2$  and 3.3, respectively, relative to the previous E373 experiment.
- Total quantity of the emulsion.  
 A total of 2.1 tons of emulsion gel, about 3 times of the previous one, was prepared, and half a year was required to produce the emulsion sheets. A total quantity of 118 emulsion modules from  $\sim 1500$  sheets was used to record the  $\Xi^-$ -induced events. Approximately one year was required for photographic developments of these sheets following the beam exposures.
- An automated  $\Xi^-$  following system [274].  
 To complete the emulsion scanning within a reasonable time frame while meeting the requirement to analyze ten times as many events, an automated track following system had been developed. This system automatically traces each track to the end point, such as stopping, decay, or passing-through, using track information from the previous sheet of the emulsion module. When an

interesting end point such a  $\Xi^-$  stop or decay is detected the system records photographic images around the point for further confirmation by human-eyes. The working speed using this system is 15 times faster than that of the semiautomatic system with human support used in the E373 experiment.

It is also important to reduce the scanning area and track candidates in the first emulsion sheet for the efficient scanning. Therefore silicon strip detectors (SSDs) having a four layer configuration and much better spatial resolution than the scintillating-fiber detectors were used as the  $\Xi^-$  tracker. The resulting resolutions were estimated to be  $15 \mu\text{m}$  and  $20 \text{mrad}$  (RMS) for the position and angle, respectively.

- Enlargement of the solid angle acceptance of the KURAMA spectrometer.

The gap of the KURAMA magnet was extended to 800 mm and the downstream detectors were enlarged. The solid angle acceptance was 280 msr.

The scanning of these emulsions is currently in progress. By September 2019, 82 % emulsion modules had been scanned at least once and 31 double-strangeness events had been observed, several of which have already been reported.

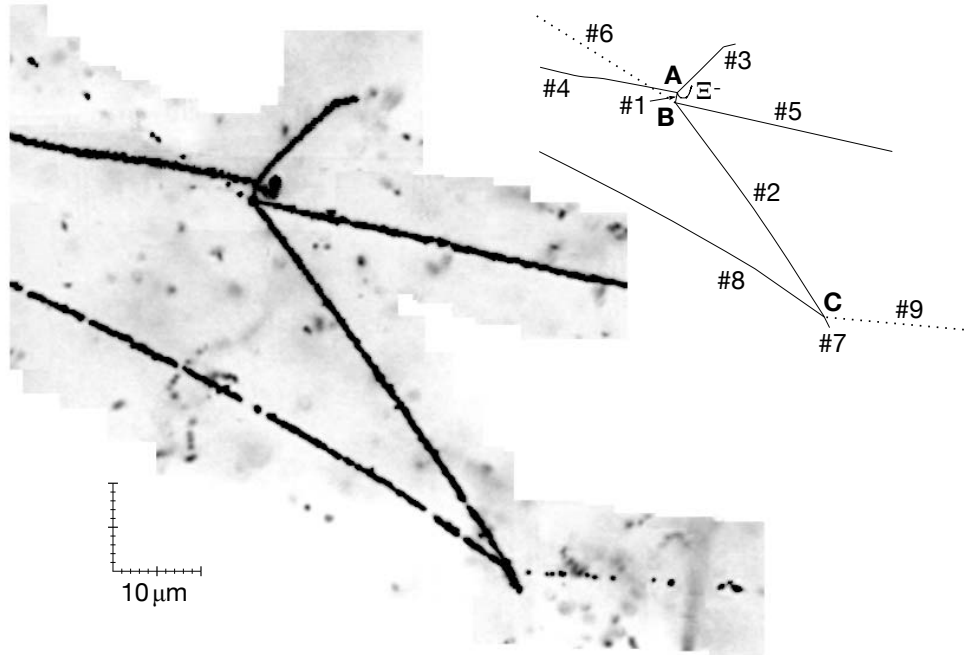
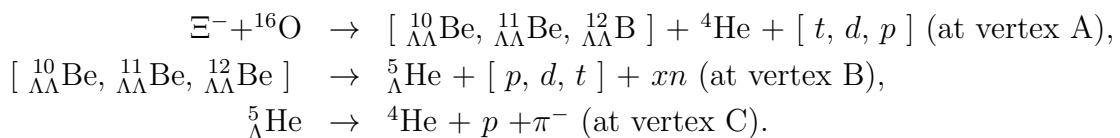


Figure 38: Overlaid photograph and its schematic drawing of the *MINO* event observed in the J-PARC E07 experiment. The figure is taken from Ref. [275].

One is *MINO* event with the topology of sequential decays as shown in Fig. 38 [275]. From the detailed kinematical analysis and assuming that the  $\Xi^-$  was captured by  $^{12}\text{C}$ ,  $^{14}\text{N}$ , or  $^{16}\text{O}$ , this event is interpreted as the following three processes involving production and decay modes:



By assuming that the  $\Xi^-$  was captured in the atomic 3D state of  $^{16}\text{O}$  with the theoretically estimated binding energy of 0.23 MeV [278], the  $B_{\Lambda\Lambda}$  values for each candidate were obtained to be  $15.05 \pm 0.09$

Table 6: Masses of hyperons and binding energies of hypernuclei used in the analysis of the *MINO* event.

	[MeV]	reference	comment
mass of $\Lambda$	$1115.683 \pm 0.006$	[45]	
mass of $\Xi^-$	$1321.71 \pm 0.006$	[45]	
$B_\Lambda(^7_\Lambda\text{Be})$	$5.16 \pm 0.08$	[276]	
$B_\Lambda(^8_\Lambda\text{Be})$	$6.84 \pm 0.05$	[276]	
$B_\Lambda(^9_\Lambda\text{Be})$	$6.71 \pm 0.04$	[276]	
$B_\Lambda(^{10}_\Lambda\text{Be})$	$8.60 \pm 0.07 \pm 0.16$	[277]	
$B_\Lambda(^{11}_\Lambda\text{Be})$	$8.2 \pm 0.5$		a linear extrapolation from $B_\Lambda$ above 4 $_\Lambda\text{Be}$ isotopes
$B_{\Xi^-}$ of $^{16}\text{O}$	0.23	[278]	atomic 3D state of $^{16}\text{O}$

Table 7: Obtained  $\Delta B_{\Lambda\Lambda}$  and  $\chi^2$  values from the kinematical fitting at vertex A for each interpretation of the *MINO* event.

Interpretations	$\Delta B_{\Lambda\Lambda}$ [MeV]	$\chi^2$
$\Xi^- + ^{16}\text{O} \rightarrow ^{10}_{\Lambda\Lambda}\text{Be} + ^4\text{He} + t$	$1.63 \pm 0.14$	11.5
$\Xi^- + ^{16}\text{O} \rightarrow ^{11}_{\Lambda\Lambda}\text{Be} + ^4\text{He} + d$	$1.87 \pm 0.37$	7.3
$\Xi^- + ^{16}\text{O} \rightarrow ^{12}_{\Lambda\Lambda}\text{Be}^* + ^4\text{He} + p$	$-2.7 \pm 1.0 (+E_X)$	11.3

(stat.)  $\pm 0.07$  (syst.),  $19.07 \pm 0.08$  (stat.)  $\pm 0.07$  (syst.), and  $13.68 \pm 0.08$  (stat.)  $\pm 0.07$  (syst.) MeV for  $^{10}_{\Lambda\Lambda}\text{Be}$ ,  $^{11}_{\Lambda\Lambda}\text{Be}$ , and  $^{12}_{\Lambda\Lambda}\text{Be}$ , respectively. The corresponding  $\Delta B_{\Lambda\Lambda}$  values are  $1.63 \pm 0.09$  (stat.)  $\pm 0.11$  (syst.),  $1.87 \pm 0.08$  (stat.)  $\pm 0.36$  (syst.), and  $-2.7 \pm 0.08$  (stat.)  $\pm 1.0$  (syst.) MeV. Those values were obtained using the mass and  $B_\Lambda$  values listed in Table 6. The negative  $\Delta B_{\Lambda\Lambda}$  for  $^{12}_{\Lambda\Lambda}\text{Be}$  seems to be inconsistent with the attractive  $\Lambda\Lambda$  interaction. However, if  $^{12}_{\Lambda\Lambda}\text{Be}$  is produced in an excited state, its excitation energy is added to  $B_{\Lambda\Lambda}$  and  $\Delta B_{\Lambda\Lambda}$ . Thus  $\Delta B_{\Lambda\Lambda}$  for the ground state of  $^{12}_{\Lambda\Lambda}\text{Be}$  may become positive. The probabilities of these three interpretations were evaluated based on the kinematical fitting. The results are shown in Table 7, together with the  $\Delta B_{\Lambda\Lambda}$  obtained from the above analysis. The  $\chi^2$  of the kinematical fitting demonstrates that the interpretation of the  $^{11}_{\Lambda\Lambda}\text{Be}$  production is the most likely.

Recently, a new scanning method, *i.e.* overall scanning, has been developed [279], in which, characteristic topologies with more than 3 vertexes are searched for without counter's information on the  $\Xi^-$  track. This method can detect latent  $\Xi^-$  capture events caused by the quasi-free  $K^- + "n" \rightarrow K^0 + \Xi^-$  reaction or by the decay of an outgoing  $K^+$  prior to the KURAMA spectrometer. Thus ten times more double-strangeness events are expected to be observed.

### 3.3.6 $\Xi$ hypernuclei

At present, only a few experimental data on the  $\Xi N$  interaction are available. Some signal events were observed in the  $\Xi$ -bound region of the missing-mass spectra for the  $^{12}\text{C}(K^-, K^+)$  reaction measured in the KEK-PS E224 [280] and BNL-AGS E885 [281] experiments. Although the peak structure could not be observed due to the insufficient experimental resolution of 10 MeV (FWHM) or worse and the poor statistics, the fitting of spectrum-shape including quasi-free  $\Xi$  production near the  $\Xi$  bound threshold suggested a weak attractive  $\Xi$ -nucleus potential with a depth of  $-14$  MeV, assuming a Wood-Saxon type potential [281]. A new impressing event named *KISO* was discovered in the emulsion exposed at the E373 experiment by applying the overall scanning method [279] which had been developed for the

E07 experiment. This event was uniquely identified as  $\Xi^- + {}^{14}\text{N} \rightarrow {}^{10}_{\Lambda}\text{Be} + {}^5_{\Lambda}\text{He}$ , although there is some uncertainty as to whether the  ${}^{10}_{\Lambda}\text{Be}$  was in the ground or excited states. Assuming that  ${}^{10}_{\Lambda}\text{Be}$  was in the excited state, which gives a lower  $\Xi$  binding energy ( $B_{\Xi}$ ), and incorporating the excitation energy predicted theoretically,  $B_{\Xi}$  was obtained to be  $1.11 \pm 0.25$  MeV. This value is much larger than 0.17 MeV for the  $\Xi$  atomic 3D orbit energy [282]. This value was later updated to be  $1.03 \pm 0.18$  MeV [283] by taking into account new experimental data on  ${}^{10}_{\Lambda}\text{Be}^*$  [277]. Thus the *KISO* event confirms the existence of a  $\Xi$  hypernucleus, and strongly suggests an attractive  $\Xi$ -nucleus potential and an attractive  $\Xi N$  interaction on average.

In the E07 experiment, a new event with a *twin event* topology was found as shown in Fig. 39. This event named *IBUKI* was uniquely identified as  $\Xi^- + {}^{14}\text{N} \rightarrow {}^{10}_{\Lambda}\text{Be}$  (#1) +  ${}^5_{\Lambda}\text{He}$  (#2). Only this mode is accepted at the first vertex where the  $\Xi^-$  was captured. The decays #1  $\rightarrow$  4-prongs and #2  $\rightarrow$  3-prongs with a  $\pi^-$  track are consistent with those of  ${}^{10}_{\Lambda}\text{Be}$  and  ${}^5_{\Lambda}\text{He}$ , respectively [284, 285]. This mode is the same as that for the *KISO* event. However, there is no possibility of  ${}^{10}_{\Lambda}\text{Be}$  being in the excited state. The  $\Xi^-$  binding energy was unambiguously determined to be  $1.27 \pm 0.21$  MeV [285], which is significantly larger than 0.17 MeV for the energy of the atomic 3D state. Therefore this event provides additional evidence for the  ${}^{15}_{\Xi}\text{C}$  hypernucleus.

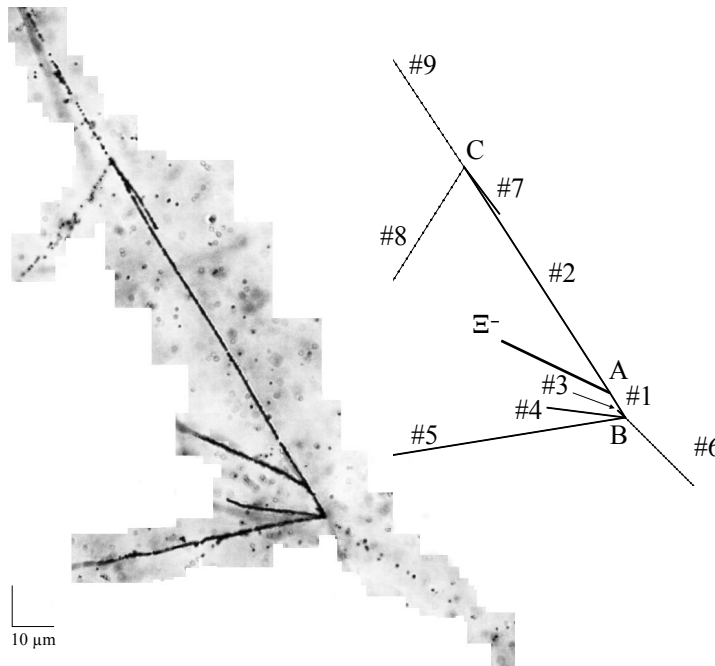


Figure 39: Overlaid photograph and its schematic drawing of the *IBUKI* event observed in the J-PARC E07 experiment. The figure is taken from Ref. [285].

A comparison of  $B_{\Xi^-}$  obtained from different events is quite interesting. There are two acceptable values that can be obtained from the *KISO* event [283]:  $1.03 \pm 0.18$  MeV in the case of the excited state of  ${}^{10}_{\Lambda}\text{Be}$  and  $3.87 \pm 0.21$  MeV in the case of the ground state. The present result from the *IBUKI* event appears to support the former case. This value also agrees with the theoretical predictions for the 2P state, which are; 1.14 MeV based on the Ehime potential [278] and 1.22 to 1.85 MeV based on the ESC08 model [286]. However the  $\Xi$  hypernuclear state may have a large width due to a strong  $\Xi N$ - $\Lambda\Lambda$  conversion in the nucleus. Therefore the latter case can not be excluded at present. Recently the *KINKA* event from the E373 experiment [269] was uniquely identified as  $\Xi^- + {}^{14}\text{N} \rightarrow {}^9_{\Lambda}\text{Be} + {}^5_{\Lambda}\text{He} + n$ , although a detailed analysis to obtain  $B_{\Xi^-}$  is still in progress. By combining the results from the *KISO*, *IBUKI*, *KINKA*, and other similar events that will presumably be observed in near future, important information can be obtained regarding not only the binding energies but also the widths of

Table 8:  $K^+$  spectrometers and their performance for the  $(K^-, K^+)$  missing-mass spectroscopy. The effects of target thickness are included in the missing-mass resolution (see text).

Spectrometer Experiment	SksPlus (E05 in the proposal)	SKS (E05)	S-2S (E70)
Magnet configuration	D+D(SKS)	D(SKS)	QQD
Acceptance [msr]	30	110	55
Missing-mass resolution (FWHM) [MeV]	3.1	5.4	< 2.0

$^{15}_{\Xi}\text{C}$  hypernuclear states.

It should be emphasized that a large number of *twin event* samples including both  $\Xi$  hypernuclei and  $\Xi^-$  absorption from atomic states provides an opportunity to confirm in which state  $\Xi^-$  absorption take place (that is, the 3D state or deeper states). This is quite important with regard to the analysis of double- $\Lambda$  hypernuclei, because the value for  $\Delta B_{\Lambda\Lambda}$  was obtained by assuming absorption in the 3D state from the theoretical calculation. If the  $\Xi^-$  is absorbed in a deeper state such as 2P, the corresponding  $\Delta B_{\Lambda\Lambda}$  value will be a larger, indicating a more attractive  $\Lambda\Lambda$  interaction.

J-PARC E05 and E70 are experiments on the  $(K^-, K^+)$  missing-mass spectroscopy aiming at observing the  $^{12}_{\Xi}\text{Be}$  hypernucleus with good resolution and high statistics, and obtaining information on  $\Xi N$  and  $\Xi N \rightarrow \Lambda\Lambda$  interactions. The original E05 plan in the proposal was to carry out the measurement using an SksPlus spectrometer with a DD configuration by adding a dipole magnet in front of the SKS magnet. The solid angle acceptance of the SksPlus is 30 msr and the missing-mass resolution is estimated to be 3.1 MeV (FWHM) with a 5.4 g/cm<sup>2</sup> carbon target (Table 8). However, the production cross section obtained from the E885 experiment is very small as  $89 \pm 14$  and  $42 \pm 5$  nb/sr for averaged from 0° to 8° and from 0° to 14°, respectively [281]. In the early stage, the MR beam power and consequently the  $K^-$  beam intensity were insufficient to allow the E05 experiment to be performed with the SksPlus. Therefore the experimental plan was reconsidered to be carried out in more realistic beam condition.

Thus, the E05 experiment was carried out by using only the SKS with a large solid angle of 110 msr and a thick carbon target of 9.36 g/cm<sup>2</sup> in 2015. In this pilot run,  $K^-$  intensity of  $6 \times 10^5$  per spill (5.52 s beam cycle) was available to use with an MR beam power of 39 kW. The experimental missing-mass resolution was found to be 5.4 MeV (FWHM) from the  $\Xi^-$  spectrum of the elementary  $p(K^-, K^+)\Xi^-$  reaction with a 9.54 g/cm<sup>2</sup> CH<sub>2</sub> target. This is the best resolution obtained to date for the missing-mass spectroscopy of  $\Xi$  hypernucleus. Elementary production data at 1.5, 1.6, 1.7, 1.8, and 1.9 GeV/ $c$  were also measured to obtain the incident momentum dependence. Cross section on the elementary  $\Xi^-$  production was confirmed to be maximum at 1.8 GeV/ $c$ , as pointed out by C.B. Dover and A. Gal [287]. This is an important result with regard to the planning of future experiments. The  $K^-$  beam at 1.8 GeV/ $c$  is evidently the most suitable to study double-strangeness systems to which  $\Xi^-$  production is doorway.

The analysis of carbon target data is in progress, but preliminary results have been reported at several conferences [288, 289]. A significant number of events ( $\sim 50$  counts) in the  $\Xi^-$  bound region were observed, suggesting the existence of  $\Xi$  hypernuclei. The production yield is also consistent with the reported cross sections, and the spectrum shape is very similar to that obtained in E885 [281], although the experimental resolution was significantly improved to 5.4 MeV (FWHM) from 10 MeV (FWHM). These results suggest either multiple bound states or a broad width for the  $\Xi$  hypernuclear state, or both.

In order to clarify this point and obtain as much information as possible, the missing-mass resolution is the most important experimental issue. Therefore in the next experiment, E70 [290], a high-resolution

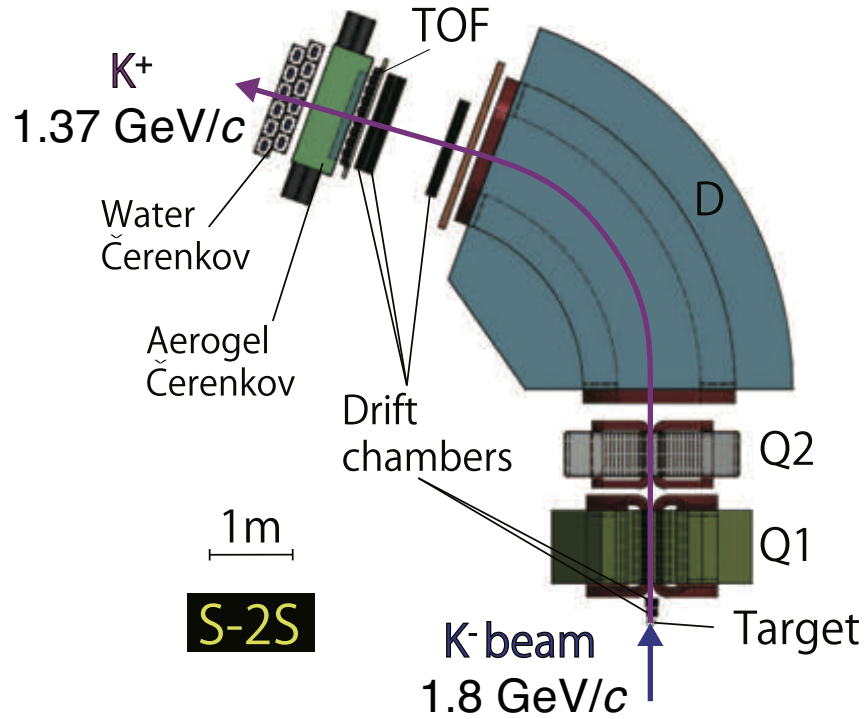


Figure 40: Schematic drawing of the S-2S to be used in the J-PARC E70 experiment. The figure is taken from the experimental proposal [290].

spectrometer S-2S (Strangeness  $-2$  Spectrometer) will be used. The S-2S has a QCD magnet configuration and good optical properties similar to those of the HKS at Jefferson Lab. [291, 292]. In this case, the experimental resolution will be primarily determined by the target thickness due to the energy loss straggling in the target. Even so, a reasonably thick target will be required to compensate for the small production cross section of  $^{12}\text{Be}$ . Therefore, an active fiber target (AFT) with a 10 cm thickness will be employed to correct the energy-loss in the target event-by-event. The resolution in this experiment is expected to be 1.4 MeV (FWHM). The recent DWIA calculation by T. Motoba *et al.* [293] using the  $\Xi N$  G-matrix interaction derived from the ESC08a model [258] predicts three prominent peaks of the  $1_1^-$ ,  $1_2^-$ , and  $1_3^-$  states. These states would be clearly observed with 1.4 MeV (FWHM) resolution in the E70. Measurements on  $^7\text{Li}(K^-, K^+)_{\Xi}^7\text{H}$  and  $^{10}\text{B}(K^-, K^+)_{\Xi}^{10}\text{Li}$  are currently under consideration in order to obtain the spin- and isospin-independent term of the  $\Xi N$  interaction [294].

Depending on the coupling strength of  $\Xi N$  and  $\Lambda\Lambda$  due to the  $\Xi N \rightarrow \Lambda\Lambda$  conversion process, a part of the production strength of  $\Xi$  hypernucleus states will be used to produce the excited states of double- $\Lambda$  hypernucleus [295]. This is a one-step process via the  $\Xi$ -doorway to produce a double- $\Lambda$  hypernucleus, similar to the one-step process via the  $\Sigma$ -doorway in the production of the neutron-rich  $\Lambda$  hypernucleus. Although the production cross section of such states is expected to be very small, the  $(K^-, K^+)$  missing-mass method is likely to be a useful means of measuring the excited states of double- $\Lambda$  hypernuclei. This method can apply to even the  $\Lambda$  unbound states that can not be identified in the emulsion analysis.

The recent lattice QCD simulation at almost physical point predicts  $S = -2$  S-wave baryon-baryon interactions [296]; the  $\Lambda\Lambda$  interaction is weakly attractive but not enough strong to produce bound or resonance dihyperon around the  $\Lambda\Lambda$  threshold. While the  $\Xi N$  interaction has relatively strong attraction in isospin-singlet, spin-singlet channel, which may lead to light  $\Xi$  hypernuclei [297]. Furthermore small  $\Xi N \rightarrow \Lambda\Lambda$  conversion is suggested. These features of the  $S = -2$  baryon-baryon interactions would be confirmed or checked by the future spectroscopy experiments.

Installation of the S-2S in the K1.8 area is planned in near future after the completion of the experiments using the KURAMA spectrometer.

### 3.3.7 X-ray spectroscopy of $\Xi^-$ -atoms

X-ray spectroscopy can be applied to the negatively charged  $\Xi^-$  hyperons to investigate the  $\Xi^-$ -nucleus potential. Since the observed level shifts and broadening of the width are connected to the  $\Xi^-$  potential in the nuclear surface region or even far from the surface, the information on the nuclear potential that is obtained is complementary to that resulting from spectroscopic studies of  $\Xi$  hypernuclei.

In the E07 experiment, X-rays were also measured in coincidence with  $\Xi^-$  production using a Hyperball-X detector, which consisted of 6 sets of clover-type Ge detectors surrounded by BGO counters, located upstream of the diamond target and the emulsion module [284]. This represented an ambitious attempt to observe  $\Xi^-$ -atomic X-rays, for the first time, from the  $\Xi^-$  atoms of heavy elements such as Ag and Br in the emulsion and C in the diamond target. In the case of Ar or Br,  $\Xi^-$  capture can be well identified by the scanning of the emulsion, thus, good S/N can be achieved although the X-ray yields would be very tiny.

In the dedicated experiment, J-PARC E03, the choice of targets is the most important to observe finite shifts and to obtain the potential information. C.J. Batty *et al.* suggested a set of 4 optimum targets, namely F ( $Z=9$ ), C ( $Z=17$ ), I ( $Z=53$ ), and Pb ( $Z=82$ ) for  $(n, l) = (3, 2), (4, 3), (7, 6),$  and  $(9, 8)$ , respectively [298], and predicted shifts on the order of 1 keV for these states. In the E03 experiment, Fe ( $Z=26$ ) was selected as the target based on considering the production rate of  $\Xi^-$ , the stopping probability of the  $\Xi^-$ , and X-ray absorption by the target material.

Figure 41 shows a schematic level scheme for the  $\Xi^-$ -Fe atom. For the  $(5, 4)$  state, both an energy shift and broadened width are expected due to the strong  $\Xi^-$ -nucleus interaction. In the case of a Wood-Saxon potential of  $-24 - 3i$  MeV, the expected shift and width ( $\Gamma$ ) are  $\sim 4$  keV and  $\sim 4$  keV, respectively. Therefore, both 176 keV and  $\sim 286$  keV X-rays will be measured for the  $(7, 6) \rightarrow (6, 5)$  and the  $(6, 5) \rightarrow (5, 4)$  transitions, respectively. Neither a level shift nor width broadening are expected in the former X-ray, while both a finite shift and width broadening are expected in the latter X-ray. In the original proposal, more than 2500 counts of  $(6, 5) \rightarrow (5, 4)$  transition X-ray will be measured to obtain shift and width information even in the case of strong absorption ( $\Gamma \sim 4$  keV). Due to the similar reason to the E05 experiment, the original plan has been changed based on a two step strategy. The goal of the first measurement is to obtain 10 % of the statistics in the original proposal. With these data, the  $(7, 6) \rightarrow (6, 5)$  transition X-rays could be observed, although no shift would be expected. In the case of weak absorption ( $\Gamma \sim 1$  keV), it may be possible to observe the  $(6, 5) \rightarrow (5, 4)$  transition X-ray and to obtain values for the finite shift, width, and absorption strength.

The first measurement is planned in near future using the KURAMA spectrometer for tagging the  $\Xi^-$  production and the Hyperball-X detector with a slightly different setup from that in the E07 experiment.

## 4 Future Prospects

Many essential results on hadron and nuclear physics have been obtained and will be obtained from the present HEF, as discussed in the previous section. However, to extend the physics programs and maintain these activities requires the capability of the HEF to be enhanced. Two new functions must be added, at least, to the HEF for future hadron and nuclear physics. One is a high intensity and high energy resolution beamline (HIHR) for high precision hadron and nuclear spectroscopy to utilize the high power beam from J-PARC MR. The other is a high intensity and high momentum particle-separated beamline (K10) to open a new door for heavy meson and baryon spectroscopy, for example. Intensive studies and efforts have been made to realize these projects among the HEF users from

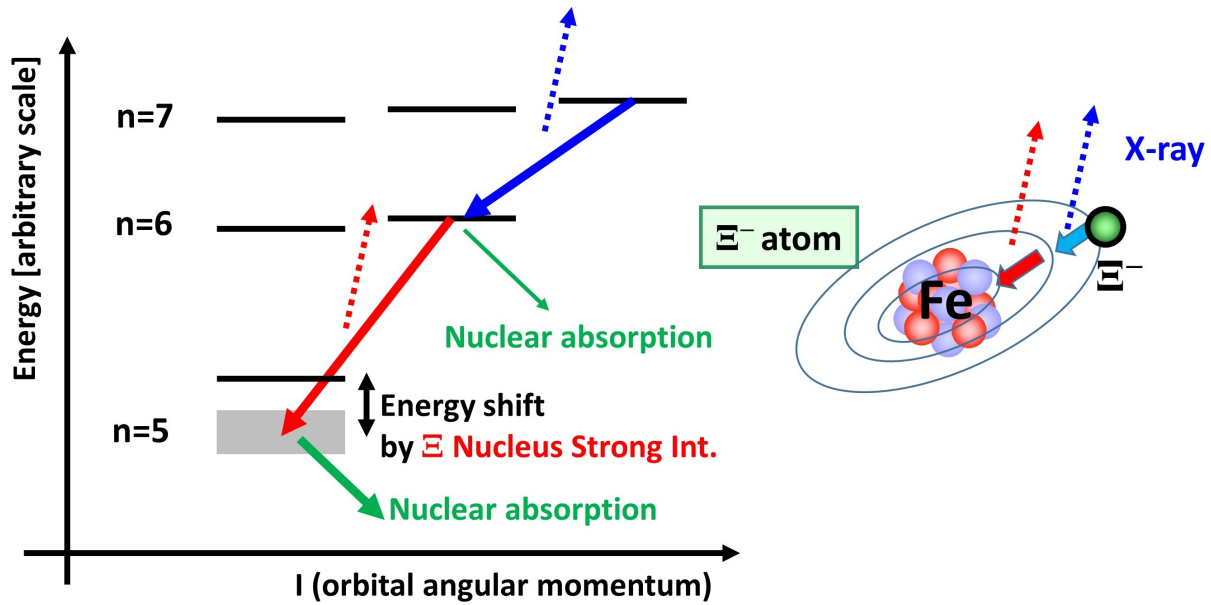


Figure 41: Schematic level scheme of  $\Xi^-$ -Fe atom.

the beginning of HEF operation, and these discussions are summarized in the HEF Extension White Paper [299, 300]. Figure 42 shows a layout of the extended HEF together with the current HEF. The size of the experimental area will be three times larger and two new production targets will be placed. Four beamlines plus one branched beamline, HIHR, K10, KL, K1.1, and K1.1BR, will be newly constructed. The specifications of the beamlines for both the present and the extended HEF are summarized in Table 9.

Physics at the new functional beamlines, HIHR and K10, and their designs are briefly described here. Details can be obtained from the HEF Extension White Paper [299, 300].

## 4.1 Physics at HIHR

The properties of high-density nuclear or hadronic matter have attracted interest in connection with neutron stars, the highest density objects in the universe. Considering that the rather high Fermi-energy with neutrons deep inside of a neutron star can be reduced by converting neutrons to hyperons and that the attractive hyperon interaction in a nucleus, at least for  $\Lambda$ , is experimentally confirmed, it is naturally expected that hyperons exist deep inside of neutron stars. The internal structure of a neutron star is theoretically studied with an equation of state (EOS) for high-density nuclear matter. There are several versions of the EOS that were constructed using realistic nuclear models with the knowledge on the properties of nuclei and interactions of nucleons or hadrons. The established models including hyperon interactions predict that hyperons appear in the inner core of neutron stars and the maximum mass of neutron stars is approximately 1.5 solar mass.

However, this natural conclusion from nuclear physics conflicts with the existence of 2 solar mass neutron stars [301, 302]. This discrepancy between the astronomical observations and the theoretical predictions in nuclear physics is referred to as the “hyperon puzzle”. The appearance of hyperons in high-density nuclear matter means the EOS must be softened and therefore such a softened EOS can not support heavy neutron stars. The hyperon puzzle thus is a significant challenge to be resolved in nuclear physics.

One of the promising approaches to solve the hyperon puzzle is to introduce a three-body repulsive force (TBRF) in the baryonic interactions with hyperons. The idea of TBRF has been discussed to

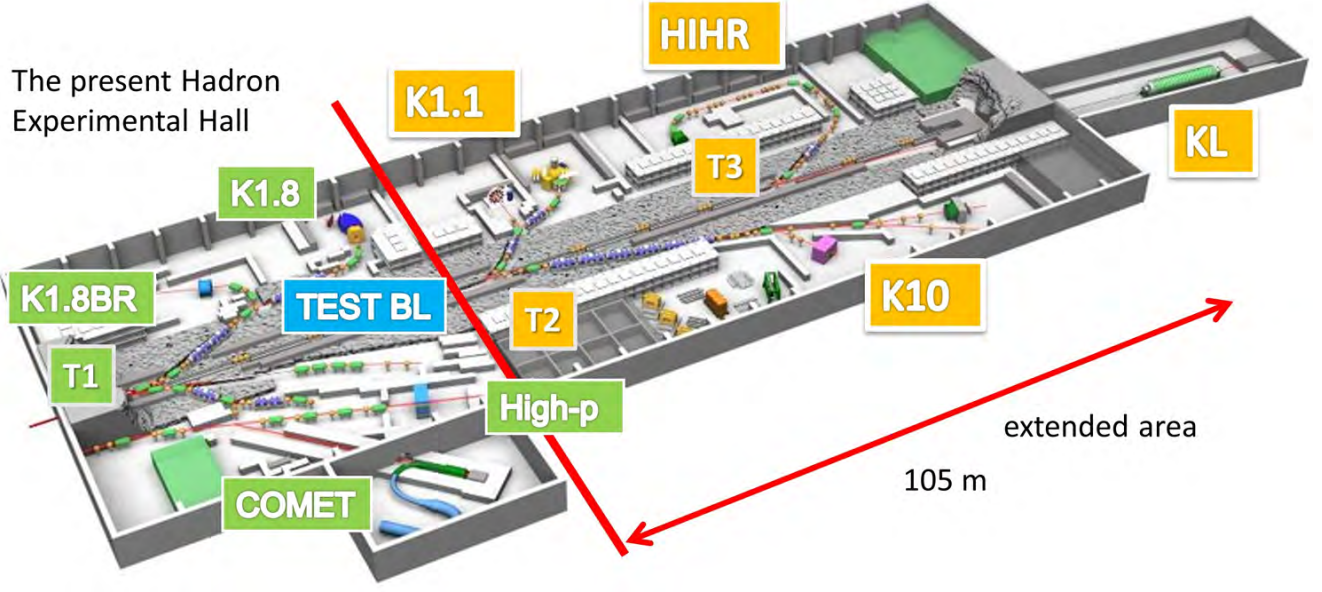


Figure 42: Layout plan of the extended HEF.

Table 9: Specifications of beamlines in the present and the extended HEF. Beam intensities at the present beamlines are typical and scaled to  $\sim 80$  kW. Those at the new beamlines are the designed values with the same protons per pulse on the production target. This table is taken from [299] with modification.

	Particles	Momentum	Intensity	Characteristics
Beamlines in the present hadron experimental facility				
K1.8	$K^\pm, \pi^\pm$	1.0 – 2.0 GeV/c	$\sim 10^6 K^-$ /spill (1.8)	mass separated
K1.8BR	$K^\pm, \pi^\pm$	< 1.1 GeV/c	$\sim 5 \times 10^5 K^-$ /spill (1.0)	mass separated
KL	$K_L$	2.1 GeV/c in ave.	$10^7 K_L$ /spill	16° extraction angle
high-p	$p$ $\pi^\pm$	< 31 GeV/c	$10^{10} p$ /spill $10^7 \pi$ /spill	primary beam (30 GeV) secondary beam
COMET	$\mu^-$			for $\mu^- \rightarrow e^-$ experiment
Beamlines in the extended area				
K1.1	$K^\pm, \pi^\pm$	< 1.2 GeV/c	$\sim 10^6 K^-$ /spill (1.1)	mass separated
K1.1BR	$K^\pm, \pi^\pm$	0.7 – 0.8 GeV/c	$\sim 10^6 K^-$ /spill	mass separated
HIHR	$\pi^\pm$	< 2.0 GeV/c	$\sim 3 \times 10^8 \pi$ /spill	mass separated $\times 10$ better $\Delta p/p$
K10	$K^\pm, \pi^\pm, \bar{p}$	< 10 GeV/c	$\sim 10^7 K^-$ /spill	mass separated
KL	$K_L$	5.2 GeV/c in ave.	$10^8 K_L$ /spill	5° extraction angle optimized $n/K_L$

overcome the softening problem of the EOS, by introducing TBRF “universally”, *i.e.* equally to the  $YN$  and  $YY$  parts, as well as  $NN$  part [303, 304]. The effects of three-body force in ordinary nuclei with  $S = 0$  has already been observed, for example, in the analyzing powers for the  $dp$  elastic scattering, [305] and the repulsive effect was suggested in the theoretical analysis of  $^{16}\text{O} + ^{16}\text{O}$  elastic scattering [306].

A baryonic TBRF affects the single particle energy of a hyperon that is bound deep inside of a hypernucleus. The effect on the  $\Lambda$  binding energy is expected to be approximately a half MeV, which is smaller than the achievable experimental resolution and hence the accuracy of the present apparatus for the missing-mass spectroscopy using meson beams. The large momentum spread of the secondary meson beams means that the momenta of the beam particles should be directly measured event-by-event; therefore, the acceptable beam intensity is limited and a thick target that degrades the experimental resolution is necessary at present.

By adopting dispersion matching techniques [307], direct measurement of the beam particle is not necessary in the HIHR. Therefore, the HIHR enables  $(\pi^\pm, K^-)$  missing-mass spectroscopy to be performed with a resolution of a few 100 keV (FWHM) through the use of high-intensity pion beams and relatively thin nuclear targets. High-resolution and high-precision spectroscopy on light to heavy  $\Lambda$  hypernuclei will reveal the existence of TBRF in hyperon interactions and hopefully solve the hyperon puzzle.

## 4.2 Physics at K10

The K10 beamline at the extended HEF is designed to handle a secondary beam up to 10 GeV/ $c$  while maintaining the intensity as high as possible. The separated beam will be available with momentum up to 4 GeV/ $c$  and 6 GeV/ $c$ , for  $K^-$  and  $\bar{p}$ , respectively. With the current design, 27 m of electrostatic (ES) separator will be used for particle separation. An RF-type separator is under discussion instead of the ES separator to extend the particle separation capability [299, 300].

The  $\Omega$  baryon nucleon interaction is one of the hot topics in hadron physics. Recently, a lattice QCD calculation suggested an attractive interaction between an  $\Omega$  baryon and a nucleon [308], which leads to the existence of the  $\Omega$ -nucleon bound state. An  $\Omega$  baryon could be produced via  $(K^-, K^+ K^{0*})$  interaction by utilizing a high momentum  $K^-$  beam. The first project could be a measurement of the  $\Omega$  production cross section in the production threshold region, *i.e.* a  $K^-$  beam momentum of approximately 6 GeV/ $c$ . At the same time, a significant amount of excited  $\Xi$  baryons are also produced, which would allow for  $\Xi^*$  baryon spectroscopy to reveal the hadron structure with  $S=-2$  baryons. High intensity and high momentum  $K^-$ , which will only be available at the K10 beamline, will allow direct  $\Omega - p$  and  $\Xi^- - p$  scattering experiments to be performed. Such information is required to achieve a complete understanding of the baryon-baryon interaction in the  $SU_f(3)$  framework [299, 300].

Investigation on charmed meson and baryon interactions is also an important subject. The formation of a charmed meson and nucleus bound state is expected [309, 310, 311] due to the attractive interaction between a charmed meson and a nucleon. To produce a charmed meson efficiently requires a high intensity anti-proton beam, which is available at the K10 beamline. However, there is no knowledge regarding  $D, \bar{D}$  production with antiprotons around the production threshold; therefore, measurement of the production cross section of a  $D\bar{D}$  pair at the production threshold with a  $\bar{p}$  beam will be the first physics program at the K10 beamline. Once the  $D\bar{D}$  production cross section is determined, the feasibility of a search for the D meson bound nucleus will be clarified. Moreover, for example, 7 GeV/ $c$   $\bar{p}$  on proton is above the production threshold of X(3872), which is known to be an exotic hadron candidate. Therefore, the study of X(3872) in a nucleus will also be a subject of interest.

Details will be reviewed in Refs. [299] and [300]

## 5 Summary

One of the biggest goals in hadron physics is to reveal fruitful phenomena predicted by QCD, especially in the low-energy non-perturbative regime. The J-PARC HEF was constructed with an aim to explore such low-energy QCD dynamics through the use of various high-intensity secondary beams as well as 30 GeV primary proton beams. Since the first beam was delivered to the J-PARC HEF in February 2009, various experiments have been performed and proposed. In this review, we have summarized the experimental results and plans that have focused on the study of the fundamental components of matter and their interactions. These experiments have been made via a wide variety of approaches, and thus have provided extremely broad and rich results.

To access information on the QCD vacuum structure, missing resonances in the non-strangeness sector will be investigated at the E45 experiment with partial wave analysis of the  $\pi N \rightarrow \pi\pi N$  and  $\pi N \rightarrow KY$  reactions. In the strangeness sector, the E72 experiment aims to determine the spin and parity of a  $\Lambda^*$  resonance at 1669 MeV produced via the  $p(K^-, \Lambda)\eta$  reaction. The exotic five-quark state with strangeness  $S = +1$ , pentaquark baryon  $\Theta^+$ , was searched for during the E19 experiment; however, no corresponding structure was observed in the missing-mass spectrum of  $p(\pi^-, K^-)X$ . The  $H$  dibaryon, six-quark state with  $S = -2$  will be searched for in the E42 experiment using the Hyperon Spectrometer with statistics an order of 100 times higher than with the previous experiment performed at KEK.

The introduction of heavy-quark symmetry is one of the best ways to study the effective degrees of freedom to describe a hadron itself. The experiment to show the di-quark correlation in charmed baryons is planned as the E50 experiment with the  $(\pi^-, D^{*-})$  reaction at up to 20 GeV/ $c$ . To investigate the origin of the QCD mass generated from the spontaneous breaking of chiral symmetry, the E16 collaboration will conduct a precise measurement of the vector-meson spectral function in medium via a dielectron channel with the 30 GeV primary proton beam. The E26 and E29 experiments are also planned to search for the  $\omega$ - and  $\phi$ -nucleus bound states with the  $(\pi^-, n)$  and  $(\bar{p}, \phi)$  reactions, respectively.

The kaon-nucleon interaction ( $\bar{K}N$ ) close to the mass thresholds provides crucial information on the interplay between spontaneous and explicit chiral symmetry breaking. To determine the individual isoscalar and isovector scattering lengths of the  $\bar{K}N$  interaction, the E57 experiment will measure the shift and width of the kaonic-deuterium  $1s$  state using many arrays of silicon drift detectors (SDDs) covering a large solid angle. For the purpose of obtaining the isospin dependence of the  $\bar{K}N$  interaction, high-resolution measurement of the kaonic- $^4\text{He}$  and  $^3\text{He}$  atoms was performed by the E62 experiment with a superconducting transition-edge-sensor (TES) microcalorimeter having resolution one order of magnitude better than conventional semi-conductor detectors.

The  $\Lambda(1405)$  state, which is widely recognized as a  $\bar{K}N$  quasi-bound state in the  $I = 0$  channel, provides essential information on the  $\bar{K}N$  interaction below the mass threshold. The E31 experiment was conducted to exclusively demonstrate the  $\Lambda(1405)$  line shape via the  $\bar{K}N \rightarrow \pi\Sigma$  channels using the  $(K^-, n)$  reaction on a deuterium target at 1.0 GeV/ $c$ . The result clearly shows the interference between the  $I = 0$  and  $I = 1$  amplitudes in the  $\pi^\pm\Sigma^\mp$  spectra, as theoretically expected. The  $\bar{K}NN$  quasi-bound state, which is one of the kaon-nucleus quasi-bound systems from the strongly attractive  $\bar{K}N$  interaction in the  $I = 0$  channel, was searched in two experiments with different reactions. The E27 collaboration measured the exclusive reaction of  $\pi^+d \rightarrow K^+X$  followed by  $X \rightarrow \Sigma^0p$  and  $\Lambda p$  decays at 1.69 GeV/ $c$ . A broad enhancement in the  $d(\pi^+, K^+)\Sigma^0p$  missing-mass spectrum was observed around 2.27 GeV/ $c^2$ , which corresponds to a  $\bar{K}NN$  binding energy of  $\sim 100$  MeV. With the  $(K^-, n)$  reaction on a  $^3\text{He}$  target at 1.0 GeV/ $c$ , the E15 collaboration observed a distinct peak with a binding energy of  $\sim 50$  MeV in the  $\Lambda p$  invariant mass of the  $\Lambda pn$  final state. Further investigation of the kaonic nuclei is planned using a new large  $4\pi$  spectrometer with neutral-particle detectors to systematically explore the light kaonic nuclei, from the most fundamental “ $\bar{K}N$ ” state (*i.e.*, the  $\Lambda(1405)$  state) to the “ $\bar{K}NNNN$ ”

via the  $(K^-, n)$  reactions.

Extension of the nuclear physics to the strangeness sector is essential to obtain further understanding of the interactions between octet baryons under flavor SU(3) symmetry. In the  $S = -1$  nuclear system, a neutron-rich hypernucleus  ${}^6_{\Lambda}\text{H}$  was investigated in the E10 experiment via the  ${}^6\text{Li}(\pi^-, K^+)$  reaction to reveal the effect of the  $\Sigma N - \Lambda N$  coupling and to obtain information on the  $\Lambda$  potential in a neutron-rich environment. However, no peak was observed in the bound region of  $\Lambda$ . In the E13 experiment, hypernuclear  $\gamma$ -rays from  ${}^4_{\Lambda}\text{He}$  and  ${}^{19}_{\Lambda}\text{F}$  were measured by Ge detectors in coincidence with hypernuclear production via the  $(K^-, \pi^-)$  reaction identified by the superconducting kaon spectrometer (SKS). The excitation energy of the  ${}^4_{\Lambda}\text{He}$   $1^+$  state obtained clearly indicated a large charge symmetry breaking between  ${}^4_{\Lambda}\text{H}$  and  ${}^4_{\Lambda}\text{He}$ . The energy spacing of the ground-state doublet of  ${}^{19}_{\Lambda}\text{F}$  is in good agreement with theoretical calculations, which shows that the theoretical framework of the  $\Lambda N$  interaction is valid, even in heavier hypernuclei. A modern  $\Sigma^{\pm}p$  scattering experiment is being performed as the E40 experiment with very high intensity  $\pi^{\pm}$  beams and liquid  $\text{H}_2$  for the  $\Sigma^{\pm}$  production and scattering targets. The experiment aims to investigate the quark Pauli effect in the  $\Sigma N(I = 3/2)$  interactions by measurement of the differential cross sections and phase shifts.

In the J-PARC HEF, efficient production of  $S = -2$  systems is possible using the world's highest-intensity  $K^-$  beam. To clarify the  $\Xi N$  interaction including  $\Xi N - \Lambda\Lambda$  coupling, the spectroscopic study of  $\Xi$  hypernuclei via the  $(K^-, K^+)$  reaction (E05 and E70) and the study of  $\Xi$ -atomic X-rays (E03 and E07) were proposed. Both the E05 and E70 experiments aim to measure the  ${}^{12}_{\Xi}\text{Be}$  hypernucleus; the E05 experiment was conducted as a pilot run using the existing SKS. A new high-resolution S-2S spectrometer will be constructed for the E70 experiment. The E07 experiment is a third-generation counter-emulsion hybrid experiment to study double strangeness nuclei such as double- $\Lambda$  and  $\Xi$  hypernuclei. The newly observed *MINO* event shows the binding (bonding) energy of two  $\Lambda$  hyperons to be  $19.07 \pm 0.11$  ( $1.87 \pm 0.37$ ) MeV for the  ${}^{11}_{\Lambda\Lambda}\text{Be}$  hypernucleus, which is the most likely explanation for the observed event. The *IBUKI* event was also uniquely identified as a  $\Xi^- + {}^{14}\text{N}$  bound nuclear system that gives  $B_{\Xi} = 1.27 \pm 0.21$  MeV. Many double strangeness nuclear events are expected to be found in future analysis. The E03 experiment will also measure the X-ray transitions from the  $\Xi$ -Fe atom to obtain the  $\Xi$ -nucleus potential around the nuclear surface region.

At the current HEF, many essential results on hadron and nuclear physics have been achieved and will be obtained from a wide variety of physics programs. However, enhancement of the HEF capabilities is mandatory to expand the physics programs to a region that has never been explored. In the HEF extension project, construction of two new beamlines is planned with the highest priority: a high-intensity and high-energy-resolution beamline (HIHR) and a high-momentum particle-separated beamline (K10). The HIHR and K10 beamlines are aimed at the high precision spectroscopy of  $\Lambda$  hypernuclei to provide keys to resolve the “hyperon puzzle”, and the heavy meson and baryon spectroscopies together with the investigation of  $\Omega$ -nucleon interaction as well as charmed meson-nucleon interactions. Intensive study and efforts have thus been made among the HEF user community toward the realization of this project.

## 6 Acknowledgments

We are grateful to all the staff members of J-PARC/KEK/JAEA for their extensive efforts on the successful operation of the facility, and thank all of collaborators and colleagues from the experiments performed in the J-PARC HEF. We are also grateful to the fruitful discussions with Prof. Tomokazu Fukuda and Prof. Makoto Oka. This work is partly supported by the MEXT Grants-in-Aid for Scientific Research on Innovative Areas “Clustering as a window on the hierarchical structure of quantum systems” Group-A02 (18H05402) and Group-B01 (18H05403), and “Nuclear matter in neutron stars investigated by experiments and astronomical observations” Group-A01 (No.24105002), and JSPS Grants-in-Aid for

Scientific Research (C) 17K05481 and (B) 18H01237, in Japan. Finally we would like to thank the Editor-in-Chief of PPNP for giving us the opportunity to contribute this review paper to PPNP in the 10th anniversary year of J-PARC.

## References

- [1] N. Isgur and G. Karl *Phys. Rev.* **D18** (1978) 4187.
- [2] Y. Nambu and G. Jona-Lasinio *Phys. Rev.* **122** (1961) 345.
- [3] Y. Nambu and G. Jona-Lasinio *Phys. Rev.* **124** (1961) 246.
- [4] S. Nagamiya *Nucl. Phys.* **A774** (2006) 895.
- [5] S. Nagamiya *Prog. Theor. Exp. Phys.* **2012** (2012) 02B001.
- [6] M. Ikegami *Prog. Theor. Exp. Phys.* **2012** (2012) 02B002.
- [7] H. Hotchi *et al.* *Prog. Theor. Exp. Phys.* **2012** (2012) 02B003.
- [8] T. Koseki *et al.* *Prog. Theor. Exp. Phys.* **2012** (2012) 02B004.
- [9] K. Abe *et al.* *Nucl. Instrum. Meth.* **A659** (2011) 106.
- [10] K. Agari *et al.* *Prog. Theor. Exp. Phys.* **2012** (2012) 02B008.
- [11] K. Agari *et al.* *Prog. Theor. Exp. Phys.* **2012** (2012) 02B009.
- [12] T. Takahashi *et al.* *Prog. Theor. Exp. Phys.* **2012** (2012) 02B010.
- [13] J. R. Sanford and C. L. Wang *BNL AGS internal reports No. BNL-11299 and No. BNL-11479* (1967) .
- [14] K. Agari *et al.* *Prog. Theor. Exp. Phys.* **2012** (2012) 02B011.
- [15] T. Yamanaka *Prog. Theor. Exp. Phys.* **2012** (2012) 02B006.
- [16] G. Adamov *et al.* [arXiv:1812.09018](https://arxiv.org/abs/1812.09018) [physics.ins-det].
- [17] H. Takahashi *et al.* *J. Radioanal. Nucl. Chem.* **305** (2015) 803.
- [18] R. S. Hayano and T. Hatsuda *Rev. Mod. Phys.* **82** (2010) 2949.
- [19] G. E. Brown and M. Rho *Phys. Rev. Lett.* **66** (1991) 2720.
- [20] T. Hatsuda and S. H. Lee *Phys. Rev.* **C46** (1992) R34.
- [21] F. Klingl, N. Kaiser, and W. Weise *Nucl. Phys.* **A624** (1997) 527.
- [22] P. Gubler and D. Satow *Prog. Part. Nucl. Phys.* **106** (2019) 1.
- [23] V. Metag, M. Nanova, and E. Ya. Paryev *Prog. Part. Nucl. Phys.* **97** (2017) 199.
- [24] T. Nakano *et al.* *Phys. Rev. Lett.* **91** (2003) 012002.
- [25] D. Diakonov, V. Petrov, and M. V. Polyakov *Z. Phys.* **A359** (1997) 305.

- [26] T. Nakano *et al. Phys. Rev.* **C79** (2009) 025210.
- [27] D. G. Ireland *et al. Phys. Rev. Lett.* **100** (2008) 052001.
- [28] M. Abdel-Bary *et al. Phys. Lett.* **B649** (2007) 252.
- [29] J. Z. Bai *et al. Phys. Rev.* **D70** (2004) 012004.
- [30] M.-Z. Wang *et al. Phys. Lett.* **B617** (2005) 141.
- [31] K. Miwa *et al. Phys. Lett.* **B635** (2006) 72.
- [32] K. Shirotori *et al. Phys. Rev. Lett.* **109** (2012) 132002.
- [33] M. Moritsu *et al. Phys. Rev.* **C90** (2014) 035205.
- [34] R. L. Jaffe *Phys. Rev. Lett.* **38** (1977) 195.
- [35] S. R. Beane *et al. Phys. Rev. Lett.* **106** (2011) 162001.
- [36] T. Inoue *et al. Phys. Rev. Lett.* **106** (2011) 162002.
- [37] J. K. Ahn *et al. Phys. Rev.* **C62** (2000) 055201.
- [38] C. J. Yoon *et al. Phys. Rev.* **C75** (2007) 022201(R).
- [39] J-PARC E42 proposal See [http://j-parc.jp/researcher/Hadron/en/Proposal\\_e.html](http://j-parc.jp/researcher/Hadron/en/Proposal_e.html) .
- [40] J. K. Ahn *PoS Hadron2017* (2018) 124.
- [41] S. H. Kim *et al. Nucl. Instrum. Meth.* **A940** (2019) 359.
- [42] J-PARC E45 proposal See [http://j-parc.jp/researcher/Hadron/en/Proposal\\_e.html](http://j-parc.jp/researcher/Hadron/en/Proposal_e.html) .
- [43] K. Tanida *AIP Conf. Proc.* **2130** (2019) 040019.
- [44] S. B. Yang *et al. Phys. Rev. Lett.* **117** (2016) 011801.
- [45] M. Tanabashi *et al. Phys. Rev.* **D98** (2018) 030001.
- [46] A. Starostin *et al. Phys. Rev.* **C64** (2001) 055205.
- [47] H. Kamano, S. X. Nakamura, T.-S. H. Lee, and T. Sato *Phys. Rev.* **C90** (2014) 065204.
- [48] H. Kamano, S. X. Nakamura, T.-S. H. Lee, and T. Sato *Phys. Rev.* **C92** (2015) 025205.
- [49] B.-C. Liu and J.-J. Xie *Phys. Rev.* **C85** (2012) 038201.
- [50] B.-C. Liu and J.-J. Xie *Phys. Rev.* **C86** (2012) 055202.
- [51] J-PARC E72 proposal See [http://j-parc.jp/researcher/Hadron/en/Proposal\\_e.html](http://j-parc.jp/researcher/Hadron/en/Proposal_e.html) .
- [52] K. Shirotori *et al. JPS Conf. Proc.* **8** (2015) 022012.
- [53] J-PARC E50 proposal See [http://j-parc.jp/researcher/Hadron/en/Proposal\\_e.html](http://j-parc.jp/researcher/Hadron/en/Proposal_e.html) .
- [54] H. Noumi *JPS Conf. Proc.* **17** (2017) 111003.

- [55] S.-H. Kim, A. Hosaka, H.-C. Kim, and H. Noumi *JPS Conf. Proc.* **10** (2016) 042004.
- [56] M. Naruki *et al. Phys. Rev. Lett.* **96** (2006) 092301.
- [57] R. Muto *et al. Phys. Rev. Lett.* **98** (2007) 042501.
- [58] M. H. Wood *et al. Phys. Rev.* **C78** (2008) 015201.
- [59] J-PARC E16 proposal See [http://j-parc.jp/researcher/Hadron/en/Proposal\\_e.html](http://j-parc.jp/researcher/Hadron/en/Proposal_e.html) .
- [60] S. H. Lee *Phys. Rev.* **C57** (1998) 927. [Erratum: *Phys. Rev.* **C58** (1998) 3771.].
- [61] H. Kim and P. Gubler [arXiv:1911.08737](https://arxiv.org/abs/1911.08737) [hep-ph].
- [62] S. Ashikaga *et al. JPS Conf. Proc.* **26** (2019) 024005.
- [63] F. Sauli *Nucl. Instrum. Meth.* **A386** (1997) 531.
- [64] Y. Komatsu *et al. Nucl. Instrum. Meth.* **A732** (2013) 241.
- [65] K. Aoki *et al. Nucl. Instrum. Meth.* **A628** (2011) 300.
- [66] K. Kanno *et al. Nucl. Instrum. Meth.* **A819** (2016) 20.
- [67] Y. Komatsu *et al. JPS Conf. Proc.* **13** (2017) 020005.
- [68] J-PARC E26 proposal See [http://j-parc.jp/researcher/Hadron/en/Proposal\\_e.html](http://j-parc.jp/researcher/Hadron/en/Proposal_e.html) .
- [69] J-PARC E29 proposal See [http://j-parc.jp/researcher/Hadron/en/Proposal\\_e.html](http://j-parc.jp/researcher/Hadron/en/Proposal_e.html) .
- [70] C. Evangelista *et al. Phys. Rev.* **D57** (1998) 5370.
- [71] M. Iwasaki *et al. Phys. Rev. Lett.* **78** (1997) 3067.
- [72] G. Beer *et al. Phys. Rev. Lett.* **94** (2005) 212302.
- [73] M. Bazzi *et al. Phys. Lett.* **B704** (2011) 113.
- [74] A. D. Martin *Nucl. Phys.* **B179** (1981) 33.
- [75] Y. Ikeda, T. Hyodo, and W. Weise *Phys. Lett.* **B706** (2011) 63.
- [76] Y. Ikeda, T. Hyodo, and W. Weise *Nucl. Phys.* **A881** (2012) 98.
- [77] A. Cieplý and J. Smejkal *Nucl. Phys.* **A881** (2012) 115.
- [78] R. H. Dalitz, T. C. Wong, and G. Rajasekaran *Phys. Rev.* **153** (1967) 1617.
- [79] F. Brau, C. Semay, and B. Silvestre-Brac *Phys. Rev.* **C66** (2002) 055202.
- [80] C. Helminen and D. O. Riska *Nucl. Phys.* **A699** (2002) 624.
- [81] R. H. Dalitz and A. Deloff *J. Phys.* **G17** (1991) 289.
- [82] Y. Akaishi and T. Yamazaki *Phys. Rev.* **C65** (2002) 044005.
- [83] J. A. Oller and U.-G. Meissner *Phys. Lett.* **B500** (2001) 263.

- [84] D. Jido, J. A. Oller, E. Oset, A. Ramos, and U.-G. Meissner *Nucl. Phys.* **A725** (2003) 181.
- [85] T. Hyodo and W. Weise *Phys. Rev.* **C77** (2008) 035204.
- [86] T. Hyodo and D. Jido *Prog. Part. Nucl. Phys.* **67** (2012) 55.
- [87] S. K. Choi *et al. Phys. Rev. Lett.* **91** (2003) 262001.
- [88] B. Aubert *et al. Phys. Rev. Lett.* **95** (2005) 142001.
- [89] S. K. Choi *et al. Phys. Rev. Lett.* **100** (2008) 142001.
- [90] R. Aaij *et al. Phys. Rev. Lett.* **115** (2015) 072001.
- [91] R. Aaij *et al. Phys. Rev. Lett.* **122** (2019) 222001.
- [92] S. Deser, M. L. Goldberger, K. Baumann, and W. E. Thirring *Phys. Rev.* **96** (1954) 774.
- [93] T. L. Trueman *Nucl. Phys.* **26** (1961) 57.
- [94] U.-G. Meissner, U. Raha, and A. Rusetsky *Eur. Phys. J.* **C35** (2004) 349.
- [95] U.-G. Meissner, U. Raha, and A. Rusetsky *Eur. Phys. J.* **C47** (2006) 473.
- [96] T. Koike, T. Harada, and Y. Akaishi *Phys. Rev.* **C53** (1996) 79.
- [97] T. S. Jensen *Frascati Physics Series* **36** (2004) 349.
- [98] M. Raeisi G. and S. Z. Kalantari *Phys. Rev.* **A79** (2009) 012510.
- [99] M. Faber *et al. Phys. Rev.* **C84** (2011) 064314.
- [100] M. Bazzi *et al. Nucl. Phys.* **A907** (2013) 69.
- [101] M. Bazzi *et al. Nucl. Phys.* **A954** (2016) 7.
- [102] C. Curceanu *et al. Rev. Mod. Phys.* **91** (2019) 025006.
- [103] A. Gal *Int. J. Mod. Phys.* **A22** (2007) 226.
- [104] M. Döring and U.-G. Meissner *Phys. Lett.* **B704** (2011) 663.
- [105] N. V. Shevchenko *Nucl. Phys.* **A890-891** (2012) 50.
- [106] T. Mizutani, C. Fayard, B. Saghai, and K. Tsushima *Phys. Rev.* **C87** (2013) 035201.
- [107] T. Hoshino, S. Ohnishi, W. Horiuchi, T. Hyodo, and W. Weise *Phys. Rev.* **C96** (2017) 045204.
- [108] J-PARC E57 proposal See [http://j-parc.jp/researcher/Hadron/en/Proposal\\_e.html](http://j-parc.jp/researcher/Hadron/en/Proposal_e.html) .
- [109] E. Gatti and P. Rehak *Nucl. Instrum. Meth.* **A225** (1984) 608.
- [110] P. Lechner *et al. Nucl. Instrum. Meth.* **A377** (1996) 346.
- [111] E. Gatti and P. Rehak *Nucl. Instrum. Meth.* **A541** (2005) 47.
- [112] R. Quaglia *et al. IEEE Trans. Nucl. Sci.* **62** (2015) 221.

- [113] E. Friedman, A. Gal, and C. J. Batty *Phys. Lett.* **B308** (1993) 6.
- [114] E. Friedman, A. Gal, and C. J. Batty *Nucl. Phys.* **A579** (1994) 518.
- [115] C. J. Batty, E. Friedman, and A. Gal *Phys. Rept.* **287** (1997) 385.
- [116] E. Friedman, A. Gal, J. Mareš, and A. Cieplý *Phys. Rev.* **C60** (1999) 024314.
- [117] A. Ramos and E. Oset *Nucl. Phys.* **A671** (2000) 481.
- [118] S. Hirenzaki, Y. Okumura, H. Toki, E. Oset, and A. Ramos *Phys. Rev.* **C61** (2000) 055205.
- [119] A. Cieplý, E. Friedman, A. Gal, and J. Mareš *Nucl. Phys.* **A696** (2001) 173.
- [120] J. Yamagata-Sekihara and S. Hirenzaki *private communication* (2015) .
- [121] J. Mareš, E. Friedman, and A. Gal *Nucl. Phys.* **A770** (2006) 84.
- [122] E. Hiyama *private communication* (2015) .
- [123] S. Okada *et al.* *Phys. Lett.* **B653** (2007) 387.
- [124] M. Bazzi *et al.* *Phys. Lett.* **B681** (2009) 310.
- [125] M. Bazzi *et al.* *Phys. Lett.* **B697** (2011) 199.
- [126] K. D. Irwin and G. Hilton *Cryogenic Particle Detection, Topics in Applied Physics* **99** (2005) 63.
- [127] W. B. Doriese *et al.* *Rev. Sci. Instrum.* **88** (2017) 053108.
- [128] H. Tatsuno *et al.* *J. Low Temp. Phys* **184** (2016) 930.
- [129] S. Okada *et al.* *Prog. Theor. Exp. Phys.* **2016** (2016) 091D01.
- [130] T. Hashimoto *et al.* *IEEE Trans. Appl. Supercond.* **27** (2017) 2100905.
- [131] J-PARC E62 proposal See [http://j-parc.jp/researcher/Hadron/en/Proposal\\_e.html](http://j-parc.jp/researcher/Hadron/en/Proposal_e.html) .
- [132] T. Hashimoto *et al.* *JPS Conf. Proc.* **26** (2019) 023013.
- [133] R. H. Dalitz and S. F. Tuan *Phys. Rev. Lett.* **2** (1959) 425.
- [134] M. H. Alston *et al.* *Phys. Rev. Lett.* **6** (1961) 698.
- [135] K. Moriya *et al.* *Phys. Rev. Lett.* **112** (2014) 082004.
- [136] J. M. M. Hall *et al.* *Phys. Rev. Lett.* **114** (2015) 132002.
- [137] M. Niiyama *et al.* *Phys. Rev.* **C78** (2008) 035202.
- [138] K. Moriya *et al.* *Phys. Rev.* **C87** (2013) 035206.
- [139] H. Y. Lu *et al.* *Phys. Rev.* **C88** (2013) 045202.
- [140] I. Zychor *et al.* *Phys. Lett.* **B660** (2008) 167.
- [141] G. Agakishiev *et al.* *Phys. Rev.* **C87** (2013) 025201.

- [142] R. J. Hemingway *Nucl. Phys.* **B253** (1985) 742.
- [143] B. Riley, I-T. Wang, J. G. Fetkovich, and J. M. Mckenzie *Phys. Rev.* **D11** (1975) 3065.
- [144] J. Esmaili, Y. Akaishi, and T. Yamazaki *Phys. Lett.* **B686** (2010) 23.
- [145] M. Hassanvand, S. Z. Kalantari, Y. Akaishi, and T. Yamazaki *Phys. Rev.* **C87** (2013) 055202.
- [146] L. Roca and E. Oset *Phys. Rev.* **C87** (2013) 055201.
- [147] S. X. Nakamura and D. Jido *Prog. Theor. Exp. Phys.* .
- [148] M. Mai and U.-G. Meissner *Eur. Phys. J.* **A51** (2015) 30.
- [149] M. Hassanvand, Y. Akaishi, and T. Yamazaki [arXiv:1704.08571](https://arxiv.org/abs/1704.08571) [nucl-th].
- [150] A. V. Anisovich *et al.* [arXiv:1905.05456](https://arxiv.org/abs/1905.05456) [nucl-ex].
- [151] S. Prakhov *et al.* *Phys. Rev.* **C70** (2004) 034605.
- [152] D. Jido, E. Oset, and T. Sekihara *Eur. Phys. J.* **A42** (2009) 257.
- [153] T. Kishimoto *Phys. Rev. Lett.* **83** (1999) 4701.
- [154] H. Asano *et al.* *AIP Conf. Proc.* **2130** (2019) 040018.
- [155] J. C. Nacher, E. Oset, H. Toki, and A. Ramos *Phys. Lett.* **B455** (1999) 55.
- [156] S. Kawasaki *et al.* *JPS Conf. Proc.* **26** (2019) 022009.
- [157] H. Kamano and T.-S. H. Lee *Phys. Rev.* **C94** (2016) 065205.
- [158] K. Miyagawa, J. Haidenbauer, and H. Kamada *Phys. Rev.* **C97** (2018) 055209.
- [159] H. Zhang, J. Tulpan, M. Shrestha, and D. M. Manley *Phys. Rev.* **C88** (2013) 035204.
- [160] E. Oset, A. Ramos, and C. Bennhold *Phys. Lett.* **B527** (2002) 99.
- [161] S. Ohnishi, Y. Ikeda, T. Hyodo, and W. Weise *Phys. Rev.* **C93** (2016) 025207.
- [162] Y. Nogami *Phys. Lett.* **7** (1963) 288.
- [163] T. Yamazaki and Y. Akaishi *Phys. Lett.* **B535** (2002) 70.
- [164] A. Doté, Y. Akaishi, H. Horiuchi, and T. Yamzaki *Phys. Lett.* **B590** (2004) 51.
- [165] A. Doté, H. Horiuchi, Y. Akaishi, and T. Yamazaki *Phys. Rev.* **C70** (2004) 044313.
- [166] N. V. Shevchenko, A. Gal, and J. Mareš *Phys. Rev. Lett.* **98** (2007) 082301.
- [167] N. V. Shevchenko, A. Gal, J. Mareš, and J. Révai *Phys. Rev.* **C76** (2007) 044004.
- [168] Y. Ikeda and T. Sato *Phys. Rev.* **C76** (2007) 035203.
- [169] Y. Ikeda and T. Sato *Phys. Rev.* **C79** (2009) 035201.
- [170] S. Wycech and A. M. Green *Phys. Rev.* **C79** (2009) 014001.

- [171] J. Révai and N. V. Shevchenko *Phys. Rev.* **C90** (2014) 034004.
- [172] A. Doté, T. Inoue, and T. Myo *Phys. Rev.* **C95** (2017) 062201(R).
- [173] S. Ohnishi, W. Horiuchi, T. Hoshino, K. Miyahara, and T. Hyodo *Phys. Rev.* **C95** (2017) 065202.
- [174] A. Doté, T. Hyodo, and W. Weise *Nucl. Phys.* **A804** (2008) 197.
- [175] A. Doté, T. Hyodo, and W. Weise *Phys. Rev.* **C79** (2009) 014003.
- [176] Y. Ikeda, H. Kamano, and T. Sato *Prog. Theor. Phys.* **124** (2010) 533.
- [177] N. Barnea, A. Gal, and E. Z. Liverts *Phys. Lett.* **B712** (2012) 132.
- [178] M. Bayar and E. Oset *Phys. Rev.* **C88** (2013) 044003.
- [179] A. Doté, T. Inoue, and T. Myo *Phys. Lett.* **B784** (2018) 405.
- [180] A. Doté, T. Inoue, and T. Myo *Prog. Theor. Exp. Phys.* **2015** (2015) 043D02.
- [181] M. Agnello *et al.* *Phys. Rev. Lett.* **94** (2005) 212303.
- [182] T. Yamazaki *et al.* *Phys. Rev. Lett.* **104** (2010) 132502.
- [183] O. Vázquez Doce *et al.* *Phys. Lett.* **B758** (2016) 134.
- [184] R. Del Grande *et al.* *Eur. Phys. J.* **C79** (2019) 190.
- [185] G. Agakishiev *et al.* *Phys. Lett.* **B742** (2015) 242.
- [186] A. O. Tokiyasu *et al.* *Phys. Lett.* **B728** (2014) 616.
- [187] T. Yamazaki and Y. Akaishi *Phys. Rev.* **C76** (2007) 045201.
- [188] Y. Ichikawa *et al.* *Prog. Theor. Exp. Phys.* **2014** (2014) 101D03.
- [189] Y. Ichikawa *et al.* *Prog. Theor. Exp. Phys.* **2015** (2015) 021D01.
- [190] T. Sekihara, D. Jido, and Y. Kanada-En'yo *Phys. Rev.* **C79** (2009) 062201(R).
- [191] D. W. Thomas, A. Engler, H. E. Fisk, and R. W. Kraemer *Nucl. Phys.* **B56** (1973) 15.
- [192] Y. Ichikawa *Ph.D thesis, Kyoto University (2015)* .
- [193] H. Garcilazo and A. Gal *Nucl. Phys.* **A897** (2013) 167.
- [194] T. Hashimoto *et al.* *Prog. Theor. Exp. Phys.* **2015** (2015) 061D01.
- [195] Y. Sada *et al.* *Prog. Theor. Exp. Phys.* **2016** (2016) 051D01.
- [196] S. Ajimura *et al.* *Phys. Lett.* **B789** (2019) 620.
- [197] T. Sekihara, E. Oset, and A. Ramos *Prog. Theor. Exp. Phys.* **2016** (2016) 123D03.
- [198] T. Sekihara, E. Oset, and A. Ramos *JPS Conf. Proc.* **26** (2019) 023009.
- [199] S. Ohnishi, Y. Ikeda, H. Kamano, and T. Sato *Phys. Rev.* **C88** (2013) 025204.

- [200] F. Sakuma *et al.* *Proceedings of the NN2018 conference, will be published in JPS Conf. Proc.* .
- [201] Letter of Intent for the J-PARC, 2019, "Letter of Intent for the Systematic Study of the Kaonic Nuclear Bound States at K1.8BR in J-PARC Hadron Hall" See [http://j-parc.jp/researcher/Hadron/en/Proposal\\_e.html](http://j-parc.jp/researcher/Hadron/en/Proposal_e.html) .
- [202] M. Oka and K. Yazaki *in Quarks and Nuclei, ed. W. Weise (World Scientific) (1985) 489.*
- [203] K. Yazaki *Nucl. Phys.* **A479** (1988) 217C.
- [204] K. Shimizu *Nucl. Phys.* **A547** (1992) 265C.
- [205] H. G. Dosch, E. Engelmann, H. Filthuth, V. Hepp, and E. Kluge *Phys. Lett.* **21** (1966) 236.
- [206] E. Engelmann, H. Filthuth, V. Hepp, and E. Kluge *Phys. Lett.* **21** (1966) 587.
- [207] H. A. Rubin and R. A. Burnstein *Phys. Rev.* **159** (1967) 1149.
- [208] G. Alexander *et al.* *Phys. Rev.* **173** (1968) 1452.
- [209] B. Sechi-Zorn, B. Kehoe, J. Twitty, and R. A. Burnstein *Phys. Rev.* **175** (1968) 1735.
- [210] G. R. Charlton *et al.* *Phys. Lett.* **32B** (1970) 720.
- [211] J. A. Kadyk, G. Alexander, J. H. Chan, P. Gaposchkin, and G. H. Trilling *Nucl. Phys.* **B27** (1971) 13.
- [212] F. Eisele, H. Filthuth, W. Föehlich, V. Hepp, and G. Zech *Phys. Lett.* **37B** (1971) 204.
- [213] J. K. Ahn *et al.* *Nucl. Phys.* **A648** (1999) 263.
- [214] Y. Kondo *et al.* *Nucl. Phys.* **A676** (2000) 371.
- [215] J. K. Ahn *et al.* *Nucl. Phys.* **A761** (2005) 41.
- [216] T. Kadowaki *et al.* *Eur. Phys. J.* **A15** (2002) 295.
- [217] K. Tanida *et al.* *Phys. Rev. Lett.* **86** (2001) 1982.
- [218] P. K. Saha *et al.* *Phys. Rev. Lett.* **94** (2005) 052502.
- [219] T. Harada, A. Umeya, and Y. Hirabayashi *Phys. Rev.* **C79** (2009) 014603.
- [220] Khin Swe Myint and Y. Akaishi *Prog. Theor. Phys. Suppl.* **146** (2003) 599.
- [221] M. Agnello *et al.* *Phys. Rev. Lett.* **108** (2012) 042501.
- [222] H. Sugimura *et al.* *Phys. Lett.* **B729** (2014) 39.
- [223] R. Honda *et al.* *Phys. Rev.* **C96** (2017) 014005.
- [224] A. A. Korshennikov *et al.* *Phys. Rev. Lett.* **87** (2001) 092501.
- [225] A. Gal and D. J. Millener *Phys. Lett.* **B725** (2013) 445.
- [226] E. Hiyama, S. Ohnishi, M. Kamimura, and Y. Yamamoto *Nucl. Phys.* **A908** (2013) 29.
- [227] A. H. Wuosmaa *et al.* *Phys. Rev.* **C95** (2017) 014310.

- [228] H. Tamura *et al.* *Phys. Rev. Lett.* **84** (2000) 5963.
- [229] Y. Miura *et al.* *Nucl. Phys.* **A754** (2005) 75c.
- [230] Y. Ma *et al.* *Eur. Phys. J.* **A33** (2007) 243.
- [231] K. Hosomi *et al.* *Prog. Theor. Exp. Phys.* .
- [232] H. Akikawa *et al.* *Phys. Rev. Lett.* **88** (2002) 082501.
- [233] M. Ukai *et al.* *Phys. Rev. Lett.* **93** (2004) 232501.
- [234] H. Tamura *et al.* *Nucl. Phys.* **A754** (2005) 58c.
- [235] M. Ukai *et al.* *Phys. Rev.* **C73** (2006) 012501(R).
- [236] D. J. Millener *Nucl. Phys.* **A754** (2005) 48c.
- [237] M. Jurič *et al.* *Nucl. Phys.* **B52** (1973) 1.
- [238] M. Bedjidian *et al.* *Phys. Lett.* **62B** (1976) 467.
- [239] M. Bedjidian *et al.* *Phys. Lett.* **83B** (1979) 252.
- [240] A. Kawachi *Ph.D thesis, Univesity of Tokyo (1997)* .
- [241] T. O. Yamamoto *et al.* *Phys. Rev. Lett.* **115** (2015) 222501.
- [242] S. B. Yang *et al.* *Phys. Rev. Lett.* **120** (2018) 132505.
- [243] T. Koike *et al.* *Nucl. Instrum. Meth.* **A770** (2015) 1.
- [244] D. J. Millener *Nucl. Phys.* **A914** (2013) 109.
- [245] Th. A. Rijken, V. G. J. Stoks, and Y. Yamamoto *Phys. Rev.* **C59** (1999) 21.
- [246] A. Umeya and T. Motoba *Nucl. Phys.* **A954** (2016) 242.
- [247] A. Esser *et al.* *Phys. Rev. Lett.* **114** (2015) 232501.
- [248] S. N. Nakamura *et al.* *Phys. Rev. Lett.* **110** (2013) 012502.
- [249] E. Botta, T. Bressani, and A. Feliciello *Nucl. Phys.* **A960** (2017) 165.
- [250] J-PARC E63 proposal *See [http://j-parc.jp/researcher/Hadron/en/Proposal\\_e.html](http://j-parc.jp/researcher/Hadron/en/Proposal_e.html)* .
- [251] M. May *et al.* *Phys. Rev. Lett.* **51** (1983) 2085.
- [252] H. Tamura *et al.* *Nucl. Phys.* **A835** (2010) 3.
- [253] R. H. Dalitz and A. Gal *Annals Phys.* **116** (1978) 167.
- [254] T. Nagae *et al.* *Phys. Rev. Lett.* **80** (1998) 1605.
- [255] P. K. Saha *et al.* *Phys. Rev.* **C70** (2004) 044613.
- [256] T. Harada and Y. Hirabayashi *Nucl. Phys.* **A759** (2005) 143.

- [257] K. Miwa *et al.* *JPS Conf. Proc.* **17** (2017) 041002.
- [258] Th. A. Rijken, M. M. Nagels, and Y. Yamamoto *Prog. Theor. Phys. Suppl.* **185** (2010) 14.
- [259] Y. Fujiwara, C. Nakamoto, and Y. Suzuki *Phys. Rev.* **C54** (1996) 2180.
- [260] Y. Fujiwara, T. Fujita, M. Kohno, C. Nakamoto, and Y. Suzuki *Phys. Rev.* **C65** (2001) 014002.
- [261] J. Haidenbauer *et al.* *Nucl. Phys.* **A915** (2013) 24.
- [262] R. Jastrow *Phys. Rev.* **81** (1951) 165.
- [263] Y. Akazawa *Ph.D thesis, Tohoku Univesity (2018)* .
- [264] L. Adamczyk *et al.* *Phys. Rev. Lett.* **114** (2015) 022301.
- [265] M. Danysz *et al.* *Nucl. Phys.* **49** (1963) 121.
- [266] D. J. Prowse *Phys. Rev. Lett.* **17** (1966) 782.
- [267] S. Aoki *et al.* *Prog. Theor. Phys.* **85** (1991) 1287.
- [268] H. Takahashi *et al.* *Phys. Rev. Lett.* **87** (2001) 212502.
- [269] J. K. Ahn *et al.* *Phys. Rev.* **C88** (2013) 014003.
- [270] E. Hiyama, M. Kamimura, Y. Yamamoto, and T. Motoba *Phys. Rev. Lett.* **104** (2010) 212502.
- [271] Y. Kanada-En'yo *Phys. Rev.* **C97** (2018) 034324.
- [272] H. Togashi, E. Hiyama, Y. Yamamoto, and M. Takano *Phys. Rev.* **C93** (2016) 035808.
- [273] Aye Moh Moh Theint *et al.* *Prog. Theor. Exp. Phys.* .
- [274] Myint Kyaw Soe *et al.* *Nucl. Instrum. Meth.* **A848** (2017) 66.
- [275] H. Ekawa *et al.* *Prog. Theor. Exp. Phys.* **2019** (2019) 021D02.
- [276] D. H. Davis and J. Pniewski *Contemp. Phys.* **27** (1986) 91.
- [277] T. Gogami *et al.* *Phys. Rev.* **C93** (2016) 034314.
- [278] M. Yamaguchi, K. Tominaga, T. Ueda, and Y. Yamamoto *Prog. Theor. Phys.* **105** (2001) 627.
- [279] J. Yoshida *et al.* *Nucl. Instrum. Meth.* **A847** (2017) 86.
- [280] T. Fukuda *et al.* *Phys. Rev.* **C58** (1998) 1306.
- [281] P. Khaustov *et al.* *Phys. Rev.* **C61** (2000) 054603.
- [282] K. Nakazawa *et al.* *Prog. Theor. Exp. Phys.* .
- [283] E. Hiyama and K. Nakazawa *Annu.Rev.Nucl.Sci.* **68** (2018) 131.
- [284] J. Yoshida *et al.* *JPS Conf. Proc.* **26** (2019) 023006.
- [285] S. Hayakawa *Ph.D thesis, Osaka Univesity (2019)* .

- [286] M. M. Nagels, Th. A. Rijken, and Y. Yamamoto [arXiv:1504.02634](#) [nucl-th].
- [287] C. B. Dover and A. Gal *Annals Phys.* **146** (1983) 309.
- [288] T. Nagae *et al.* *PoS INPC2016* (2017) 038.
- [289] T. Nagae *et al.* *AIP Conf. Proc.* **2130** (2019) 020015.
- [290] J-PARC E70 proposal *See [http://j-parc.jp/researcher/Hadron/en/Proposal\\_e.html](http://j-parc.jp/researcher/Hadron/en/Proposal_e.html)* .
- [291] Y. Fujii *et al.* *Nucl. Instrum. Meth.* **A795** (2015) 351.
- [292] T. Gogami *et al.* *Nucl. Instrum. Meth.* **A900** (2018) 69.
- [293] T. Motoba and S. Sugimoto *Nucl. Phys.* **A835** (2010) 223.
- [294] E. Hiyama, Y. Yamamoto, T. Motoba, Th. A. Rijken, and M. Kamimura *Phys. Rev.* **C78** (2008) 054316.
- [295] T. Harada, Y. Hirabayashi, and A. Umeya *Nucl. Phys.* **A914** (2013) 85.
- [296] K. Sasaki *et al.* [arXiv:1912.08630](#) [hep-lat].
- [297] E. Hiyama, K. Sasaki, T. Miyamoto, T. Doi, T. Hatsuda, Y. Yamamoto, and T. A. Rijken [arXiv:1910.02864](#) [nucl-th].
- [298] C. J. Batty, E. Friedman, and A. Gal *Phys. Rev.* **C59** (1999) 295.
- [299] H. Fujioka *et al.* [arXiv:1706.07916](#) [nucl-ex].
- [300] P. Achenbach *et al.* [arXiv:1906.02357](#) [nucl-ex].
- [301] P. B. Demorest, T. Pennucci, S. M. Ransom, M. S. E. Roberts, and J. W. T. Hessels *Nature* **467** (2010) 1081.
- [302] J. Antoniadis *et al.* *Science* **340** (2013) 1233232.
- [303] S. Nishizaki, T. Takatsuka, and Y. Yamamoto *Prog. Theor. Phys.* **105** (2001) 607.
- [304] S. Nishizaki, T. Takatsuka, and Y. Yamamoto *Prog. Theor. Phys.* **108** (2002) 703.
- [305] K. Sekiguchi *et al.* *Phys. Rev.* **C83** (2011) 061001(R).
- [306] T. Furumoto, Y. Sakuragi, and Y. Yamamoto *Phys. Rev.* **C79** (2009) 011601(R).
- [307] Y. Fujita *et al.* *Nucl. Instrum. Meth.* **B126** (1997) 274.
- [308] T. Iritani *et al.* *Phys. Lett.* **B792** (2019) 284.
- [309] A. Hayashigaki *Phys. Lett.* **B487** (2000) 96.
- [310] K. Tsushima, D. H. Lu, A. W. Thomas, K. Saito, and R. H. Landau *Phys. Rev.* **C59** (1999) 2824.
- [311] A. Sibirtsev, K. Tsushima, and A. W. Thomas *Eur. Phys. J.* **A6** (1999) 351.